

الجمهورية الجزائرية الديمقراطية الشعبية
République Algérienne Démocratique et Populaire
وزارة التعليم العالي والبحث العلمي
Ministère de l'enseignement supérieur et de la recherche scientifique

Université Mohamed Khider de Biskra
Faculté des Sciences et de la technologie
Département : Génie Electrique
Réf.



جامعة محمد خيضر بسكرة
كلية العلوم والتكنولوجيا
قسم: الهندسة الكهربائية
المرجع:

Thèse présentée en vue de l'obtention
Du diplôme de
Doctorat LMD en Energies Renouvelables
Option : Energies Renouvelables Solaire Photovoltaïque

***Détection et localisation des défauts d'un
système PV par les techniques soft
computing***

Présentée par :

Marah BACHA

Soutenue publiquement le : 03/07/2025

Devant le jury composé de :

Salah Eddine ZOUZOU	Professeur	Université de Biskra	Président
Amel TERKI	Professeur	Université de Biskra	Rapporteur
Said DRID	Professeur	Ecole supérieur Nationale ER2SD. Batna	Examineur
Mohamed Yacine HAMMOUDI	Professeur	Université de Biskra	Examineur

الجمهورية الجزائرية الديمقراطية الشعبية
People's Democratic Republic of Algeria
وزارة التعليم العالي والبحث العلمي
Ministry of Higher Education & Scientific Research

University Mohamed Khider – Biskra
Faculty of Science and Technology
Department of Electrical Engineering
Ref.....



جامعة محمد خيضر بسكرة
كلية العلوم والتكنولوجيا
قسم: الهندسة الكهربائية
المرجع:

A thesis submitted for the fulfillment of
The degree of

LMD Doctoral Thesis in Renewable Energies

Option: Renewable Energies Solar Photovoltaic

Detection and localization of faults in a PV system using soft computing techniques

Presented by:

Marah BACHA

Thesis defended publicly on: 03/07/2025

In front of a jury composed of:

Salah Eddine ZOUZOU	Professor	University of Biskra	President
Amel TERKI	Professor	University of Biskra	Thesis Supervisor
Said DRID	Professor	Higher National School ER2SD of Batna	Examiner
Mohamed Yacine HAMMOUDI	Professor	University of Biskra	Examiner

Dedication

I dedicate this modest work to my beloved parents and my beloved grandmother who have been my source of inspiration and strength, who continually provide their moral, spiritual and emotional support.

To my beloved sisters, Madjda and Manel, and my dear brother Marouane, your love, patience, and unwavering belief in me have been my strength to complete this thesis.

To my cherished best friends, Hadia and Chaima, and to all the relatives whose kind words, advice, and encouragement lifted my spirits, your presence in my life has been a beautiful reminder of love, strength, and unwavering support.

A special dedication to all LGEB members from friends, colleagues, and teachers whose unwavering support and encouragement have been a guiding light throughout this journey.

To my dear aunt who left us, she was very generous and always smiling, may God keep you in his vast paradise.

I say thank you

Acknowledgment

First of all, I thank Allah, the Almighty, who gave me the strength, patience and will to accomplish this modest work.

Also, my thesis supervisor Pr. Amel Terki, of the LGEB Laboratory at the University of Biskra for her supervision, her directives and her availability. Also, I thank her for his encouragement and sympathy throughout the period of preparing my work.

My thanks also go to the jury members, Professor Zouzou Salah Eddine, from the University of Biskra, who honored me by chairing my thesis, Professor Hammoudi Mohamed Yacine, also from the University of Biskra, and Professor Drid Said from Higher National School ER2SD of Batna, for their presence and for the time they were willing to devote to evaluating this work.

My sincere appreciation goes to the current head of the Laboratory of Electrical Engineering (LGEB), Professor Naimi Djemai, and the former head Professor Zouzou Salah Eddine, for fostering an ideal research and experimental work environment. This work wouldn't have reached fruition without their assistance and the collective support of the LGEB members.

I also thank all the teachers of the electrical engineering department of Mohamed Khider Biskra University who participated in my training throughout the university cycle.

I cannot conclude without expressing my heartfelt thanks to my family my parents, my sisters, my brother, and friends both in my social and academic life, whose unwavering love and support have lightened the burdens of this journey.

Finally, to everyone who has offered help, encouragement, or information, and to all who have believed in me, giving me the energy to persevere and succeed, I offer my sincerest thanks.

Abstract

Ensuring the reliability and efficiency of photovoltaic (PV) systems requires robust fault detection and diagnosis methods. This thesis presents a comprehensive study on the detection, classification, and localization of PV faults using Artificial Neural Networks (ANN) and Fuzzy Logic (FL) techniques, validated through both simulation and experimental approaches. In the first phase, a simulation model was developed in Matlab/Simulink® to describe the system behavior for both healthy and faulty operations. To deal with this concern, a Matlab/Simulink® co-simulation strategy is developed to elaborate a trusted simulation model. This model requires the use of the One Diode Model (ODM) electrical parameters. For this, an efficient strategy, based on the War Strategy Optimization (WSO) algorithm, is applied to identify the ODM parameters. Finally, the ODM identified parameters are used to elaborate an efficient strategy of maximum power point (MPP) estimation. The efficiency of the developed strategies is experimentally evaluated by using real measured data. In the first phase, the thresholding method and FL classifier demonstrated high fault detection capabilities to diagnose eight types of faults occurring in PV cells, achieving approximately 100% accuracy in the simulation and experimental tests. In the second phase, an Artificial Neural Network (ANN)-based fault detection and classification approach was successfully implemented and validated through both simulation and experimental analysis. Five distinct single- and multi-fault types, including partial shading, open circuit and bypass diode failures, were applied to a PV module through the dSPACE DS1104 controller, confirmed the model's robustness and reliability. The ANN-based method achieved an impressive classification accuracy of 99.7%, proving its efficiency in detecting PV faults under varying conditions. In the third phase, a comprehensive study has substantiated that both Artificial Neural Networks (ANN) and Fuzzy Logic (FL) are capable of detecting and classifying all single- and multi-fault types effectively. However, when moving from simulation to experimental tests using the dSPACE DS1104 platform, the results unequivocally showcased the superiority of the ANN classifier over the FL classifier. The ANN classifier exhibited superior accuracy (99.6%) and faster fault classification compared to the FL classifier (99.2%) in real-time conditions. The findings of this research highlight the ANN-based approach as an efficient solution for PV fault diagnosis, offering enhanced accuracy and faster processing. These results underscore the potential of integrating ANN techniques into real-time monitoring systems to improve the performance, reliability, and safety of photovoltaic installations.

Key words: Photovoltaic systems, Fault detection, Artificial Neural Networks, Fuzzy Logic, War Strategy Optimization, Matlab/Simulink, Real-time monitoring.

Résumé

Assurer la fiabilité et l'efficacité des systèmes photovoltaïques (PV) nécessite des méthodes robustes de détection et de diagnostic des défauts. Cette thèse présente une étude approfondie de la détection, de la classification et de la localisation des défauts PV à l'aide de techniques de réseaux de neurones artificiels (ANN) et de logique floue (FL), validées par des approches de simulation et expérimentales. Dans un premier temps, un modèle de simulation a été développé sous Matlab/Simulink® afin de décrire le comportement du système, qu'il soit en fonctionnement normal ou en fonctionnement défectueux. Pour répondre à cette problématique, une stratégie de co-simulation Matlab/Simulink® a été développée afin d'élaborer un modèle de simulation fiable. Ce modèle nécessite l'utilisation des paramètres électriques du modèle à une diode (ODM). Pour cela, une stratégie efficace, basée sur l'algorithme d'optimisation de stratégie de guerre (WSO), est appliquée pour identifier les paramètres ODM. Enfin, les paramètres ODM identifiés sont utilisés pour élaborer une stratégie efficace d'estimation du point de puissance maximale (MPP). L'efficacité des stratégies développées est évaluée expérimentalement à l'aide de données réelles mesurées. Lors de la première phase, la méthode de seuillage et le classificateur FL ont démontré une capacité élevée de détection des défauts pour diagnostiquer huit types de défauts survenant dans les cellules photovoltaïques, atteignant une précision d'environ 100 % lors des simulations et des tests expérimentaux. Lors de la deuxième phase, une approche de détection et de classification des défauts basée sur un réseau de neurones artificiels (ANN) a été mise en œuvre avec succès et validée par simulation et analyse expérimentale. Cinq types distincts de défauts simples et multiples, dont l'ombrage partiel, le circuit ouvert et les défaillances de diodes de dérivation, ont été appliqués à un module photovoltaïque via le contrôleur dSPACE DS1104, confirmant la robustesse et la fiabilité du modèle. La méthode basée sur le RNA a atteint une précision de classification impressionnante de 99,7 %, prouvant son efficacité dans la détection des défauts photovoltaïques dans diverses conditions. Lors de la troisième phase, une étude approfondie a démontré que les réseaux de neurones artificiels (ANN) et la logique floue (FL) sont capables de détecter et de classer efficacement tous les types de défauts simples et multiples. Cependant, en passant de la simulation aux tests expérimentaux avec la plateforme dSPACE DS1104, les résultats ont clairement démontré la supériorité du classificateur ANN sur le classificateur FL. Le classificateur ANN a affiché une précision supérieure (99,6 %) et une classification des défauts plus rapide que le classificateur FL (99,2 %) en conditions temps réel. Les résultats de cette recherche mettent en évidence l'approche basée sur les ANN comme une solution efficace pour le diagnostic des défauts photovoltaïques, offrant une précision accrue et un traitement plus rapide. Ces résultats soulignent le potentiel de l'intégration des techniques ANN dans les systèmes de surveillance en temps réel pour améliorer les performances, la fiabilité et la sécurité des installations photovoltaïques.

Mots-clés : Systèmes photovoltaïques, Détection de défauts, Réseaux de neurones artificiels, Logique floue, Optimisation de stratégie de guerre, Matlab/Simulink, Surveillance en temps réel.

يتطلب ضمان موثوقية وكفاءة أنظمة الطاقة الكهروضوئية (PV) أساليب قوية للكشف عن الأعطال وتشخيصها. تقدم هذه الأطروحة دراسة شاملة حول الكشف عن أعطال الطاقة الكهروضوئية وتصنيفها وتحديد مواقعها باستخدام تقنيات الشبكات العصبية الاصطناعية (ANN) والمنطق الضبابي (FL)، والتي تم التحقق من صحتها من خلال كل من المحاكاة والنهج التجريبية. في المرحلة الأولى، تم تطوير نموذج محاكاة في Matlab/Simulink® لوصف سلوك النظام لكل من العمليات السليمة والمعيبة. للتعامل مع هذه المشكلة، تم تطوير استراتيجية محاكاة مشتركة Matlab/Simulink® لوضع نموذج محاكاة موثوق به. يتطلب هذا النموذج استخدام المعلومات الكهربائية لنموذج الصمام الثنائي الموحد (ODM). ولهذا، يتم تطبيق استراتيجية فعالة، تستند إلى خوارزمية تحسين استراتيجية الحرب (WSO)، لتحديد معلمات ODM. وأخيراً، يتم استخدام معلمات ODM المحددة لوضع استراتيجية فعالة لتقدير نقطة القدرة القصوى (MPP). يتم تقييم كفاءة الاستراتيجيات المطورة تجريبياً باستخدام بيانات مقاسة حقيقية. في المرحلة الأولى، أظهرت طريقة تحديد العتبات ومصنف FL قدرات عالية في اكتشاف الأعطال لتشخيص ثمانية أنواع من الأعطال التي تحدث في الخلايا الكهروضوئية، محققين دقة تقارب 100% في اختبارات المحاكاة والاختبارات التجريبية. في المرحلة الثانية، تم بنجاح تنفيذ نهج اكتشاف وتصنيف الأعطال القائم على الشبكة العصبية الاصطناعية (ANN) والتحقق من صحته من خلال كل من المحاكاة والتحليل التجريبي. تم تطبيق خمسة أنواع مميزة من الأعطال المفردة والمتعددة، بما في ذلك التظليل الجزئي والدائرة المفتوحة وفشل الصمام الثنائي الالتفافية، على وحدة كهروضوئية من خلال وحدة التحكم dSPACE DS1104، مما أكد متانة النموذج وموثوقيته. حققت الطريقة القائمة على ANN دقة تصنيف رائعة بلغت 99.7%، مما يثبت كفاءتها في اكتشاف أعطال الخلايا الكهروضوئية في ظل ظروف مختلفة. في المرحلة الثالثة، أثبتت دراسة شاملة أن كلاً من الشبكات العصبية الاصطناعية (ANN) والمنطق الضبابي (FL) قادران على اكتشاف وتصنيف جميع أنواع الأعطال المفردة والمتعددة بشكل فعال. ومع ذلك، عند الانتقال من المحاكاة إلى الاختبارات التجريبية باستخدام منصة dSPACE DS1104، أظهرت النتائج بوضوح تفوق مُصنّف الشبكات العصبية الاصطناعية (ANN) على مُصنّف FL. أظهر مُصنّف الشبكات العصبية الاصطناعية دقة فائقة (99.6%) وتصنيفاً أسرع للأعطال مقارنةً بمُصنّف FL (99.2%) في الظروف اللحظية. تُسلط نتائج هذا البحث الضوء على النهج القائم على الشبكات العصبية الاصطناعية (ANN) كحلٍ فعالٍ لتشخيص أعطال الخلايا الكهروضوئية، حيث يُوفّر دقةً مُحسّنةً ومعالجةً أسرع. تُؤكّد هذه النتائج على إمكانية دمج تقنيات الشبكات العصبية الاصطناعية في أنظمة المراقبة اللحظية لتحسين أداء وموثوقية وسلامة منشآت الطاقة الكهروضوئية.

الكلمات المفتاحية:

الأنظمة الكهروضوئية، اكتشاف الأخطاء، الشبكات العصبية الاصطناعية، المنطق الضبابي، تحسين استراتيجية الحرب، Matlab/Simulink، المراقبة في الوقت الحقيقي.

TABLE OF CONTENTS**General Introduction****Chapter 1: State of the Art in PV System Fault Diagnosis: Types, Detection Methods, and Analysis**

1.1.Introduction.....	6
1.2. Description of a photovoltaic system.....	6
I.2.1. Photovoltaic Conversion	7
1.2.2. Current–voltage and power–voltage characteristics.....	7
I.2.3. Structure of a photovoltaic module	9
1.2.4. Protection System	10
1.2.4.1. Bypass Diode	10
1.2.4.2. Blocking Diode	12
1.3. Losses, defects, and possible faults in PV systems	12
I.3.1. Fault classification	12
I.3.2. PV array faults	13
I.3.2.1. Cell-level faults	13
I.3.2.2. Module-level faults	14
I.3.2.3. Array-level faults	16
1.4. Fault detection and diagnosis in PV systems	19
A. Monitoring	20
B. Diagnosis	20
1.4.1. Faults Detection Techniques	21
1. Visual Inspection	21

2. Infrared (IR) and Electroluminescence (EL) Imaging Inspections	22
3. I-V Curve Analysis	23
4. Signal Processing Techniques	24
5. Analytical Monitoring	24
5.1 Real-Time Difference Measurement (RDM)	24
5.2. Statistical Approaches (SA)	25
5.3. Machine Learning Techniques (MLT)	25
1.6. Conclusion.....	27
 Chapter 2 : Diagnosis based on Fuzzy Logic: Simulation and real-time experimentation	
2.1. Introduction.....	29
2.2. Part 1: Modeling and simulation	29
2.2.1. Photovoltaic module modeling	29
2.2.1.1. PV module characteristics	29
2.2.1.2. PV Module Parameters Identification.....	30
2.2.2. PV Module Faults	36
2.2.3. Fault Diagnosis PV System	37
2.2.3.1. Thresholding method (Algorithm 1)	38
2.2.3.2 Fuzzy Logic Method (Algorithm 2)	40
2.2.4. Results and Discussion	43
2.3. Part 2: Experimental Validation	44
2.3.1. Experimental components Description	44
2.3.2. Real-time Implementation: Results and Discussion	47
2.4. Conclusion.....	49

Chapitre 3 : Diagnosis based on Artificial Neural Network: Simulation and real-time experimentation

3.1 Introduction.....	51
3.2. Description of Monitoring and Diagnosis PV System.....	51
3.2.1. Monitoring Unit	53
3.2.2. Photovoltaic System Modeling	53
3.3. PV Faults	56
3.4. Implementation of the Artificial Neural Network Classifier	57
3.5. Simulation results	58
3.6. Experimental Validation.....	60
3.7 Conclusion.....	65

Chapter 4 : Comparative Study of Real-Time Photovoltaic Fault Diagnosis: Fuzzy Logic and Neural Network Approaches

4.1 Introduction.....	67
4.2 Explanation of the Photovoltaic System and the Strategy for Detecting and Diagnosing Faults.....	67
4.2.1 PV system description.....	67
4.2.2. The Implemented Diagnosis Technique	69
4.2.2.1. PV Module Faults.....	69
4.2.2.2 Photovoltaic System Fault Detection.....	71
4.3 Results Analysis	76
4.3.1. Simulation results for Simulink Model	76
4.3.1.1.Evaluation of the Proposed Method's Effectiveness.....	77

4.4. Experimental validation.....	79
4.4.1. Investigated Faults	81
4.4.2. Experimental data Test off-line implementation	82
4.5. Real-time Experimental Application Results and Discussion	83
4.6. Comparative Study with Other ANN Solutions	89
4.7 Conclusion.....	89
General conclusion	
Bibliography	
Scientific Productions	

LIST OF FIGURES

Chapter 1

Figure I.1: Photovoltaics: Cells to Modules to Arrays.....	6
Figure I.2: Structure of a of a silicon photovoltaic cell.....	7
Figure I.3: Solar cell equivalent circuit.....	8
Figure I.4: Current voltage (IV) curve of a solar cell.....	9
Figure I.5: Structure of a photovoltaic module.....	10
Figure I.6: modules with non- overlapped and overlapped bypass diodes.....	10
Figure I.7: Protection of a PV generator by bypass diode and blocking diode.....	11
Figure I.8: PV module under shading of a cell.....	11
Figure I.9: Classification of PV faults.	12
Figure 1.10: Representative degradation modes of silicon PV modules for the last 10 years.....	19
Figure I.10: Block diagram of PV monitoring system.....	20
Figure I.11: Block diagram of PV fault diagnosis scheme.....	20
Figure I.12: Faults Detection and Identification techniques.	21
Figure I.13: Imaging inspection process utilizing an IR camera.....	22
Figure I.14: Illustrates the Smart I-V Curve diagnosis method developed by Huawei....	23
Figure I.15: Presents a fault detection diagram that analyzes the output signal to identify anomalies and classify faults in the PV system	24

Chapter 2

Figure 2.1: Schematic of PV panel.....	30
Figure 2.2: Schematic of the experimental proposed technique.....	31

Figure 2.3: Attack strategy in WSO.....	32
Figure 2.4: The convergence rate of the WSO algorithm during the parameter extraction process for PV module.....	34
Figure 2.5: I-V Performance of a photovoltaic module under STC.....	35
Figure 2.6: P-V Performance of a photovoltaic module under STC.....	35
Figure 2.7: Concept of objective function calculation with WSO.....	35
Figure 2.8: Convergence rate of WSO algorithm during the extraction process of ISO FOTON106/12 PV module.	36
Figure 2.9: Schematic diagram of PV panel with various faults.....	37
Figure 2.10: Diagnosis PV system.....	38
Figure 2.11: Output of fault 5 which is displayed in the command window.....	38
Figure 2.12: Diagnosis Model based on Threshold method.....	39
Figure 2.13: I-V Curves of different type of faults.	40
Figure 2.14: Diagnosis Model after integration of the fuzzy logic.	40
Figure.2.15: Fuzzy Classifier structure and input variables.....	41
Figure.2.16: Flowchart of the diagnosis algorithm.....	42
Figure.2.17: Diagnosis PV system results for F1 fault.....	43
Figure.2.18: Diagnosis PV system results for F2 fault.....	44
Figure. 2.19: Schematic of the experimental proposed technique.	45
Figure 2.20: The investigated faults: (a) Shading 1 cell 50%, (b) Shading horizontal line of cells at 100%, (c) Shading vertical line of cells at 100%, (d) one diode by-pass short circuited.	46
Figure 2.21: Experimental SET-UP.....	47
Figure. 2.22: The user-interface ControlDesk.	48

Chapter 3

Figure 3.1: Schematic Representation of the Electrical Configuration for the Experimental PV System.	52
--	-----------

Figure 3.2: Diagram Depicting the Proposed Monitoring and Diagnosis system.....	53
Figure 3.3: PV module BP diode connections.....	54
Figure 3.4: I-V curve of a photovoltaic module under STC.....	55
Figure 3.5: P-V curve of a photovoltaic module under STC.	55
Figure 3.6: Illustrates the convergence rate of the WSO algorithm during the parameter extraction process for PV module	55
Figure. 3.7: The Investigated faults.....	56
Figure. 3.8: Schematic representation of a photovoltaic panel exhibiting the five faults.	56
Figure 3.9: ANN configuration.....	57
Figure 3.10: Schematic of the used ANN architecture.....	58
Figure 3.11: (a). Progression of Mean Squared Error (MSE) for the MLP Network. (b). Confusion Matrix for Classification in the MLP Network.	59
Figure 3.12: Detection and classification of Fault 2.....	59
Figure 3.13: The investigated faults.....	61
Figure 3.14: The ControlDesk User Interface Presents Real-Time Measurement Data in the Monitored PV Panel (Normal operation)	62
Figure 3.15: The ControlDesk User Interface Presents Real-Time Measurement Data in the Monitored PV Panel (Fault 1).....	62
Figure 3.16: The ControlDesk User Interface Presents Real-Time Measurement Data in the Monitored PV Panel (Fault 2).	63
Figure 3.17: The ControlDesk User Interface Presents Real-Time Measurement Data in the Monitored PV Panel (Fault 3).	63
Figure 3.18: The ControlDesk User Interface Presents Real-Time Measurement Data in the Monitored PV Panel (Fault 4).	64
Figure 3.19: The ControlDesk User Interface Presents Real-Time Measurement Data in the Monitored PV Panel (Fault 5).	64

Chapter 4

Figure 4.1: Schematic representation of the electrical configuration for the experimental PV system.	68
Figure. 4.2: Schematic representation of the six faults.	69
Figure 4.3: I-V Performance for various types of faults.....	70
Figure 4.4: The proposed fault diagnosis technique.....	72
Figure 4.5: Photovoltaic System Fault Detection.....	72
Figure 4.6: Result of the first fault, presented within the command window.....	73
Figure 4.7: Structure of the fuzzy classifier and its input parameters.	75
Figure 4.8: ANN configuration.	76
Figure 4.9: Schematic of the used ANN architecture.....	76
Figure 4.10: (a). Progression of Mean Squared Error (MSE) for the MLP Network. (b). Confusion Matrix for Classification in the MLP Network.....	78
Figure 4.11: Detection of bypass diode CC fault.	79
Figure 4.12: The experimental test bench setup.	80
Figure 4.13: Diagram Depicting the Proposed Technique for Fault Diagnosis.....	80
Figure 4.14: (a). PV module characteristics: case of soiling, shadow effect, shadow effect and bypass diode fault. (b). PV module characteristics: case of bypass diode faults.	81
Figure 4.15: The investigated faults.....	82
Figure 4.16: (a). Progression of Mean Squared Error (MSE) for the MLP Network. (b). Confusion Matrix for Classification in the MLP Network	83
Figure 4.17: The ControlDesk User Interface Presents Real-Time Measurement Data and Detects Fault 1 in the Monitored PV Panel	85
Figure 4.18: The ControlDesk User Interface Presents Real-Time Measurement Data and Detects Fault 2 in the Monitored PV Panel.....	85
Figure 4.19: The ControlDesk User Interface Presents Real-Time Measurement Data and Detects Fault 3 in the Monitored PV Panel	86
Figure 4.20: The ControlDesk User Interface Presents Real-Time Measurement Data and Detects Fault 4 in the Monitored PV Panel	86
Figure 4.21: The ControlDesk User Interface Presents Real-Time Measurement Data and Detects Fault 5 in the Monitored PV Panel.	87
Figure 4.22: The ControlDesk User Interface Presents Real-Time Measurement Data and Detects Fault 6 in the Monitored PV Panel.	87

LIST OF TABLES

Table GI.1: Performance comparison of the most recent fault detection methodologies	3
Table 1.1: Cell-level faults.....	13
Table 1.2: Module-level faults.. ..	14
Table 1.3: Array-level faults.....	17
Table 1.4: Impact of different defects on cell parameters.....	18
Table 2.1: Electrical characteristics of the SUNTECH PV module.	30
Table 2.2: The final identified parameters of the SUNTECH PV module.....	34
Table 2.3: The comparative study of the three optimization algorithms.	36
Table 2.4: Different type of faults chosen for the diagnosis.	37
Table 2.5: The signature of faults after using the threshold method.....	39
Table 2.6: Fuzzy Rule base and Defuzzification for Fuzzy Classifier (Case 1).....	42
Table 2.7: Fuzzy Rule base and Defuzzification for Fuzzy Classifier (Case 2).....	42
Table 2.8: The signatures of each of the symptom for each fault after integration of the fuzzy logic.	44
Table 3.1: Electric Properties of the SUNTECH Photovoltaic Module.....	54
Table 4.1: Various categories of faults selected for the diagnosis.	69
Table 4.2: The distinctive signature of faults following the application of the threshold technique.	73
Table 4.3: Fuzzy rule set and the process of defuzzification employed in the fuzzy classifier (Case 1).	74
Table 4.4: Fuzzy rule set and the process of defuzzification employed in the fuzzy classifier (Case 1).	74
Table 4.5: The Symptom Signatures for Individual Faults after Fuzzy Logic Integration.....	77
Table 4.7: The output DA and the execution time with FL and with ANN system.....	88
Table 4.8: ANN techniques for PV diagnosis and faults identification.	89

LIST OF ABBREVIATIONS AND SYMBOLS

Abbreviations

AI	Artificial intelligence
ABC	Artificial bee colony
ANN	Artificial neural network
ANMSSA	Adaptive nonlinear mutual sparrow search algorithm
BFM	Blending fitting model
CNN	Convolutional neural network
DL	Deep learning
DNN	Deep neural network
DT	Decision tree
DWT	Discrete wavelet transform
IoT	Internet of Things
MIFNet	Multi-source information fusion network
OVMD	Optimized variational mode decomposition
PSO	Particle Swarm Optimization
SAE-CA	Stacked auto-encoder and clustering algorithm
SVM	Support Vector Machines
RFCs	Random Forest Classifiers
WSO	War Strategy Optimization
UHWSPR	Hourly weather status pattern recognition
XGBoost	Extreme Gradient Boosting

Symbols

AC	Alternating Current
DC	Direct Current
FCM	Fuzzy C-Means

FDD	Fault Detection and Diagnosis
GC	Grid Connected
MLP	Multi-Layer Perceptron
MPP	Maximum Power-Point
PNN	Probabilistic Neural Network
PS	Partial Shading
PSC	Partial shading conditions
PV	Photovoltaic
SC	Short Circuit
SDM	Single Diode Model
BP	By-pass diode
STC	Standard Test Condition
I	PV current
I_d	Diode current
I_0	Diode saturation current
I_{sh}	current (short circuit of solar cell)
V_{oc}	Open Circuit Voltage
I–V	Current–voltage
P–V	Power–voltage
T	Temperature
I_r	Irradiance
K	Boltzmann’s constant
V_{mp}	Maximum DC voltage of module
I_{mp}	Maximum DC current of module
MPPT	Maximum power point tracking
R_s	Series intrinsic resistance
R_{sh}	Shunt resistance
V_t	Thermal potential
I_{pv}	PV current
V_{pv}	PV voltage
PR	Power Ratio
IR	Current Ratio
OCR	Open Circuit Ratio

Introduction

Introduction

Photovoltaic (PV) systems play a crucial role in the conversion of solar energy into electrical power. Nevertheless, the performance and reliability of PV systems are encountering various real-time operational challenges. Researchers have identified these issues and proposed numerous solutions. Factors like solar irradiance and module temperature [1], shading [2], module degradation [3], soiling, and by-pass diode faults [4,5], impact the performance and energy output of PV modules potentially accelerating their degradation. Accurate energy yield forecasting under these varying conditions is crucial, making it important to consider these factors during the design and operation of PV systems. Additionally, without proper supervision, users find it difficult to identify the exact type of faults in the system. Although increasing data for better monitoring can complicate the system, accurate fault detection and diagnosis are essential for maintaining and ensuring the reliability of photovoltaic arrays. Selecting the right indicators for monitoring enhances fault diagnosis techniques and simplifies the system. Thus, power engineers need assistance in interpreting data and focusing on the most useful information. To keep costs down, only the essential electrical features of the PV system should be monitored and analyzed. Hence, the accurate diagnosis of these PV system faults is imperative to ensure proper functionality and to avert significant economic repercussions.

With the rapid development of the PV industry and the increase in the installed capacity, efficient operation and maintenance strategies are increasingly required [6]. In fact, manufacturing, transportation, installation, and operating conditions can cause PV cell or module failures [7], [8]. In the case of a PV array or power plant, which is composed of several electrically connected modules, any fault in one cell or module affects the performance of the whole array or system. The PV faults could cause a severe safety hazard, e.g., fire risk, electrical shock, physical danger [9], or power loss [10]. Therefore, to assure the reliability, availability and safety of the PV installations, their health status should be monitored regularly to prevent from failures and contribute to an efficient condition-based maintenance policy. To this end, efficient PV fault detection and diagnosis (FDD) strategies are required. Recently, several methods have been suggested for detecting PV problems, such as the utilization of fuzzy logic (FL) [11-14] and artificial neural network (ANN) techniques [15-17]. Both techniques have shown significant potential in the field of fault diagnostics for PV systems.

Problem statement

Despite the development of various defect diagnosis techniques, many existing methods demonstrate limitations in accurately identifying compound faults, often simplifying them as single faults. Additionally, while several deep learning approaches have been introduced, there remains a lack of comprehensive comparative analysis with the latest methodologies. Most current models also fall short in handling multi-label fault scenarios effectively. Therefore, there is a need for a diagnostic approach capable of accurately identifying both single and compound faults in offline and online real-time applications. This study addresses this gap by proposing advanced diagnostic models and evaluating their performance against state-of-the-art multi-label learning algorithms (SAE-CA, PSO-SVM-OVMD, UHWSR-BFM, Random Forest, BA-XGBoost, ANMSSA-MIFNet, and a weighted ensemble learning model) based on monitored parameters, fault detection capabilities, and diagnostic accuracy.

Table GI.1. Performance comparison of the most recent fault detection methodologies.

Ref./Year	Monitored Parameters	Considered faults Detection & identification	Method	Accuracy (%)
[18]/ 2021	Current, voltage and power	Short-circuit, degradation, partial-shading, partial-shading with the by-pass diode open-circuit defect, partial-shading with the by-pass diode short-circuit, short-circuit with the degradation defect	SAE-CA	98.3%
[19]/ 2022	Current	DC Arc fault	PSO-SVM-OVMD	98.21%
[20]/ 2022	Power	Line to line, line to ground	UHWSR- BFM	99.29%
[21]/ 2023	Current, voltage and power	Line-to-line defects Open-circuit failures Partial shading	Random forest	99.17%
[22]/ 2024	Current, voltage and power	Short-circuited modules, disconnected strings	BA-XGBoost	87.56%
[23] / 2024	Current, voltage and power	Shading, short circuits, open circuits, and degradation of solar cells	ANMSSA-MIFNet	99.64%
[24] / 2024	T, Ir, Imp, Vmp, and, Maximum Power Point (MPP)	Line-to-line defects Open-circuit failures Partial shading	Random Forest Classifiers	99.4%
[25] / 2024	Short circuit current, open-circuit voltage, Maximum Power Point (MPP), half short-circuit current, and half open-circuit voltage	line-ground (LG), line-line (LL), open-circuit (OC), string degradation, and array degradation faults	Weighted ensemble learning model	98.37%

Thesis outline

The aim of this thesis is to evaluate the efficacy of two artificial intelligence techniques: fuzzy logic (FL) and artificial neural networks (ANN) in diagnosing defects in photovoltaic (PV) systems. The created model seeks to identify and categories single and multiple fault types that may arise in photovoltaic panels for real-time applications, including partial shading, soiling, open circuit, short circuit of one bypass diode, short circuit of two bypass diodes, bypass diode shunting, and bypass diode disconnection. The detection methods depend on the analysis of

three input ratios: Power Ratio (PR), Current Ratio (IR), and Open Circuit Ratio (OCR). These ratios are derived from measurements and simulations performed under both standard and defective settings. The comparison is conducted via simulation and experimentation utilizing Matlab/Simulink® software. The model is tested with dSPACE DS1104 controller to facilitate real-time testing of its efficacy in diagnosing photovoltaic module, in terms of accuracy, speed and feasibility in real conditions. The thesis comprises of four chapters, the last three chapters representing original works that have been previously published.

Chapter One provides a general overview of photovoltaic (PV) systems, including an examination of various types of faults that can occur. Additionally, a comprehensive literature review will be presented, focusing on existing fault detection and diagnosis techniques.

Chapter Two is devoted entirely to PV array modeling. It begins with an introduction to the One-Diode Model (ODM) of PV modules. Subsequently, five electrical parameters of this model will be identified using the war strategy optimization algorithm (WSO) [26, 27]. Following by the implementation of fuzzy logic for fault diagnosis. The fuzzy logic models were developed and simulated using MATLAB/Simulink before being experimentally implemented on dSPACE DS1104 platform. The results demonstrated the effectiveness of fuzzy logic in identifying and diagnosing various faults, such as partial shading, shorted bypass diodes, and other common faults.

Chapter Three focuses on the application of ANNs to PV system fault diagnosis. An ANN model is trained using experimental databases and simulated using MATLAB/Simulink. This model is then implemented on dSPACE DS1104 platform to evaluate its real-time performance. The results demonstrate remarkable accuracy in term of detection and diagnosis single and multi-type faults.

Chapter Four compares the two approaches (FL and ANN) in terms of accuracy, speed, and real-time adaptability. Experimental results reveal that ANNs slightly outperform fuzzy logic, particularly in terms of execution speed, making them a more practical solution for industrial applications.

The work concludes with a conclusion that summarizes the main contributions of the thesis, highlighting the value of the studied approaches for real-time monitoring of photovoltaic systems, as well as the anticipated future prospects.

Chapter 1

State of the Art in PV System Fault Diagnosis: Types, Detection Methods, and Analysis

1.1. Introduction

A photovoltaic (PV) array fault refers to a defect that either reduces output power or poses a safety hazard. However, variations in appearance due to manufacturing that do not impact safety or performance are not classified as faults. Outdoor PV arrays are exposed to various internal and external factors, making them susceptible to a wide range of faults that can affect nearly all components. These faults can result in different degrees of degradation, power loss, or even fire hazards. Therefore, a thorough understanding of common PV array faults is crucial before developing effective detection and diagnosis strategies. This chapter aims to provide a comprehensive state of the art on common PV array faults and diagnosis methods. Section I.2 introduces the structure of PV panel and protection system, while in Section I.3, we present the faults in detail and their impact in terms of power loss and safety. In Section I.4, we analyze the fault detection techniques, and Section I.5 closes the chapter.

1.2. Description of a photovoltaic system

Solar cells are typically arranged in an assembly of one or more units and then encapsulated under glass to form a photovoltaic (PV) module. A PV generator consists of multiple interconnected modules, creating a unit capable of generating high continuous power suitable for standard electrical equipment (Figure 1.1). To enhance the output voltage and current, PV modules are usually connected in a series-parallel configuration. These interconnected modules are mounted on metal structures and tilted at an optimal angle based on the installation location, collectively referred to as a PV array [28].

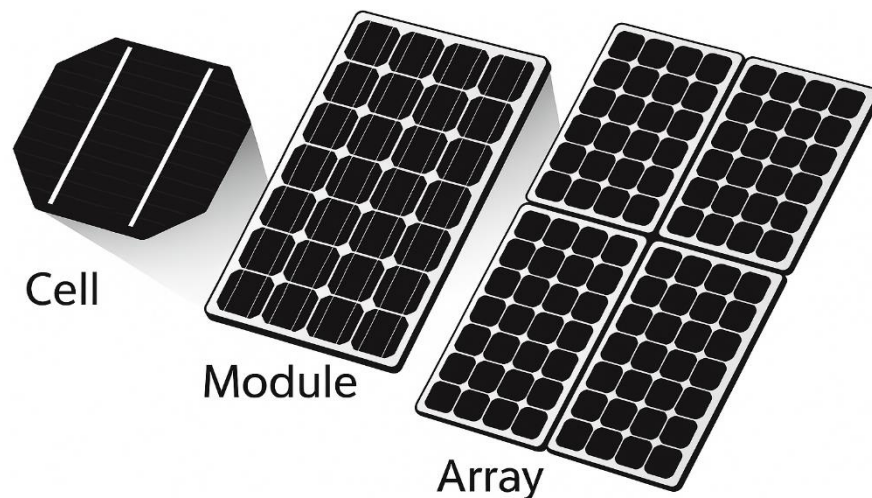


Figure 1.1. Photovoltaics: Cells to Modules to Arrays.

1.2.1. Photovoltaic Conversion

A photovoltaic cell is a device that converts sunlight into electricity. It works by using the properties of semiconductor materials to absorb light and create an electric current. The materials used to make photovoltaic cells are chosen based on how easily they can release electrons when exposed to light. When these electrons are released, they flow through the cell and create an electrical current. This phenomenon is called the photovoltaic effect. Figure 1.2 shows the structure of a silicon photovoltaic cell.

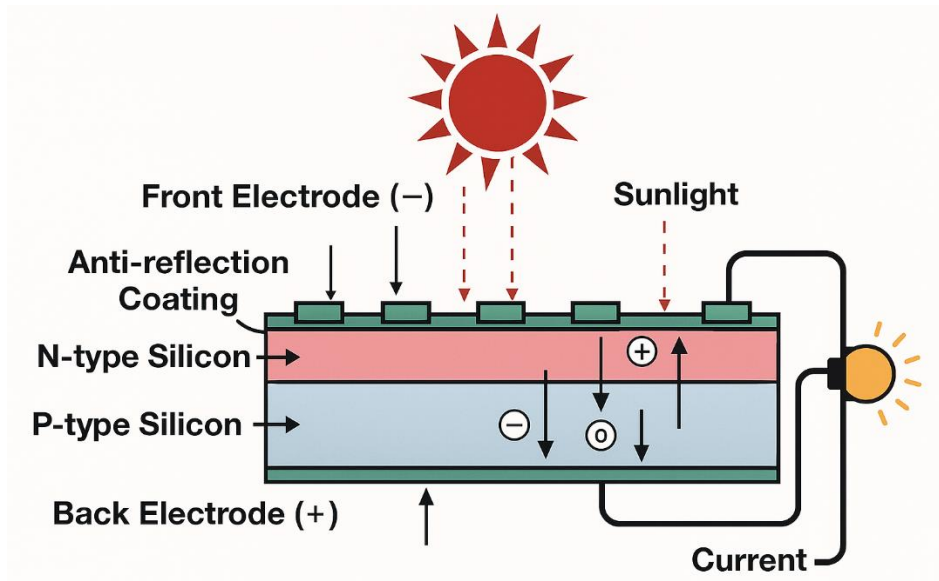


Figure 1.2: Structure of a of a silicon photovoltaic cell.

1.2.2 Current–voltage and power–voltage characteristics

Most commonly available solar cells have a diode structure, consisting of a junction between p-type and n-type semiconductor materials. In some designs, an insulating layer is added to form a p-n junction, or multiple junctions are created. However, in terms of electrical behavior, the overall characteristics remain similar. The relationship between current (I) and voltage (V) is ideally described by Eq. (1.1), which represents the standard diode equation. This equation incorporates the light-generated current I_{ph} and a diode factor (n), which accounts for the recombination mechanisms within the cell, as shown in Figure 1.3.

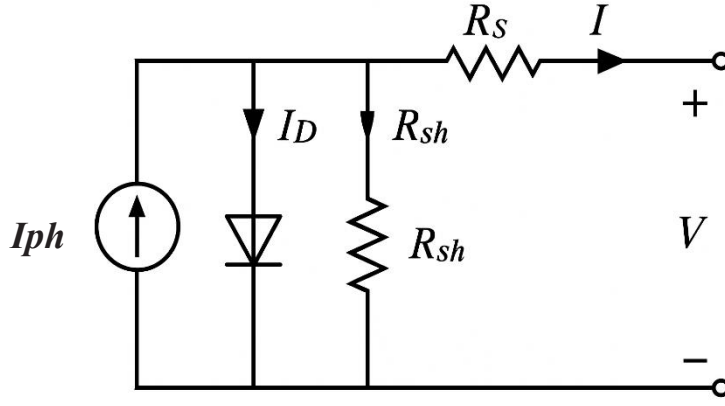


Figure.1.3. Solar cell equivalent circuit.

$$I = I_{ph} - I_0 \left[\exp \left(\frac{V + R_s I}{V_t n} \right) - 1 \right] - \frac{V + R_s I}{R_{sh}} \quad (1.1)$$

Where V_t is defined by:

$$V_t = \frac{N_s K T}{q} \quad (1.2)$$

Whereas

V = Voltage of the cell [V].

q = Electron charge.

k = Boltzmann constant.

T = absolute temperature [$^{\circ}\text{K}$].

I_{sc} = Saturation current of the diode [A].

R_s = Series resistance.

R_{sh} = Shunt resistance.

n = Ideality Factor.

The I-V curve represents the fundamental relationship between the output current and voltage of a solar cell, providing crucial insights into its performance and operational behavior under different conditions, as shown in Figure 1.4. Excluding the known parameters, there are five unknown parameters I_{ph} , I_0 , R_{sh} , R_s , n that are needed to be estimated.

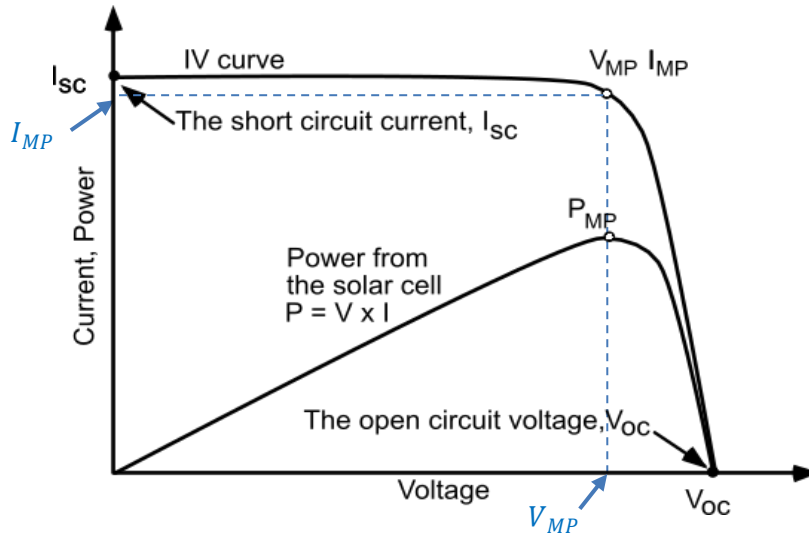


Figure I.4: Current voltage (IV) curve of a solar cell.

1.2.3 Structure of a photovoltaic module

The photovoltaic module is a collection of assembled cells designed to generate usable electrical power when exposed to light. This series assembly must be protected to make the panel suitable for outdoor use. The cells are indeed fragile and susceptible to corrosion, requiring mechanical protection and shelter from harsh weather conditions such as humidity and temperature variations [28]. A "standard" module typically contains 36 or 72 cells, though modules with 40, 54, or 60 cells are also available on the market. Figure I-5 illustrates the structure of a photovoltaic module, showing its front and back sides with 36 cells [29]. Depending on the manufacturer and the number of cells, each module may include from 2 to 5 bypass diodes [30]. The cells are connected in series to form a PV array (figure 1.5). Each array is connected in parallel with bypass diodes in an anti-parallel configuration to protect them from reverse operation (for example, during shading).

The ideal approach is to connect a bypass diode for each cell [31], but this technique is not commonly used due to its complexity and high cost. Two different configurations are possible for the installation of bypass diodes, as shown in Figures 1.6 [32]. Typically, there are 18 cells per bypass diode; however, this number can vary among different manufacturers of the modules. In the case of PV modules with overlapped diodes (see (b) in Figure 1.6), these proposals are not widely applied due to manufacturing difficulties. In contrast, in PV modules with non-overlapped diodes (see (a) in Figure 1.6), energy losses are caused solely by the consumption of the bypass diodes.

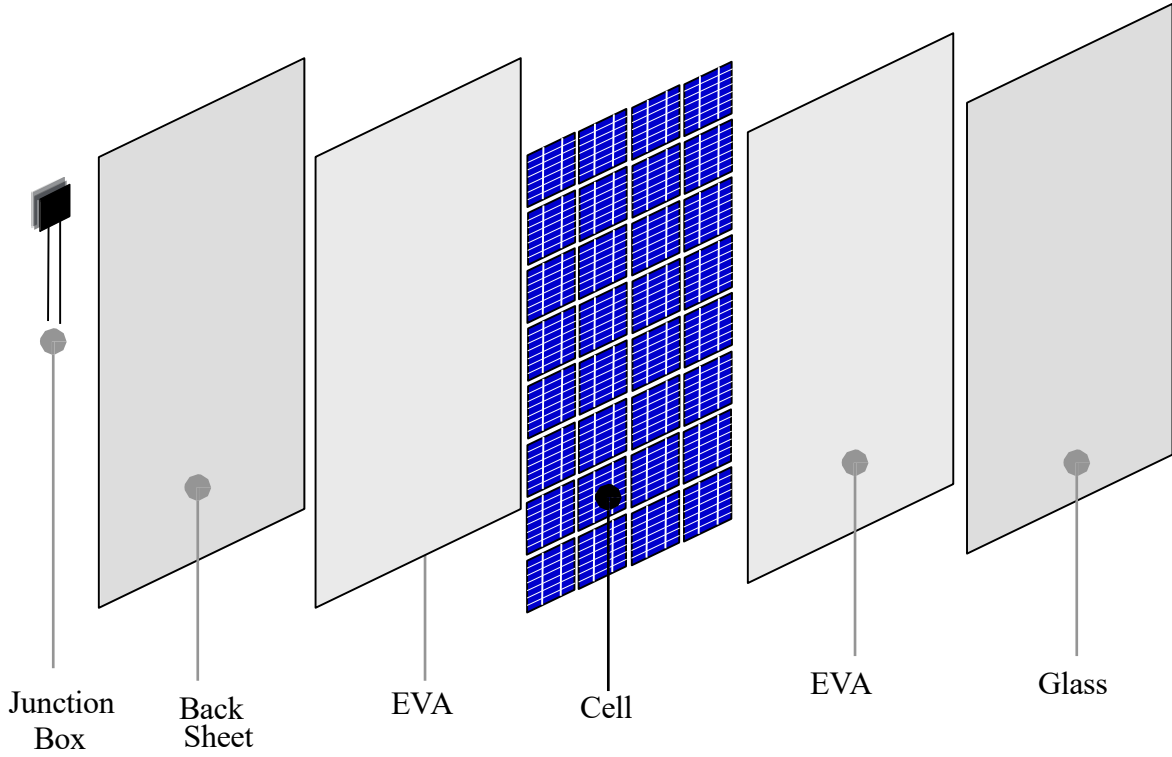


Figure 1.5: Structure of a photovoltaic module.

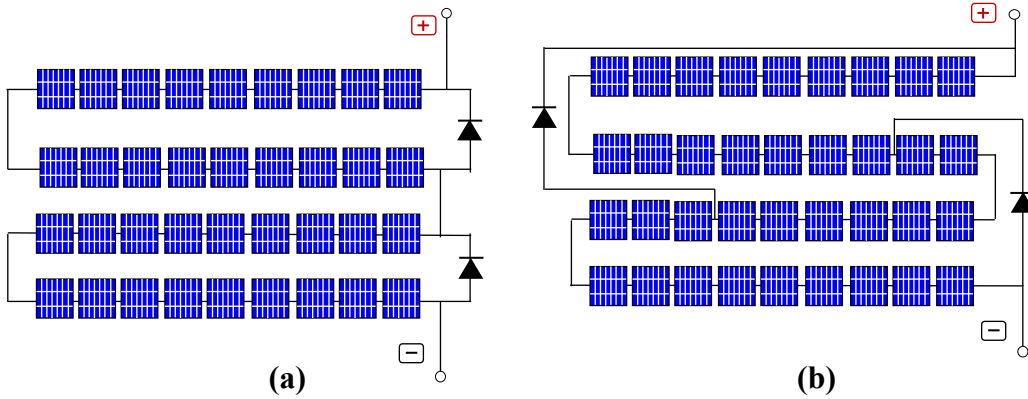


Figure 1.6: PV modules with non- overlapped and overlapped bypass diodes.

1.2.4 Protection System

Several types of protection can be used in a photovoltaic installation, similar to other electrical installations: protection for operators, protection against lightning, and protection for the PV generator. Since we will be discussing faults or anomalies that lead to decreased production, we will focus solely on the components that protect the PV generator.

1.2.4.1 Bypass Diode

As mentioned earlier, the bypass diode is connected in parallel with a group of cells to protect the weaker cells from reverse bias (see Figure 1.7). Under the influence of factors such as shading or temperature variations, the electrical characteristics of series-connected photovoltaic

cells may differ and their electrical properties can change due to shading or temperature differences. Cells that receive more sunlight generate more current than shaded ones, creating an imbalance. This can lead to overheating, which may deform or even break the glass panel of the solar module. To prevent excessive heating, bypass diodes are used. When a submodule is shaded, its bypass diode activates, allowing excess current to flow through it instead of the shaded cell. This helps reduce overheating in the affected area as shown in Figure 1.8 [33].

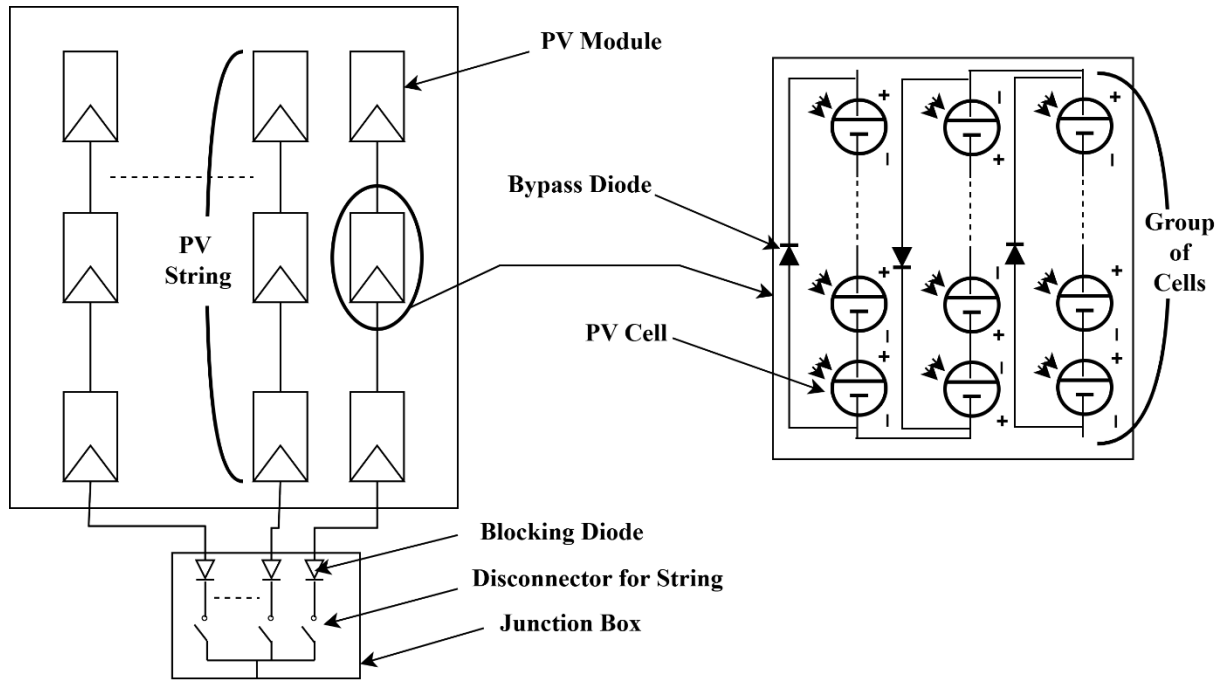


Figure 1.7: Protection of a PV generator by bypass diode and blocking diode.

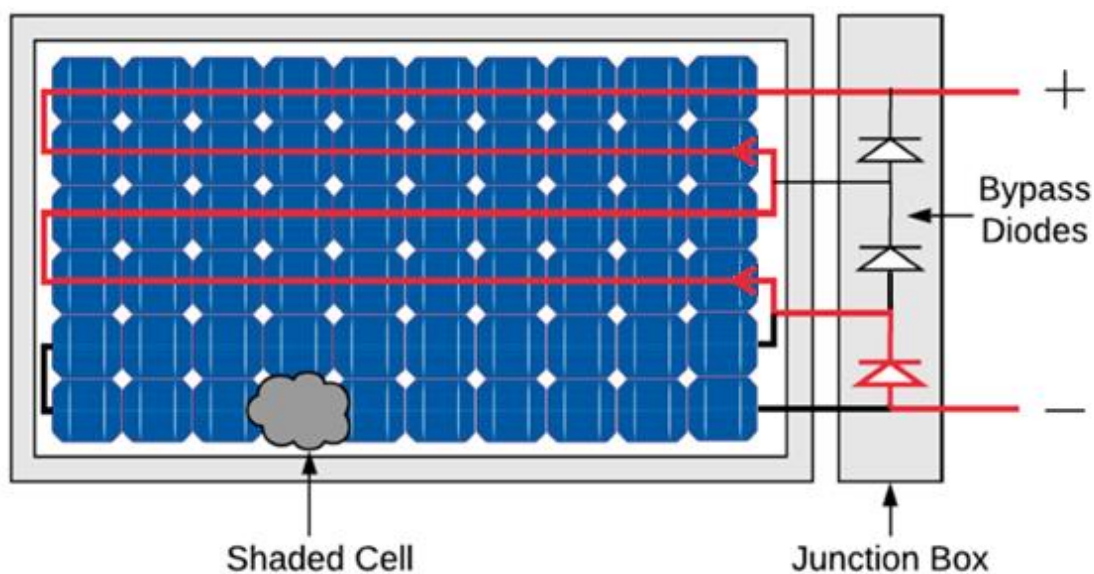


Figure 1.8: PV module under shading of a cell.

1.2.4.2 Blocking Diode

The voltage produced by each string may be different. When these strings are connected in parallel to form a field, the string with the lowest voltage can absorb reverse current from the other strings. This leads to reduced production, and the modules in the string experiencing reverse current could also be at risk of failure. To prevent these reverse currents, a blocking diode is placed at the end of each string, as shown in Figure 1.7 [34].

1.3 Losses, defects, and possible faults in PV systems

1.3.1. Fault classification

Photovoltaic arrays and cells are highly sensitive instruments that must be installed in unobstructed surroundings to optimize solar radiation exposure. Nevertheless, existing in such environments exposes them to considerable environmental and physical stress all the time. This stress can result in physical damage, including corrosion, cracks, and delamination, so diminishing their effectiveness. Photovoltaic cells depend on sun radiation to generate electrical current; in its absence, they are incapable of producing any current. Partial shading of the array can result in significant variations in the IV properties, resulting in elevated temperatures and perhaps catastrophic damage to the cells. Alongside environmental and physical causes, electrical problems frequently occur in photovoltaic systems [35-37]. Figure 1.9 presents the classification of PV faults.

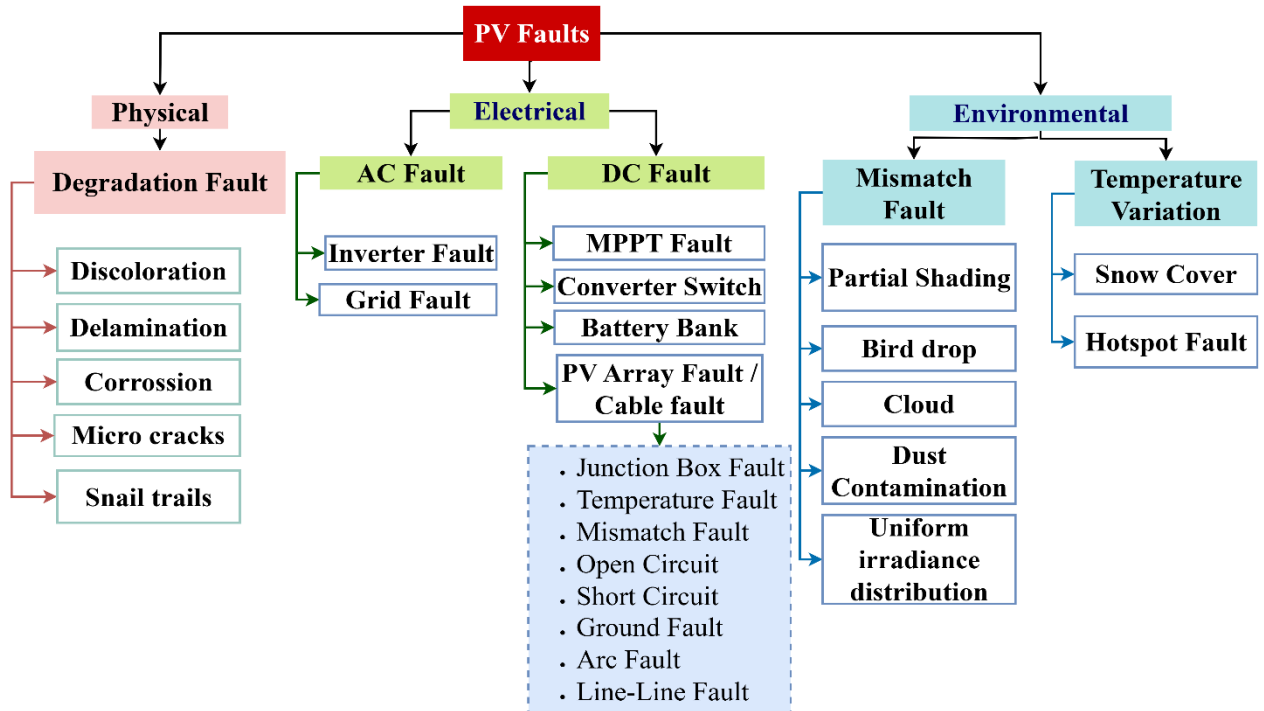


Figure 1.9: Classification of PV faults.

I.3.2. PV array faults

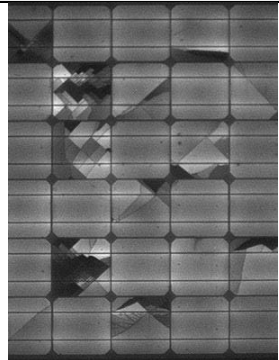

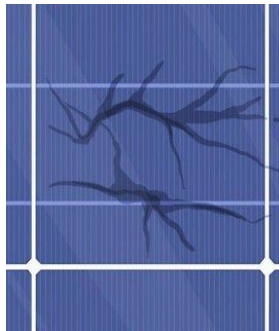
The following sections provide a detailed explanation of typical PV faults associated with the three levels.

I.3.2.1. Cell-level faults

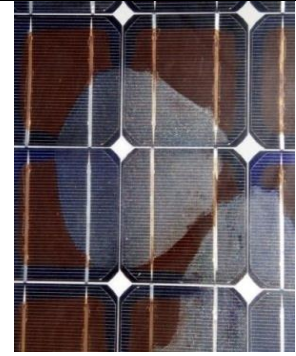
Cell-level faults are PV faults that impact an individual PV cell. While they may gradually extend to neighboring areas, they typically do not affect the entire surface of the PV module.

Table 1.1 provides an overview of these faults along with corresponding images.

Table 1.1: Cell-level faults.

Fault	Description	Example
Cell crack	Cell cracks are fractures in the silicon substrate of photovoltaic cells caused by mechanical stress, often invisible to the naked eye. They can occur during manufacturing, transportation, installation, or operation. The cracks vary in shape, length, and orientation within a single solar cell. The resulting power loss depends on the extent of the ‘inactive’ area affected by the crack.	 [38]
Discoloration	Discoloration is generally related to the PV modules using EVA (Ethylene Vinyl Acetate) as the encapsulant material. Discoloration refers to the yellowing or browning of PV cells. It causes a change in the transmission of solar irradiance reaching the cell surface and consequently a reduction in production. Nowadays, this fault is greatly eased for the PV modules with new encapsulant material. For example, for thermoplastic polyolefin, the discoloration rate is reported around 9 times lower [39].	
Snail track	Snail tracks appear as grey or black discoloration on the silver paste of the front metallization in screen-printed solar cells. This discoloration typically develops between three months and one year after the PV module is installed. Studies in [40,41] indicate that humidity plays a role in the formation of snail trails. However, there is no evidence that this phenomenon reduces the efficiency of the PV module or affects its output power.	 [42]

Delamination Delamination is the adhesion loss between the glass, encapsulant, active layer and back layer. For thin-film PV type, the Transparent conductive oxide (TCO) may as well delaminate from the adjacent glass layer. Bubble is also a form of delamination. Delamination will lead to optical reflection and therefore cause the decrease in power output. It also causes moisture penetration, which then leads to various chemical and physical degradation.







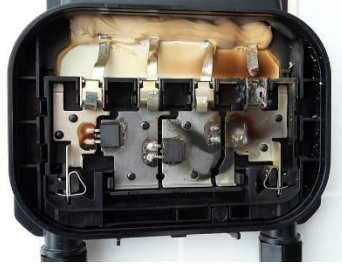

[43]

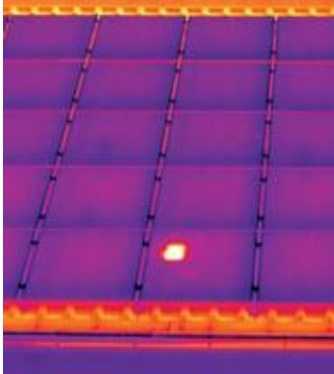
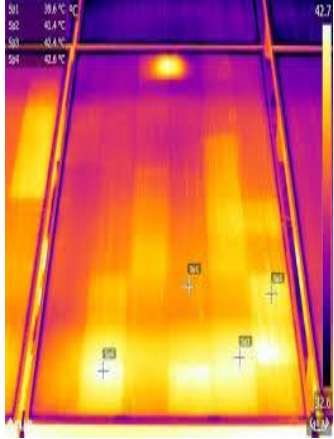
I.3.2.2. Module-level faults

At the module level, common PV faults can be classified into three main categories: shading, structural, and electrical faults. Additionally, hot spots resulting from a combination of diode faults, partial shading, or mismatches are also considered module-level faults. A detailed overview of these faults is provided in Table 1.2.

Table 1.2: Module-level faults.

Fault	Description	Example
Shading/soiling	Shading and partial shading (PS) are typically caused by obstructions such as buildings, trees, or moving clouds. Soiling, on the other hand, occurs when the PV module's surface is covered by snow, dirt, dust, or other particles. Both shading and soiling can be categorized as either hard or soft, as well as permanent or temporary and leads to a current reduction in the shaded cells, leading to varying degrees of power loss.	
		[44]
Frame breakage	The primary cause of frame breakage is the accumulation of heavy snow, which gradually moves downward and enters the gap between the frame and the glass. This process deforms the module and can cause the frame to detach from the PV glass, ultimately leading to power loss.	
		[45]

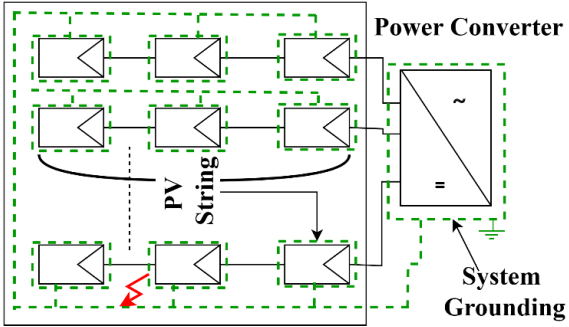
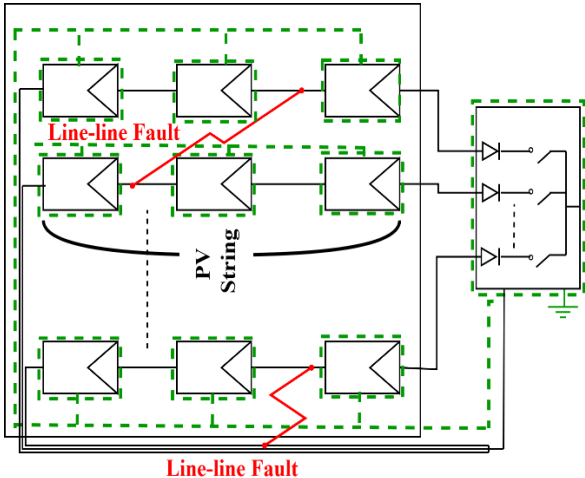
Back sheet Adhesion loss	<p>The causes of back-sheet adhesion loss in PV modules vary based on the material type but are generally similar to those of delamination, including factors such as temperature, moisture, and mechanical stress. This issue leads to insulation failure, increasing the risk of exposure to active electrical components, particularly when it occurs near a junction box or the module's edge.</p>	
Junction Box fault	<p>Junction box faults commonly include poor fixation, faulty wiring, and broken connections. These issues are primarily caused by energy overstress, cable rework during installation, connector rework, and prolonged heat exposure. Such faults can lead to moisture ingress, internal arcing, and power loss.</p>	
Diode fault	<p>A common diode fault occurs in the bypass diode (BPD) due to excessive current levels and inadequate or improper heat dissipation. Limited airflow within the junction box also plays a significant role, especially during rapid transitions between shadow and sunlight. A burnt BPD can result in a short circuit, open circuit, shunted diode, or an inversed diode, leading to varying degrees of power loss.</p>	
Burn mark	<p>Partial shading combined with a BPD fault or other mismatch issues, such as a low resistance defect in c-Si, can result in energy being consumed in the mismatched area rather than being generated. This leads to localized overheating of the cell and the formation of burn marks. Additionally, a DC arc fault can also cause burn marks, potentially resulting in overheating, delamination, or material melting.</p>	

Shunt Hot Spot	<p>Partial shading can cause a cell to enter a reverse-biased voltage state, to which thin-film cells are particularly sensitive. This results in module current concentrating along the shunt path, leading to the formation of hot spots. Unlike hot spots in c-Si modules, where the BPD helps limit reverse voltage, thin-film modules lack this protection. While overheating is less likely, this condition can lead to glass breakage and an increased risk of electrical shock.</p>	
PID	<p>Potential Induced Degradation (PID) is a performance loss in photovoltaic (PV) modules caused by high voltage differences between the solar cell and grounded components, such as the module frame. This voltage stress can lead to leakage currents and the migration of ions (like sodium) through the encapsulant, resulting in reduced power output and degraded cell performance. PID typically occurs under high system voltages, elevated temperatures, and humid conditions, and can significantly shorten the lifespan of PV modules if not properly mitigated.</p>	
Abnormal degradation	<p>Abnormal degradation is a combined effect of multiple faults, such as delamination, bubbles, snail tracks, PID, and the associated corrosion of the PV module [52]. Its impact is primarily observed through power loss and alterations in the slope of the module's I-V curve.</p>	<p>[51]</p>

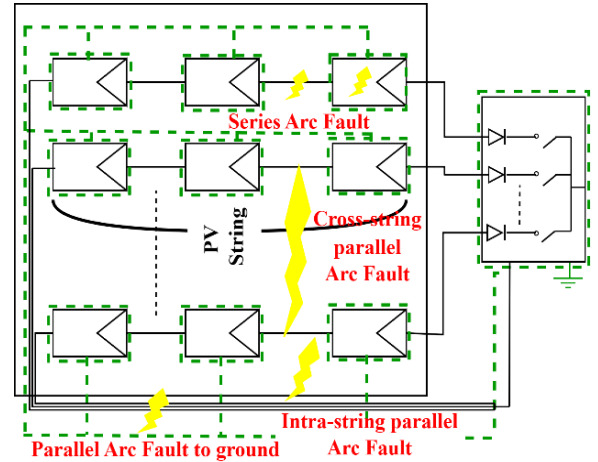
I.3.2.3. Array-level faults

At the array level, the main type of fault is the connection fault, which generally includes the earth fault, the line fault and the arc fault, as shown in Table 1.3.

Table 1.3: Array-level faults

Fault	Description	Example
Ground fault (GF)	<p>It occurs when an unintended low-impedance path forms between the Current Carrying Conductor (CCC) and the ground. In grounded PV systems, ground faults result in a high current flowing through a designated circulating path. In ungrounded systems, they create a residual magnetic field between the forward and return current flow. This leads to changes in insulation resistance and a sustained power loss.</p>	
Line-line fault (LLF)	<p>Line-to-Line Fault (LLF) occurs due to an unintended low-resistance path between two Current Carrying Conductors (CCC) with different electrical potentials. It can result from poor insulation in string connectors, accidental short circuits between CCCs, improper mounting, or external damage. This fault causes a high reverse current determined by the potential difference at the fault location flowing through the faulty path, leading to persistent power loss. LLF is categorized into two types: intra-string and cross-string LLF. Equipment damage: May damage modules, strings, or MPPT units. Standard detection method: Current/voltage monitoring, insulation resistance test.</p>	

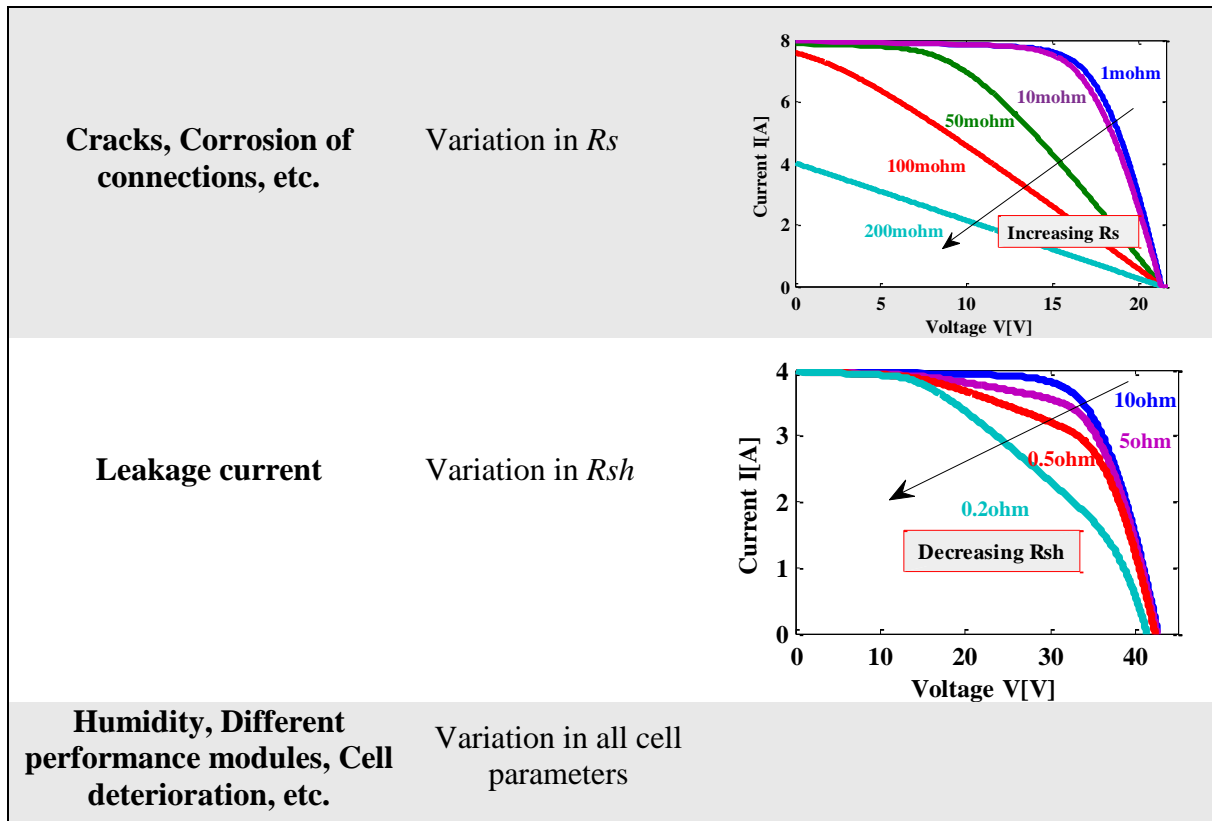
Arc fault (AF) Various external factors can cause discontinuity or insulation failure in Current Carrying Conductors (CCC), creating an air gap that leads to an arc fault. Arc faults are classified into two types: series and parallel AF, with the latter further divided into intrastring, cross-string, and parallel-to-ground faults. These faults can occur at almost any connection point or structural component within the PV array, including cells, busbars, modules, diodes, strings, and safety devices. They generate brief but extremely high temperatures that can burn the module's metal coating. Additionally, arc faults produce high-frequency components, leading to significant nonlinear distortions in current and voltage. **Equipment damage:** Can destroy connectors, modules, and protective devices. **Standard detection method:** Needs high-frequency signature analysis or arc fault detection devices.



Below, we present the impact of defects on the various parameters of the PV panel (see Table 1.4).

Table 1.4: Impact of different defects on cell parameters [33].

Nature of defects	Affected parameters
Shading (leaves, snow, sand, etc.)	Variation in I_{ph}
Cell heating	Variation in T



As shown in Figure 1.10, the most common degradation modes in modules for the last 10 years were hot spots (33%) followed by ribbon discoloration (20%), glass breakage (12%), encapsulant discoloration (10%), cell breakage (9%), and potential-induced degradation (PID, 8%) [53].

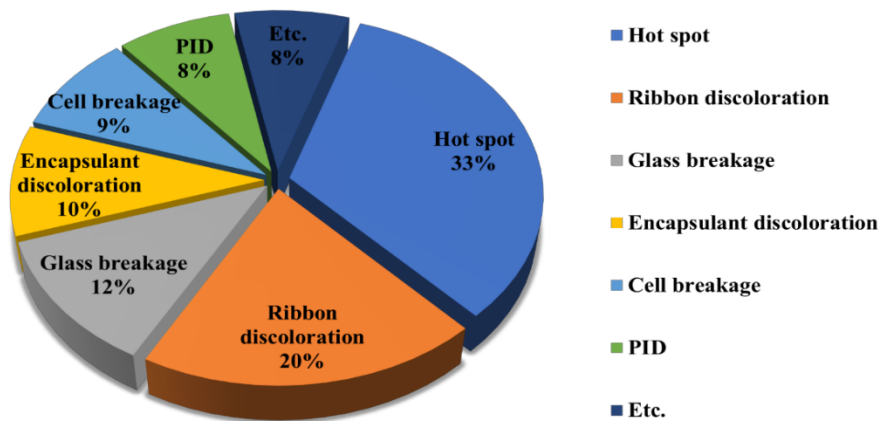


Figure 1.10: Representative degradation modes of silicon PV modules for the last 10 years [53].

1.4 Fault detection and diagnosis in PV systems

A fault detector is an additional component in both off-line and on-line PV systems, designed to assist operators in identifying faults, determining their type, and locating them within the system. It comprises various sensors, processing units, actuators, transducers, protective relays,

and circuit breakers, and can be installed at any node marked by the dashed polylines. At the output level, the fault detector features alarms, buzzers, and various Graphical User Interfaces (GUI) to notify field workers of any fault occurrences. The fault detection process is carried out in two key stages: *monitoring* and *diagnosis*.

A. Monitoring

To assess the performance of a PV system, the monitoring system gathers and analyzes various parameters such as voltage, current, and power [54]. This process is essential as a preliminary step before fault detection, ensuring continuous tracking of electrical power generation. Sensors serve as the primary input for data acquisition, with the collected data being transmitted through signal processing units. In the final stage, the data is stored for further analysis [54,55]. Figure 1.11 illustrates the cascaded monitoring process of a PV system, integrated within a fault detection framework.



Figure 1.11: Block diagram of PV monitoring system.

B. Diagnosis

The monitoring system outputs acquired data, which serves as the primary input for the fault diagnosis framework. By comparing this data with reference values, the system determines whether a fault is present or not [56,57]. The data source whether from the DC or AC side of the PV system helps guide the fault detector in its investigation. Figure 1.12 illustrates the sequential steps of PV fault diagnosis, starting with data analysis and concluding with the activation of alarms.

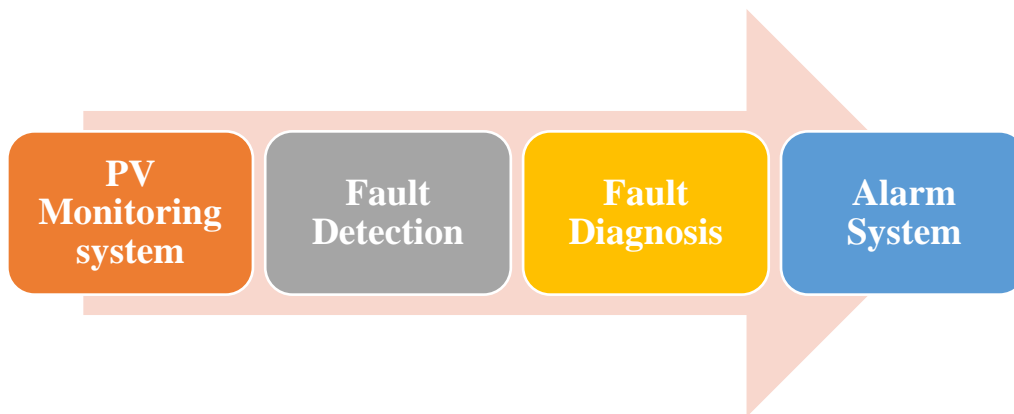


Figure 1.12: Block diagram of PV fault diagnosis scheme.

1.4.1 Faults Detection Techniques

Photovoltaic (PV) systems are prone to various faults that can degrade their performance, reduce energy output, and cause safety hazards. To ensure reliability and efficiency, different fault detection and identification techniques have been developed [58-61]. These techniques can be broadly classified into visual inspection, imaging-based techniques, electrical analysis, signal processing, analytical monitoring, and other advanced methods. The following sections provide an in-depth discussion of each approach. Figure 1.13 illustrates the Faults Detection and Identification techniques investigated in this sub-section.

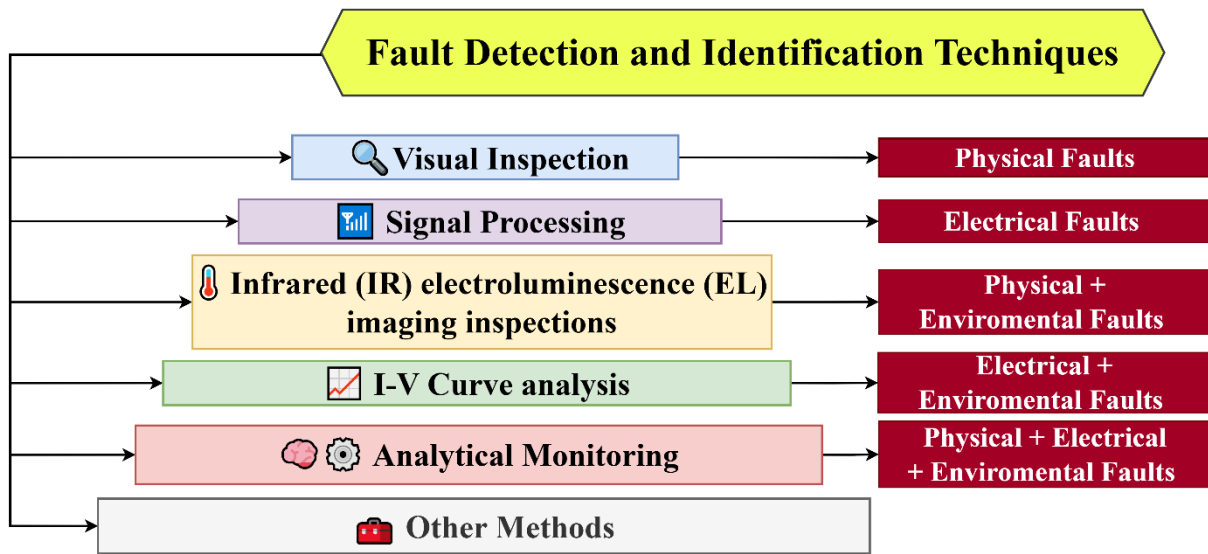


Figure 1.13: Faults Detection and Identification techniques.

1. Visual Inspection

Visual inspection is the most straightforward method for fault detection in PV systems. It involves manually examining solar panels, wiring, and electrical connections to identify visible defects. Technicians physically inspect the PV modules for signs of wear, damage, or dirt accumulation.

Some of the common issues detected through visual inspection include:

- **Broken or cracked solar cells** – Can be caused by external impacts, thermal stress, or material defects.
- **Burn marks or discoloration** – Indicate overheating, electrical faults, or aging of the module.
- **Loose connections and damaged wiring** – Poor connections can lead to power losses and even fire hazards.
- **Dust, dirt, and shading effects** – Obstructions on the module surface can reduce power generation efficiency.

While visual inspection is useful in detecting physical faults, it has several limitations. It is **time-consuming, labor-intensive, and cannot identify internal or electrical faults**. As a result, it is often combined with other advanced techniques to provide a more comprehensive fault detection approach.

2. Infrared (IR) and Electroluminescence (EL) Imaging Inspections

Numerous Operations and Maintenance firms provide routine Infrared (IR) and Electroluminescence (EL) imaging inspections of photovoltaic (PV) plants to guarantee optimal performance and safety of the PV array [62]. Infrared (IR) and electroluminescence (EL) imaging are non-destructive measurement techniques that can deliver high-resolution images of photovoltaic (PV) modules in real-time. Nonetheless, not all imperfections in PV modules result in a temperature rise; thus, a combination of infrared and electroluminescence monitoring techniques is essential for accurately identifying the most prevalent flaws in PV modules [63]. In recent years, numerous Machine Learning (ML) techniques have been employed to autonomously process sequences of images captured by infrared (IR) and electro-optical (EL) cameras mounted on Unmanned Aerial Vehicles (UAVs) [64-67], significantly reducing inspection durations and precisely analyzing diverse defects and failures in photovoltaic (PV) arrays. Figure 1.14 illustrates the imaging inspection procedure utilizing an infrared camera mounted on the drone platform to identify and pinpoint anomalies and failures inside the photovoltaic array. The IR and EL imaging approaches are complimentary, each possessing distinct strengths and shortcomings [63]. While these procedures necessitate complex equipment.

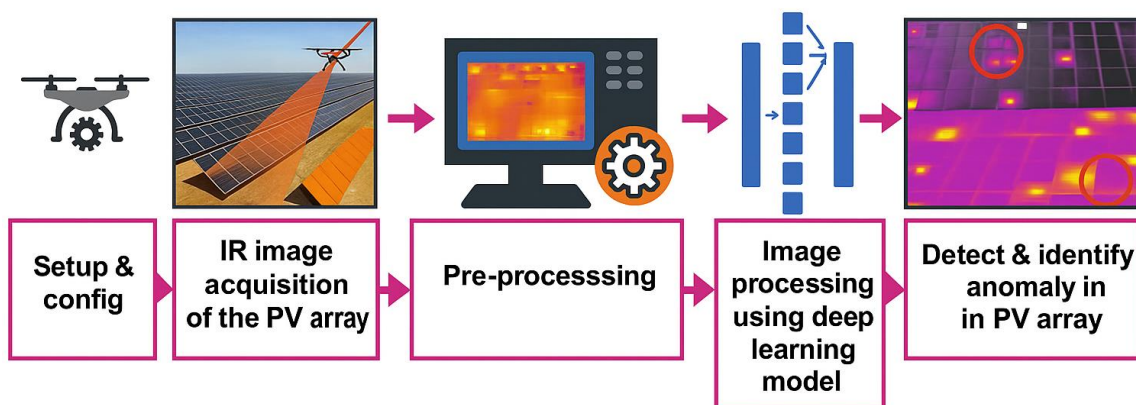


Figure 1.14: Imaging inspection process utilizing an IR camera [68].

3. I-V Curve Analysis

I-V (current-voltage) curve analysis is a commonly used electrical method for diagnosing PV system faults. This technique involves measuring the **I-V characteristics of a PV module or array** and comparing the results with a reference (healthy) curve [69,70].

Key parameters extracted from the I-V curve include:

- **Short-circuit current (I_{sc}):** The maximum current.
- **Open-circuit voltage (V_{oc}):** The highest voltage output when no load is connected.
- **Maximum power point (P_{max}):** The point where the module generates peak power.

By analyzing deviations in these parameters, different types of faults can be identified:

- **Open-circuit faults:** Sudden drops in current indicate disconnected panels or broken interconnections.
- **Short-circuit faults:** A significant reduction in voltage suggests a bypass diode failure or internal short-circuiting.
- **Partial shading effects:** A distorted I-V curve indicates uneven solar exposure across the PV array.

I-V curve analysis is widely used in both simulation and real-time monitoring. However, it requires accurate data acquisition and controlled test conditions for effective diagnosis (see figure 1.15).

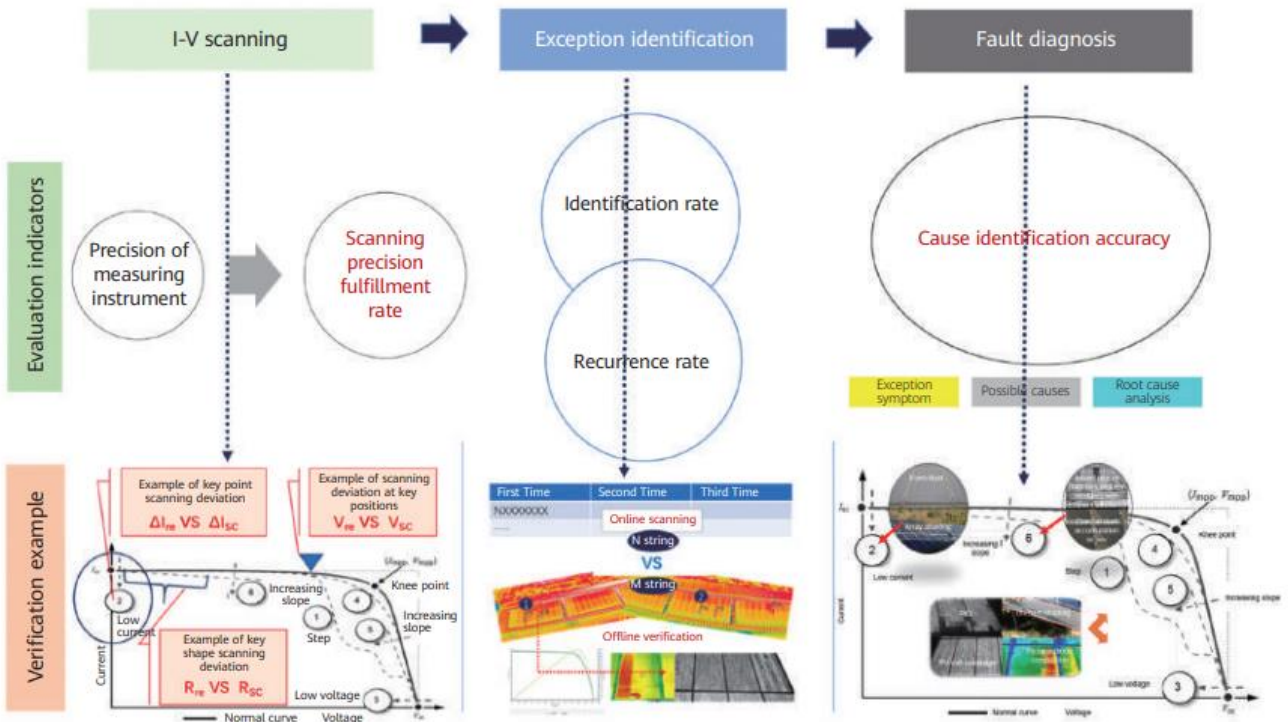


Figure 1.15: Illustrates the Smart I-V Curve diagnosis method developed by Huawei [71].

4. Signal Processing Techniques

Signal processing methods analyze electrical signals, such as voltage, current, and power, to identify fault patterns. These techniques utilize mathematical transformations to extract features from measured data and detect anomalies as shown in Figure 1.16 [72-75].

Common signal processing approaches include:

- **Fast Fourier Transform (FFT):** Converts time-domain signals into frequency domain to detect periodic faults.
- **Wavelet Transform (WT):** Identifies transient variations in electrical signals caused by sudden faults.
- **Hilbert-Huang Transform (HHT):** Used for analyzing nonlinear and non-stationary electrical patterns in PV systems.

Signal processing techniques are highly effective for detecting arc faults, ground faults, and inverter malfunctions. However, they require advanced computational tools and expert knowledge for accurate implementation.

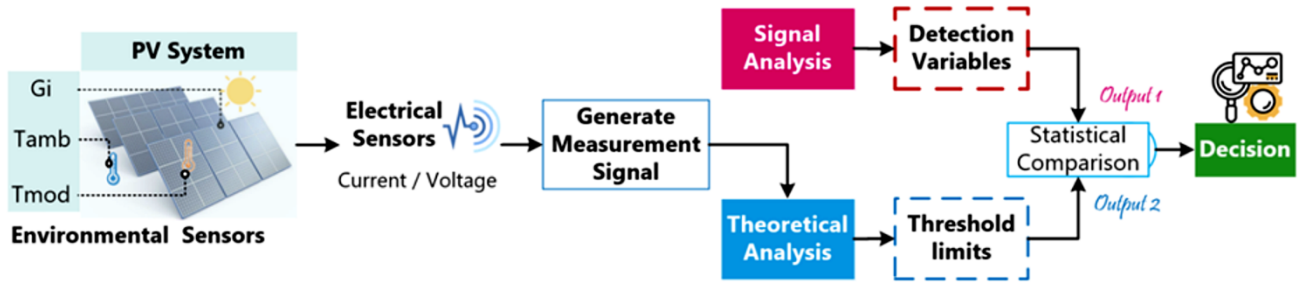


Figure 1.16: Presents a fault detection diagram that analyzes the output signal to identify anomalies and classify faults in the PV system [30].

5. Analytical Monitoring

Analytical monitoring techniques use mathematical models, statistical tools, and artificial intelligence to detect faults in PV systems. These methods are particularly effective for real-time fault diagnosis and classification.

5.1 Real-Time Difference Measurement (RDM)

RDM compares real-time voltage, current, and power measurements with expected values under normal conditions. Any deviation beyond a predefined threshold is flagged as a potential fault. This method is widely used in real-time monitoring systems for rapid fault detection. Threshold logic serves as the fundamental mechanism for executing a binary decision. The

threshold crossing, as indicated by the feature, signifies the system's health status, either functioning properly or malfunctioning [76-80].

5.2 Statistical Approaches (SA)

The statistical qualities of features can also be utilized for decision-making, as previously indicated for feature extraction. Numerous tools for statistical analysis are documented in literature [81]. Regression analysis is a collection of statistical methods used to estimate the associations between a dependent variable and one or more independent variables [82,83]. The aim of regression is to determine the coefficients of the curve (linear or non-linear) that most accurately fit the data based on an optimization criterion. It can be utilized for both prediction and categorization.

5.3 Machine Learning Techniques (MLT)

Machine learning (ML) models use historical data to train algorithms that can automatically detect and classify faults. Machine Learning (ML) techniques have become essential in PV fault detection due to their ability to analyze large datasets, recognize complex patterns, and make real-time decisions [84]. These methods rely on historical and real-time data to identify deviations from normal operation, allowing for efficient classification of different fault types [85]. By utilizing intelligent algorithms, ML techniques reduce the need for manual inspections, enhance system reliability, and improve predictive maintenance. Among the most commonly used ML techniques are **Artificial Neural Networks (ANNs)**, **Support Vector Machines (SVMs)**, **Fuzzy Logic Systems**, and **Decision Trees (DTs)**.

- **Artificial Neural Networks (ANNs):**

Artificial Neural Networks (ANNs) are computational models inspired by the structure and function of the human brain [86]. They consist of interconnected layers of artificial neurons that process input data and learn from experience. In PV fault detection, ANNs are trained using datasets containing various system parameters, such as voltage, current, and power, enabling them to classify normal and faulty conditions accurately. The multi-layered structure of ANNs allows them to extract meaningful features from complex, nonlinear data, making them highly effective in diagnosing different types of faults [87]. Once trained, an ANN can automatically detect abnormalities in real-time, making it a powerful tool for intelligent monitoring of PV systems.

- **Support Vector Machines (SVMs):**

Support Vector Machines (SVMs) are supervised learning models used for classification and regression tasks [88]. They operate by mapping input data into a high-dimensional space and finding an optimal hyperplane that best separates different fault categories. SVMs are particularly effective when dealing with binary classification problems, such as distinguishing between normal and faulty PV system conditions. By using kernel functions, they can also handle complex, nonlinear relationships between input parameters [89-90]. Their ability to generalize well with limited training data makes them a reliable choice for PV fault detection, ensuring accurate classification even when environmental conditions vary.

- **Fuzzy Logic Systems:**

Fuzzy Logic Systems provide a rule-based approach to PV fault detection by handling imprecise or uncertain information. Unlike traditional binary classification methods [91], which make rigid decisions, fuzzy logic assigns degrees of membership to different fault conditions, allowing for more flexible and human-like reasoning. The system relies on a set of IF-THEN rules that describe how input variables, such as voltage and current, relate to potential faults. By processing uncertain or noisy data, fuzzy logic effectively diagnoses faults and provides interpretable results, making it a valuable tool for real-time monitoring in dynamic PV environments.

- **Decision Trees (DTs)**

DT is a decision-making instrument that utilizes a tree-structured model [92]. It typically operates from top to bottom, selecting a variable at each stage that optimally divides the set of elements [93]. It typically comprises three types of nodes: root node, child nodes, and leaf nodes. The primary challenge in creating a decision tree is to identify the optimal splits. In PV fault detection, DTs segment data based on predefined conditions, allowing for a clear and structured classification of different fault types. Their ability to break down complex relationships into an intuitive, rule-based system makes them a widely used approach in automated fault diagnosis.

6. Other Methods

In addition to the above approaches, employing a signal transmission technique specifically for the PV array enables the detection of local disconnections in interconnect cables within PV modules and open-circuit failures of bypass diodes. The signal transmission device is compact,

lightweight, and cost-effective. It comprises two components: a transmitter and a receiver [94]. The identification of each defective module inside arrays facilitates rapid fault detection; however, this necessitates a substantial financial commitment owing to the enormous quantity of sensors needed.

5. Conclusion

This chapter has presented an overview of photovoltaic (PV) systems, their prevalent defects, and the approaches employed for fault detection and diagnosis (FDD). We have examined the operation of photovoltaic systems, the potential issues they may face, and the several methods utilized to identify and resolve these problems. A varied array of tools is available for monitoring and supervising photovoltaic (PV) systems, varying from traditional model-based procedures to advanced artificial intelligence (AI) technologies. These methodologies include system performance simulation and data analysis with machine learning techniques, all directed towards achieving optimal system efficiency and reliability. This chapter's findings enhance our comprehension of PV system maintenance and establish a foundation for further progress in renewable energy technology. In our pursuit of a more sustainable future, the proficient management of photovoltaic system defects will be essential for optimizing energy output and reducing environmental impact, which is the objective of the next chapters.

Chapter 2

Diagnosis based on Fuzzy Logic: Simulation and real-time experimentation

2.1. Introduction

Fault detection and diagnosis in photovoltaic (PV) systems are crucial for ensuring their efficiency and longevity. This chapter presents both simulation and experimental approaches to identifying, classifying, and localizing various PV faults using fuzzy logic-based techniques.

In the first part, a Fuzzy Logic Classifier is developed in Matlab/Simulink to diagnose eight types of faults occurring in PV cells, series resistance, shunt resistance, and bypass diodes. A diagnostic model is designed to simulate both healthy and faulty conditions of a PV panel, enabling the identification of faults through two distinct algorithms. The first algorithm employs a thresholding method to detect faults with distinct symptoms, while the second utilizes a fuzzy logic classifier to distinguish faults with overlapping characteristics.

The second part focuses on the experimental validation of the proposed fault detection approach. A fault classification algorithm is implemented to diagnose different shading conditions and short-circuit faults in bypass diodes. This method leverages an experimental database of climatic and electrical parameters from a PV panel, with the developed model integrated into Matlab/Simulink and interfaced with dSPACE DS1104 controller for real-time diagnosis. By combining simulation and experimental analysis, this chapter provides a comprehensive framework for detecting and classifying PV faults, enhancing the reliability and performance of solar energy systems.

2.2. Part 1: Modeling and simulation

2.2.1. Photovoltaic module modeling

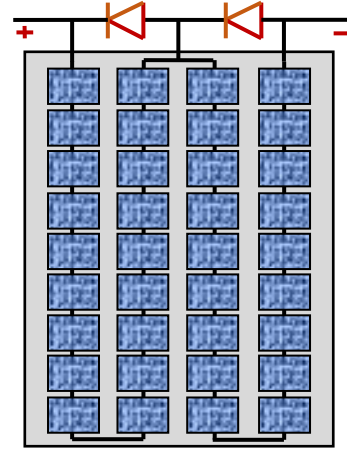
To evaluate the performance of photovoltaic panels under different operating conditions, the single diode model is generally considered as the most used model for describe the electrical behavior of PV cell as shown in Figure 1.3.

2.2.1.1 PV module characteristics

The PV panel used in this work is a SUNTECH PV module, composed of 36 PV cells and two bypass diodes as shown in Figure 2.1, with power 46.71 watt of type poly crystalline silicon and its electrical characteristics are presented in Table 2.1.

Table 2.1. Electrical characteristics of the SUNTECH PV module.

Electrical characteristics	
Pmax: Maximum power	46.71W
Vmp: Voltage at Maximum power	14.15 V
Imp: Current at Maximum power	3.3 A
Voc : Open Circuit Voltage	20.8 V
Isc: Short Circuit Current	3.67 A
The total number of cells connected in series	36
Number of bypass diodes	2

**Figure.2.1:** Schematic of PV panel.

2.2.1.2 PV Module Parameters Identification

- **Fundamental Principle**

The key objective is to reduce the error between the simulated and experimental results in the evaluation of the solar PV cell parameters. The root mean square error (RMSE) is an objective function that can be built in such a way that optimal values for the solar PV model parameters can be achieved. As given bellow:

$$RMSE = \sqrt{\frac{1}{N} \left(\sum_{i=1}^N [I_{meas} - I_{estim}]^2 \right)} \quad (2.1)$$

Where:

$$f(I_{ph}, I_0, R_{sh}, R_s, n) = I_{ph} - I_0 \cdot \left[\exp\left(\frac{V + R_s \cdot I}{V_t \cdot n}\right) - 1 \right] - \frac{V + R_s \cdot I}{R_{sh}} - I \quad (2.2)$$

Where N is the number of samples, I_{meas} is the measured current, I_{estim} is the calculated current which obtained by solving the nonlinear Equations (2.2) for a given voltage value using the Newton Raphson method. The current RMSE is calculated using these current values by using Equation (2.1).

The objective of this part is to use metaheuristic optimization techniques to estimate the parameters of a solar PV panel based on current and voltage measurements. The objective function is based on the RMSE values between the measured and expected current values. The parameters identification schema is highlighted in Figure 2.2.

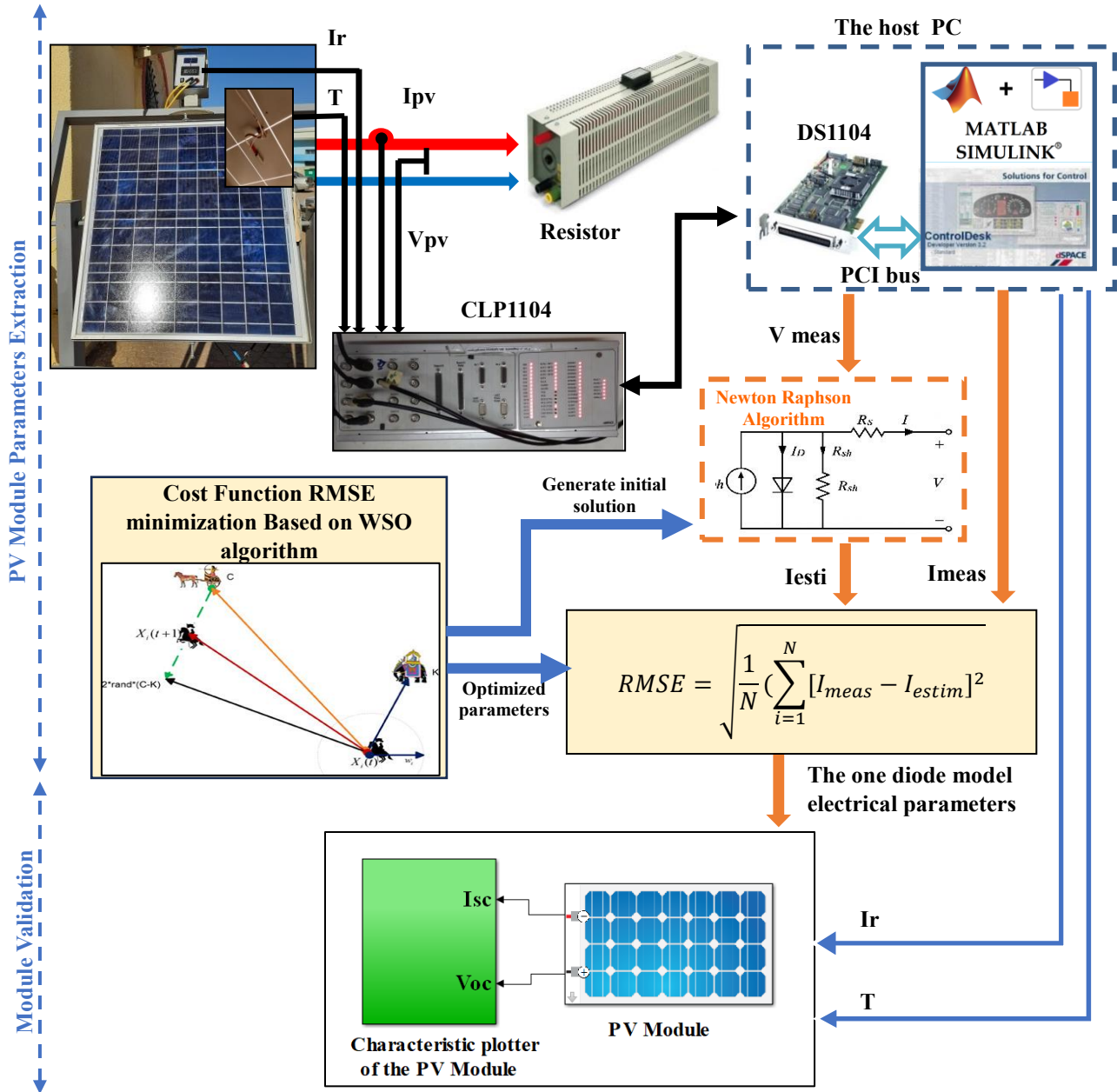


Figure. 2.2: Schematic of the experimental proposed technique.

• War Strategy Optimization (WSO) algorithm

The War Strategy Optimization (WSO) Algorithm is inspired by ancient kingdoms' military tactics during wars, where armies (infantry, chariots, elephants) arranged themselves into specific formations called *Vyuha* to achieve strategic objectives. The King and Commander coordinated troop movements using visible signals (like flags) and audible signals (like drum beats). The strategy adapted dynamically based on real-time battlefield situations.

The main steps in WSO include:

Random Attack: Troops are randomly and uniformly distributed; the King (leader) directs multiple army chiefs.

Attack Strategy: Focuses on identifying and exploiting the opponent's weaknesses. Soldiers adjust their positions dynamically based on the King's and Commander's locations, promoting successful soldiers and reverting unsuccessful ones.

Signaling by Drums: Drums are used to communicate strategic changes instantly to the soldiers.

Defense Strategy: Prioritizes protecting the King by forming a defensive chain around him, with soldiers adjusting positions relative to neighbors and the King, while exploring the battlefield to confuse the enemy.

The WSO algorithm is dynamic, adaptive, and decentralized, mimicking these historical tactics to solve optimization problems.

- **Mathematical modeling of the war strategy**

The War Strategy Optimization (WSO) Algorithm models two main war strategies inspired by ancient battlefield tactics. In the **first strategy**, each soldier updates their position based on the King's and the Commander's locations. This attacking model is pictorially explained in Figure 2.3.

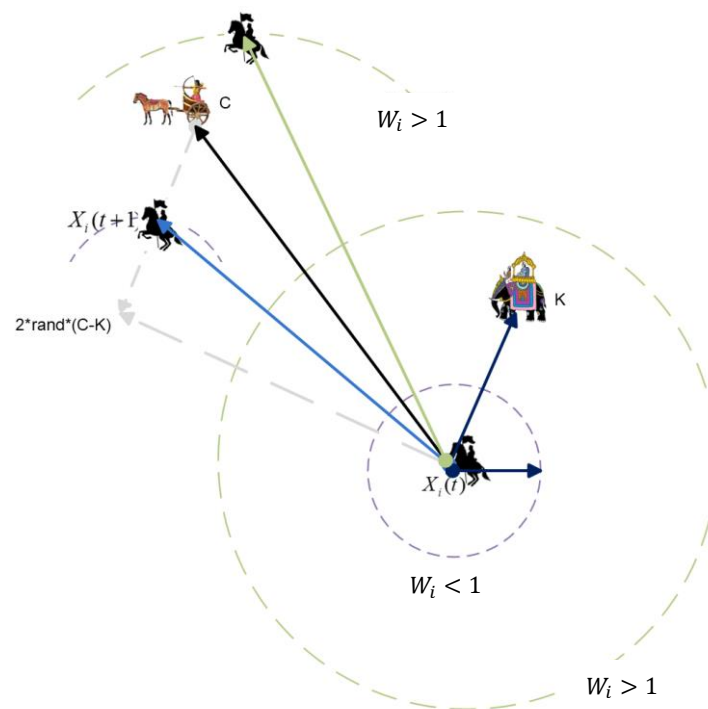


Figure. 2.3: Attack strategy in WSO.

Initially, all soldiers have the same rank and weight, symbolizing equal status. The "King" is the soldier with the highest attack force (best fitness value). As the war progresses, soldiers who successfully improve their attack force by moving to better positions are promoted in rank, and

their weights are updated accordingly. The movement rule combines the influence of the King and the Commander, and random variations. Where $X_i(t+1)$ is a new position, $X_i(t)$ is the previous position, C is the position of the commander, K is the position of the King, W_i is the weight.

$$X_i(t+1) = X_i(t) + 2 \times \sigma \times (c - K) + rand \times (W_i \times K - X_i(t)) \quad (2.3)$$

If a new position (fitness) leads to a worse attack force (F_n), the soldier reverts to their previous location (F_p).

$$X_i(t+1) = (X_i(t+1)) \times (F_n < F_p) + (X_i(t)) \times (F_n \geq F_p) \quad (2.4)$$

If the soldier updates the position successfully, the rank (R_i) of the soldier will be upgraded.

$$R_i = (R_i + 1) \times (F_n < F_p) + (R_i) \times (F_n \geq F_p) \quad (2.5)$$

The weights dynamically adapt over time, encouraging large exploratory moves at the beginning of the war and smaller, more precise movements toward the end. Where α is a tunable parameter.

$$W_i = W_i \times \left(1 - \frac{R_i}{Max_iter}\right)^\alpha \quad (2.6)$$

In the second strategy, position updates depend not only on the King and Commander but also on a randomly selected soldier, which introduces more randomness into the search process. This enhances the algorithm's exploration ability, allowing the army (search agents) to cover a broader search space and avoid premature convergence.

$$X_i(t+1) = X_i(t) + 2 \times \sigma \times (K - X_{rand}(t)) + rand \times W_i \times (C - X_i(t)) \quad (2.7)$$

• Parameters Identification Results

The War Strategy Optimization (WSO) technique is employed to ascertain the five unknown parameters I_{ph} , I_o , R_{sh} , R_s , and n of a single diode model with conjunction of the Newton Raphson method. This technique is employed to compute the value of the objective function during parameter optimization. Throughout the optimization process, the algorithm sends the photovoltaic parameters to the Newton-Raphson method for the computation of the objective function. Subsequently, the Newton-Raphson approach resolves the nonlinear equation in (2.2)

at a defined voltage, producing an output current with an absolute error (ε) significantly less than $1\text{E-}4$.

Table 2.2 displays the estimated parameters and the RMSE errors derived from WSO [26,27]. Figure 2.4 illustrates the convergence curves for the established goal functions, whereas Figures 2.5 and 2.6 compare the I-V and P-V curves of the photovoltaic cell utilizing both empirical and calculated parameters. These attributes were modeled via Simulink/Matlab under standard test conditions (STC). The basic steps of the WSO algorithm are summarized in Figure 2.7.

Table 2.2. The final identified parameters of the SUNTECH PV module.

Extracted Parameters					
R_s	R_{sh}	I_{ph}	I_0	n	RMSE
0.0356 Ω	18.4709 Ω	3.6658A	8.3e-10A	1.1567	2.245253e-07

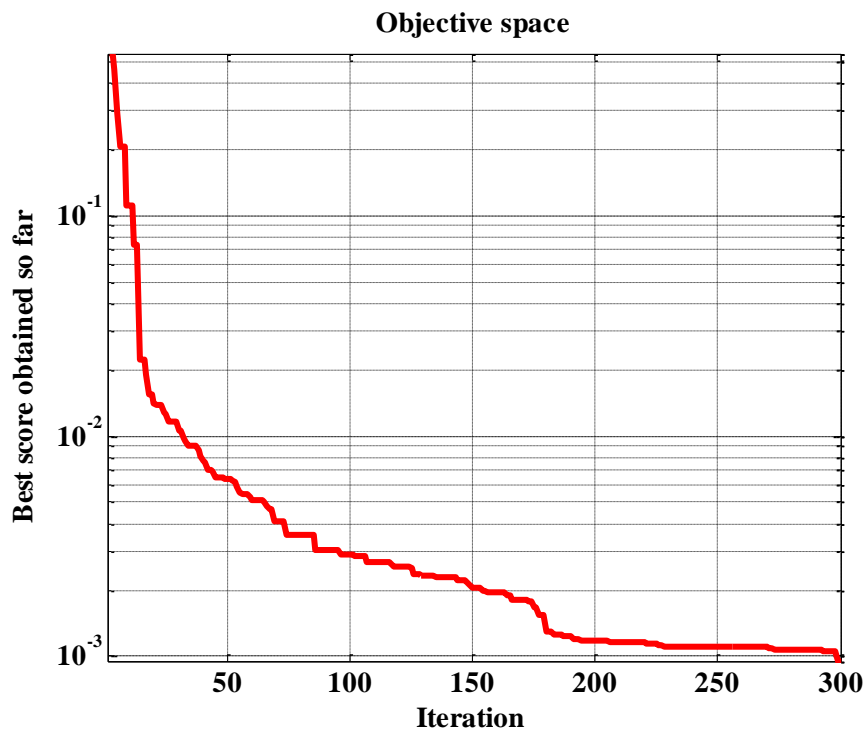


Figure. 2.4: The convergence rate of the WSO algorithm during the parameter extraction process for PV module.

The comparison of the extracted parameters from the WSO of the experimental and anticipated I-V and P-V curves demonstrates a strong concordance in both results and structure (refer to Figures 2.5 and 2.6). The smallest given RMSE (2.245253e-07A) from Table 2.2 and the best parameters fit expressed the efficiency of the proposed optimization algorithm and its convergence rate. Furthermore, as stated in [95], the highest absolute error remains below 0.06,

reinforcing the low RMSE value does not surpass 0.05 as a maximum value demonstrates the remarkable predictive accuracy of the WSO algorithm in selecting optimal parameter values. Moreover, the algorithm efficiently achieves this with a satisfactory convergence rate, as depicted in Figure 2.4.

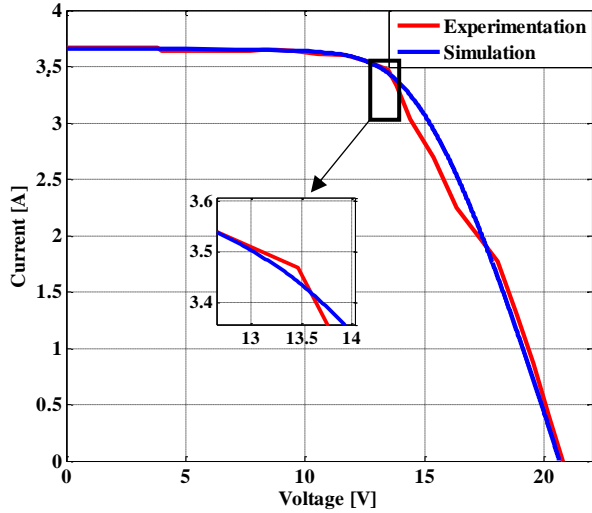


Figure 2.5: I-V Performance of a photovoltaic module under STC.

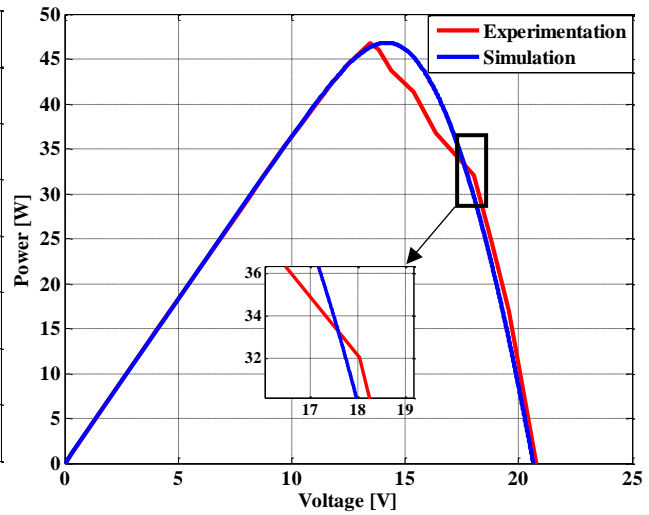


Figure 2.6: P-V Performance of a photovoltaic module under STC.

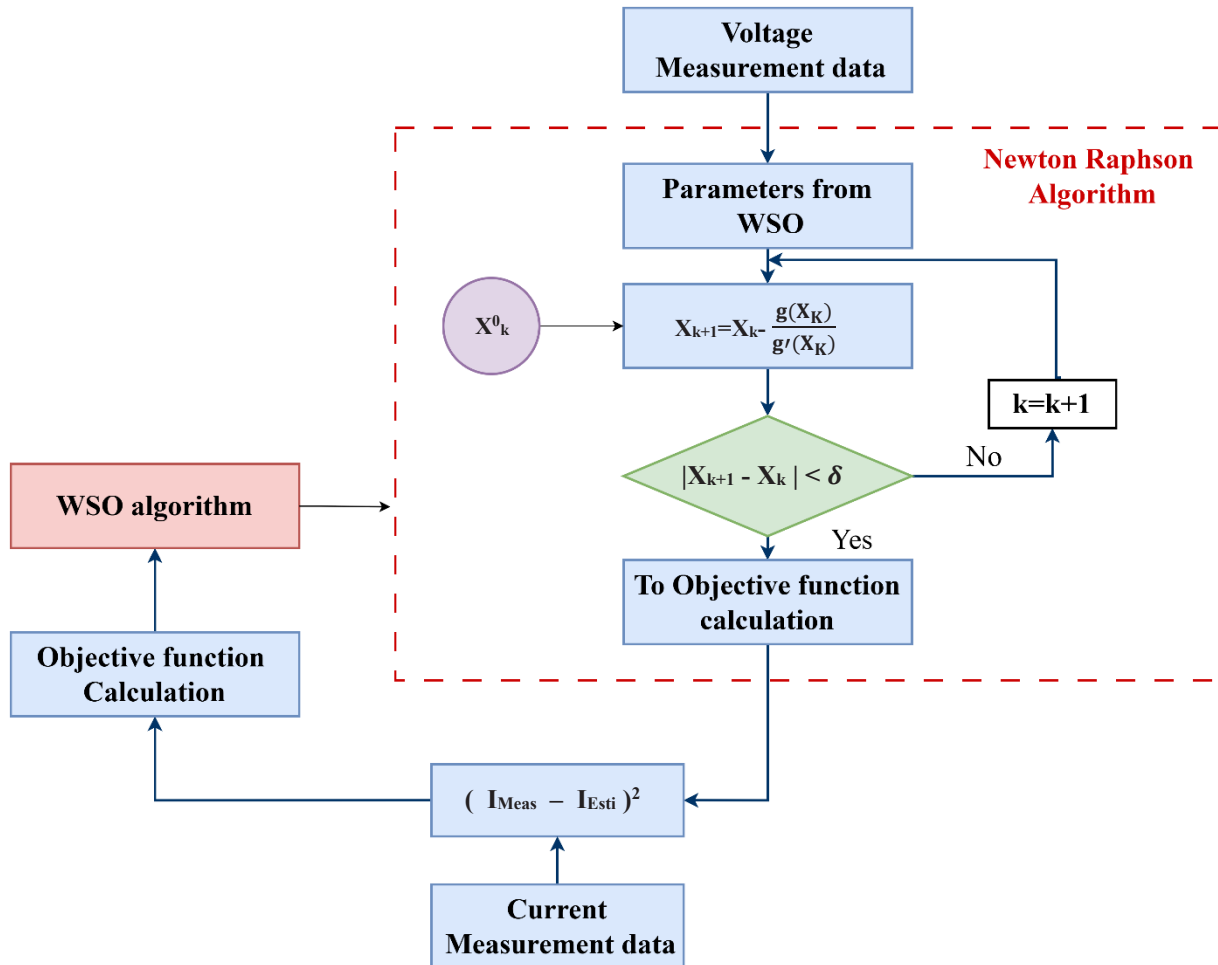


Figure 2.7: Concept of objective function calculation with WSO.

To evaluate the performance of the proposed WSO algorithm, a comparative study was conducted using the ISO FOTON 106/12 PV module alongside two other optimization algorithms from the literature [96]: Artificial Bee Colony (ABC) and Practical Swarm Optimization algorithms (PSO). As shown in Table 2.3, the results clearly demonstrate that the WSO algorithm outperforms both ABC and PSO.

Table 2.3. The comparative study of the three optimization algorithms.

Item	WSO	ABC	PSO
I_{ph}	6.5579	6.73	6.73
I_o	5.0308e-4	1.38e-05	1e- 5
n	63.018	61.76	60.24
R_s	0.21	0.12	0.13
R_{sh}	105	103	95.50
RMSE	0.012	0.015	0.018

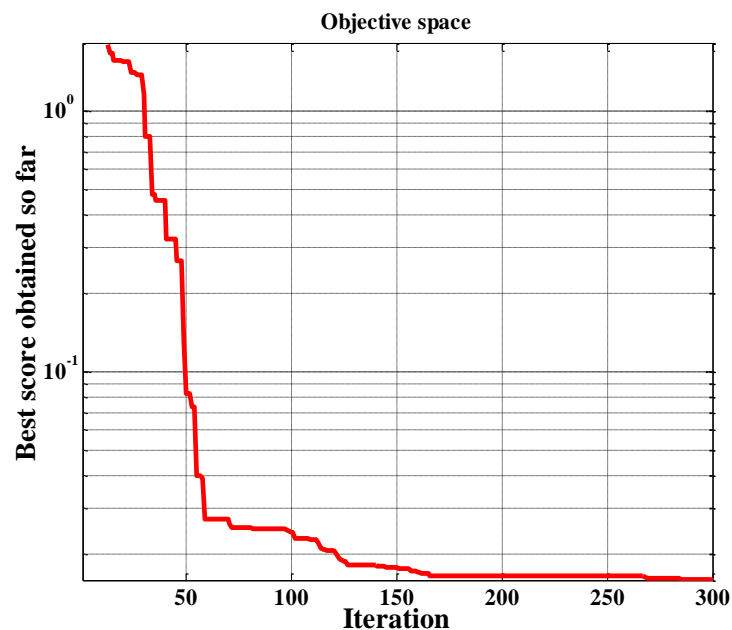


Figure 2.8: Convergence rate of WSO algorithm during the extraction process of ISO FOTON106/12 PV module.

2.2.2 PV Module Faults

Although it is desirable to maintain a regular solar radiation over the panel with each cell performing at its Maximum Power Point (MPP). In reality, PV panels often experience several abnormal conditions that negatively affect their efficiency and the total output power. In this part, eight faults on

PV module are chosen to be achieved as listed in Table 2.4 with Schematic diagram of PV panel with various faults highlighted in Figure 2.9.

Table 2.4. Different type of faults chosen for the diagnosis.

Symbol	Fault type
F1:	Shading of one cell in submodule of the panel at 50 %.
F2:	Shading of one cell in submodule of the panel at 100 %.
F3:	Shading of a cell of the submodule 1 and another of the submodule 2 of the panel at 50 %.
F4:	Shading of a cell of the submodule 1 and another of the submodule 2 of the panel at 100 %.
F5:	Increase the serie resistors ($R_s = 0.09\Omega$) module.
F6:	By-pass diode disconnected.
F7:	By-pass diode short circuited.
F8:	Decrease the shunt resistors ($R_p = 0.4\Omega$) module.

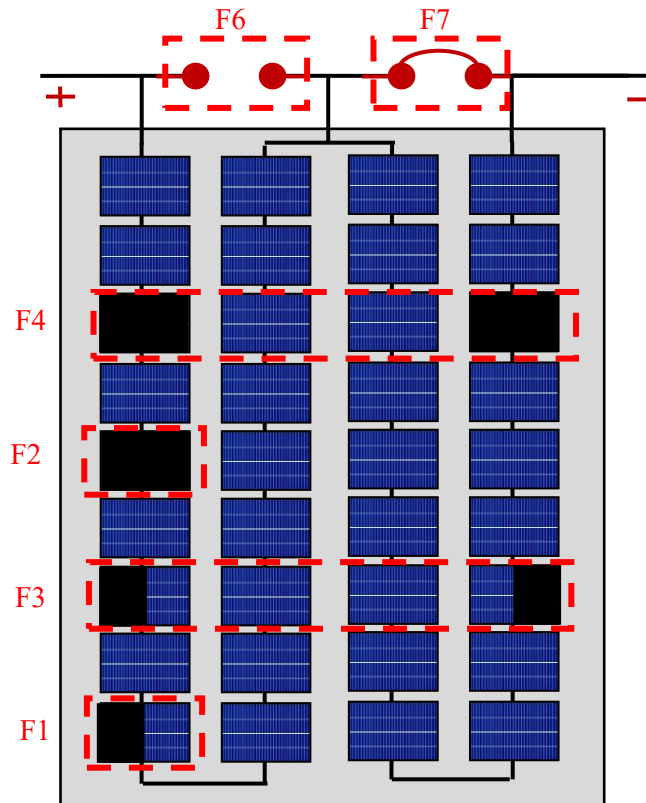


Figure.2.9. Schematic diagram of PV panel with various faults.

2.2.3 Fault Diagnosis PV System

The simulated diagnosis PV system is composed of two SUNTECH PV modules, these modules consist of 36 cells and two bypass diodes each. As a first step we simulate the normal PV panel (healthy) which used as a reference module and the faulty PV panel as a tested module for different chosen faults. In the second step, for each I-V curve three parameters (P_{max} , V_{oc} ,

I_{sc}) are extracted, and in the third step, a diagnosis algorithm is used to detect and classify PV module faults into two groups:

- Faults with different combination of symptoms. These faults are isolated using a signal threshold-based approach.
- Faults with the same combination of symptoms. This type of faults is isolated using a Fuzzy Logic Classifier.

Each fault generates a set of symptoms which are displayed with a message on the Command Window illustrate the fault type as shown in Figure 2.11. Simulink/Matlab has been used to implement this configuration illustrated in Figure 2.10.

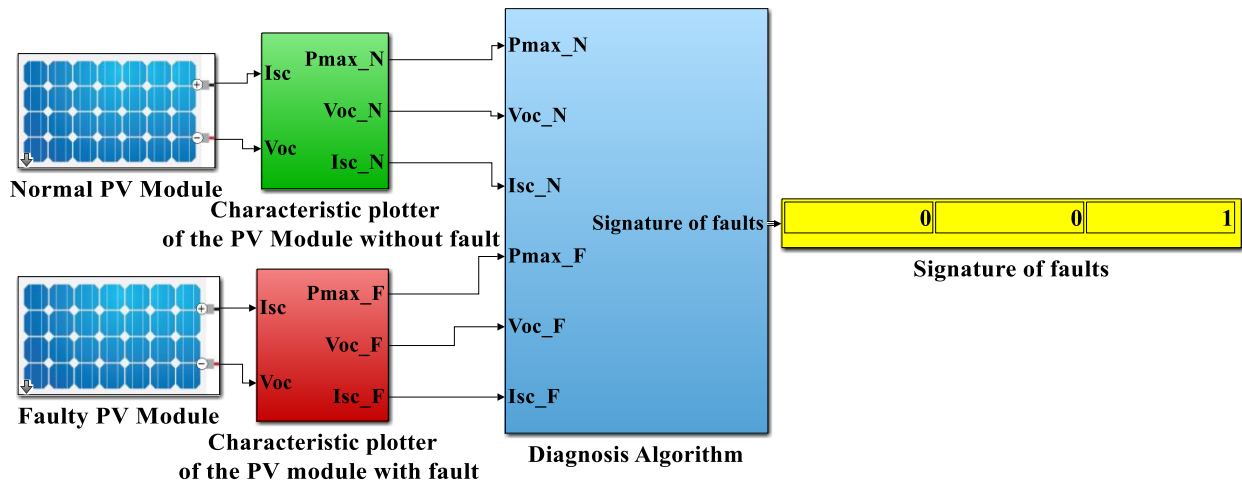


Figure.2.10. Diagnosis PV system.

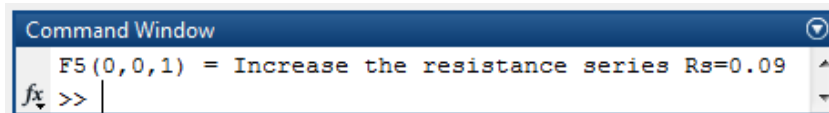


Figure 2.11. Output of fault 5 which is displayed in the command window.

2.2.3.1 Thresholding method (Algorithm 1)

In this part as shown in Figure 2.12, after extraction the three parameters (P_{max} , V_{oc} , I_{sc}) from each I-V curve (Normal and faulty module), the resulting parameters are compared to obtain (ΔP_{max} , ΔV_{oc} , ΔI_{sc}). In the second Step, the obtained parameters will compare to three relative errors associated to power, voltage and current, which these errors are related to measurement and the model errors. From the standard IEC 61724 [97], that indicates a relative error of 2 %, 1 %, and 1 % while measuring power, voltage, and current, respectively. The model uncertainty is related to the industrialization tolerance and sensors noise. The maximum error due by this uncertainty is calculated, according to [33], by adding a dispersion parameter to the simulation model parameters. The obtained relative errors associated to power,

voltage, and current are equal to 5%, 3 %, and 6 %, respectively. The detection of faults is considered effective when these chosen thresholds are exceeded.

After using the threshold method, five groups of faults can be achieved as shown in Table 2.5:

Table 2.5. The signature of faults after using the threshold method.

Groups	Fault type	Symptoms [S1,S2,S3]		
1	[F1,F5]	S1=1	S2=0	S3=0
2	[F2,F7,F8]	S1= 1	S2=1	S3 =0
3	[F3]	S1=1	S2=0	S3=1
4	[F4]	S1=1	S2=1	S3=1
5	[F6]	S1=0	S2=0	S3=0

According to these results, the first algorithm cannot discriminate between the faults (F1, F5), and (F2, F7, F8), which have the same combination of symptoms. Therefore, to isolate these faults, a very efficient technique of classification is required.

The simulation of the previous faults allowed us to obtain different curves as shown in Figure 2.13, which the outputs of our Simulink model are illustrated in the same figure.

- The symptom S1: Reduction of maximum power of the PV module.
- The symptom S2: Reduction of V_{oc} of the PV module.
- The symptom S3: Reduction of I_{sc} of the PV module.

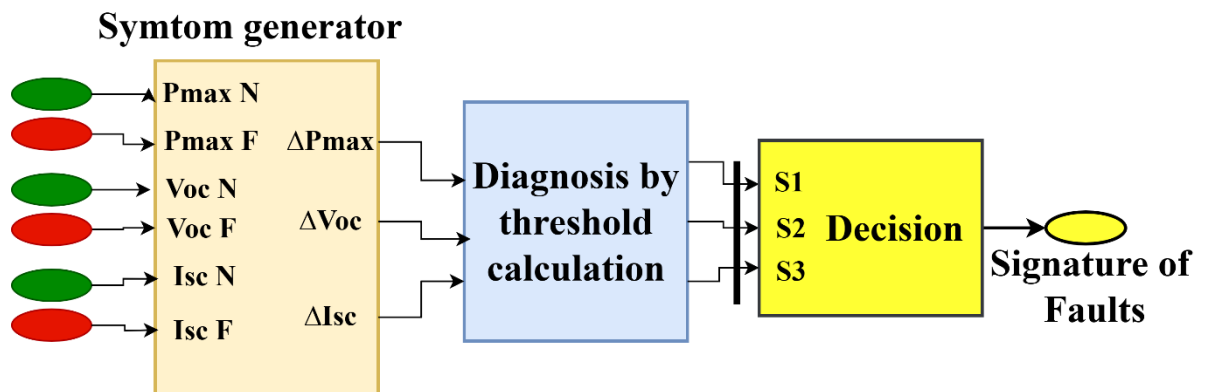


Figure 2.12: Diagnosis Model based on Threshold method.

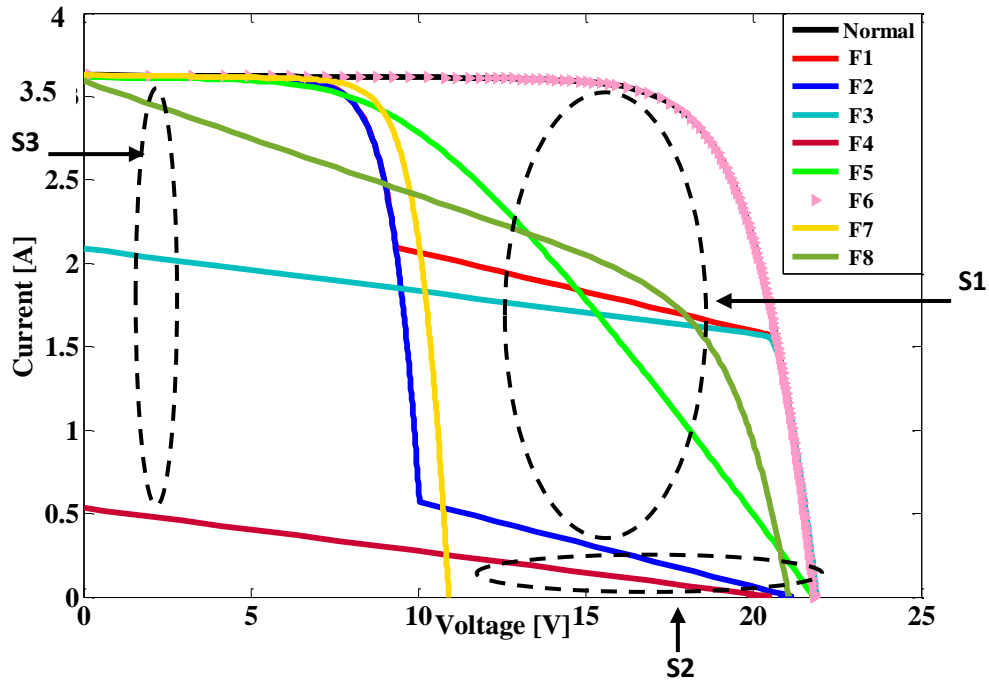


Figure 2.13: I-V Curves of different type of faults.

2.2.3.2 Fuzzy Logic Method (Algorithm 2)

To solve this problem A Fuzzy Logic (FL) method will be applied. From Figure 2.14, the threshold algorithm block remains the same. Therefore, the modification consists in integrating two diagnosis blocks by Fuzzy Logic Classifier in the system, with (ΔP_{max} , ΔV_{oc}) as inputs. The 1st FL block works only in the case where $(S1, S2, S3) = (1, 1, 0)$ and the 2nd block works only in the case where $(S1, S2, S3) = (1, 0, 0)$. The algorithm used is summarized in Figure 2.16.

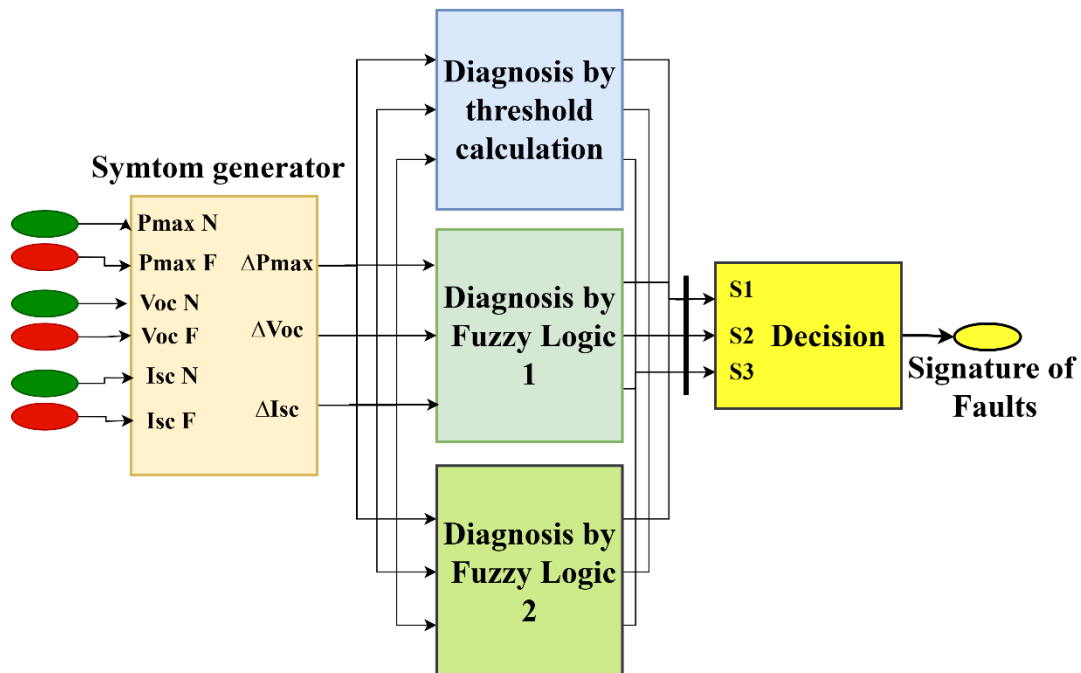


Figure 2.14: Diagnosis Model after integration of the fuzzy logic.

To construct a classifier, we have to use data mentioned in the previous paragraph as inputs. As shown in Figure 2.15, in the case 1 and 2, fuzzy classifier (FC) starts by fuzzification of these inputs by using the membership functions.

Then we have to construct a fuzzy inference base rule IF/THEN, the fuzzy rules are chosen to distinguish the defects which have the same indication signature. As presented in Table 2.6 and 2.7, precise bases discriminate between the three faults (in case 1) and the two faults (in case 2) have been constructed. Which Table 2.6 contains 3 rules and Table 2.7 contains 2 rules.

Finally, the values obtained have been defuzzified. This has been performed by applying the Takagi-Sugeno-Kang type one FL method at the output of a FC. Therefore, the outputs membership functions are constants.

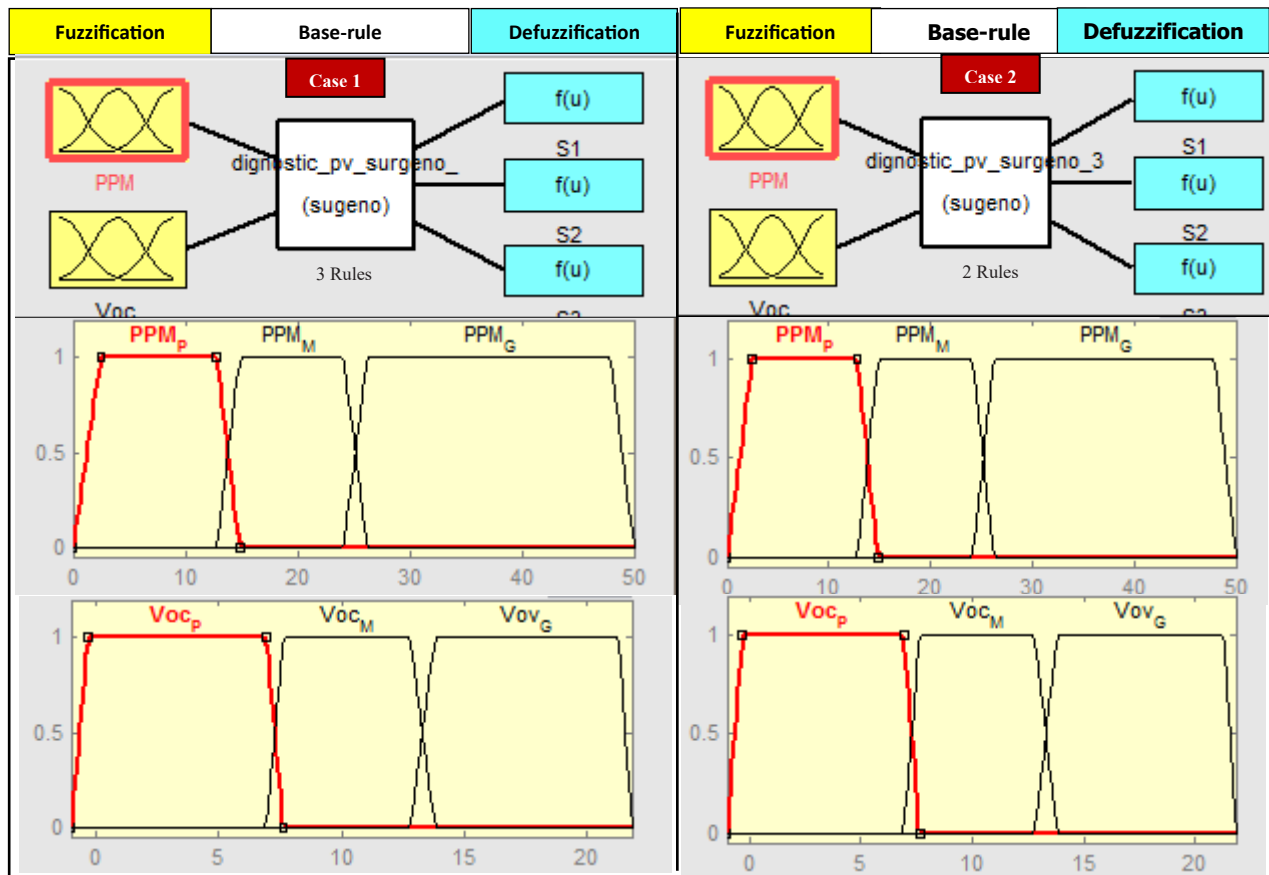


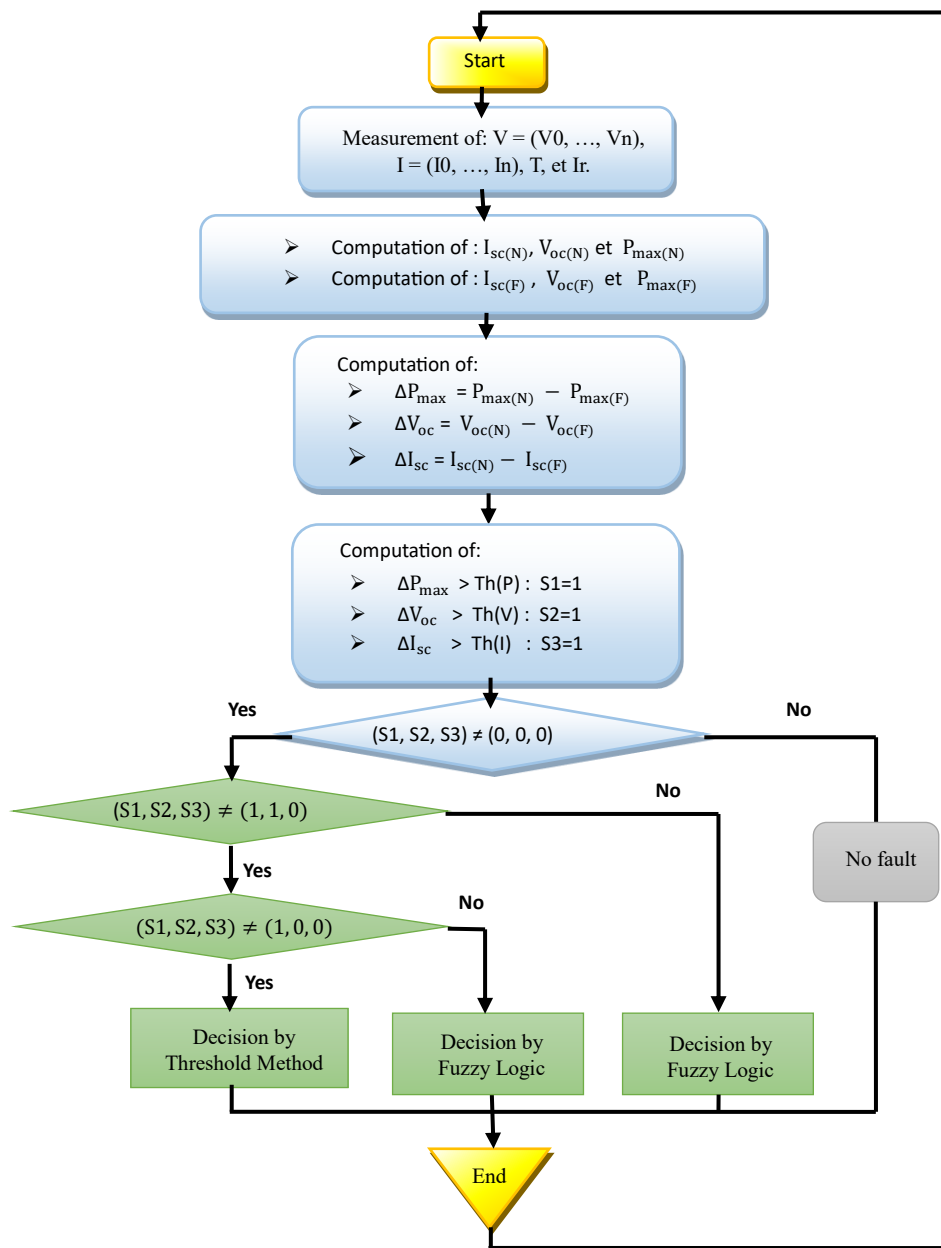
Figure.2.15: Fuzzy Classifier structure and input variables.

Table 2.6. Fuzzy Rule base and Defuzzification for Fuzzy Classifier (Case 1).

Rule N°	IF		THEN			Defuzzification
	PPM	Voc	S1	S2	S3	
1	PPM_G	Vco_P	S1=0	S2=1	S3=0	[0 1 0]
2	PPM_M	Vco_M	S1=0	S2=1	S3=1	[0 1 1]
3	PPM_M	Vco_P	S1=1	S2=1	S3=0	[1 1 0]

Table 2.7. Fuzzy Rule base and Defuzzification for Fuzzy Classifier (Case 2).

Rule N°	IF		THEN			Defuzzification
	PPM	Voc	S1	S2	S3	
1	PPM_M	Vco_P	S1=1	S2=0	S3=0	[1 0 0]
2	PPM_G	Vco_P	S1=0	S2=0	S3=1	[0 0 1]

**Figure.2.16:** Flowchart of the diagnosis algorithm.

2.2.4 Results and discussion

This part presents the results of the Simscape based model as well as the performance of the proposed fault diagnosis technique for the PV module (SUNTECH) system is simulated.

As example, Figure 2.17 shows the results given by the technique used in the case of shading 1 cell at 50%, Figure 2.18 shows the results given in the case of shading 1 cell at 100%.

The different chosen faults are applied in a singular way on the faulty PV module, so then the algorithm detects and classifies the fault to different combination of symptoms. The obtained symptoms send a signal to decision block (shown in Figure 2.14) to gives its accurate location.

The results of different fault scenarios for Sugeno FL and thresholding method are illustrated in Table 2.8. For eight different case scenarios have been tested, all different faults have been detected except the fault 6, which does not affect in the power generation of the system. Hence, it can be seen clearly from these obtained results that these two methods have proved to be able to detect and classify and locate different faults in PV panels accurately and efficiently.

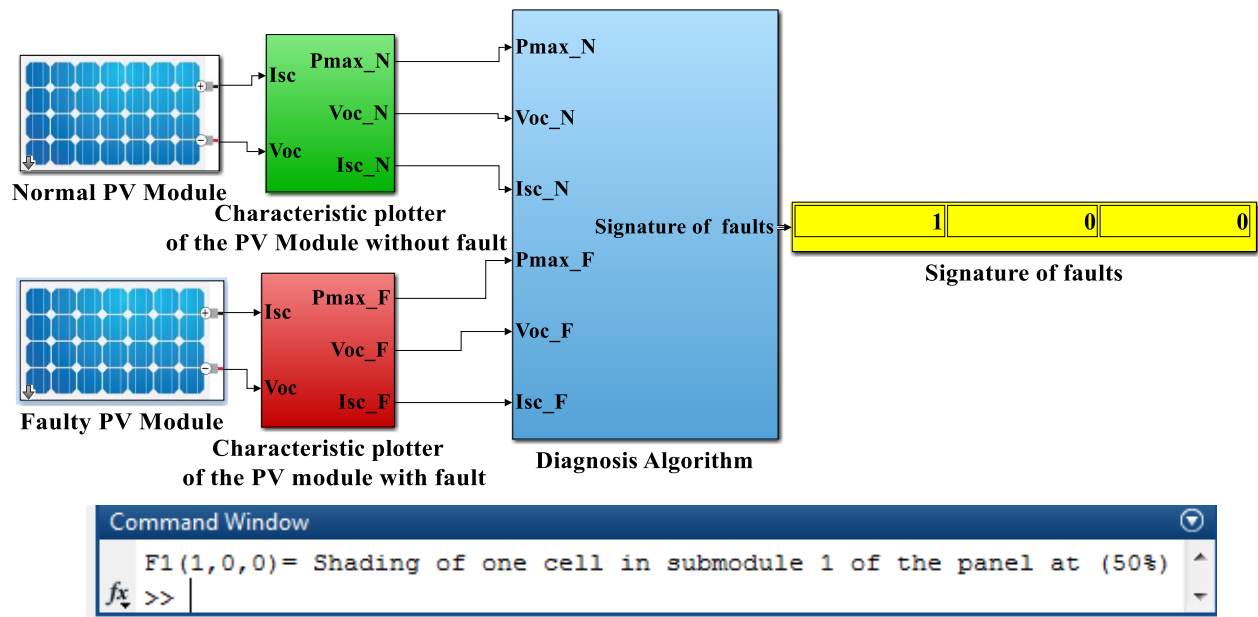


Figure.2.17: Diagnosis PV system results for F1 fault.

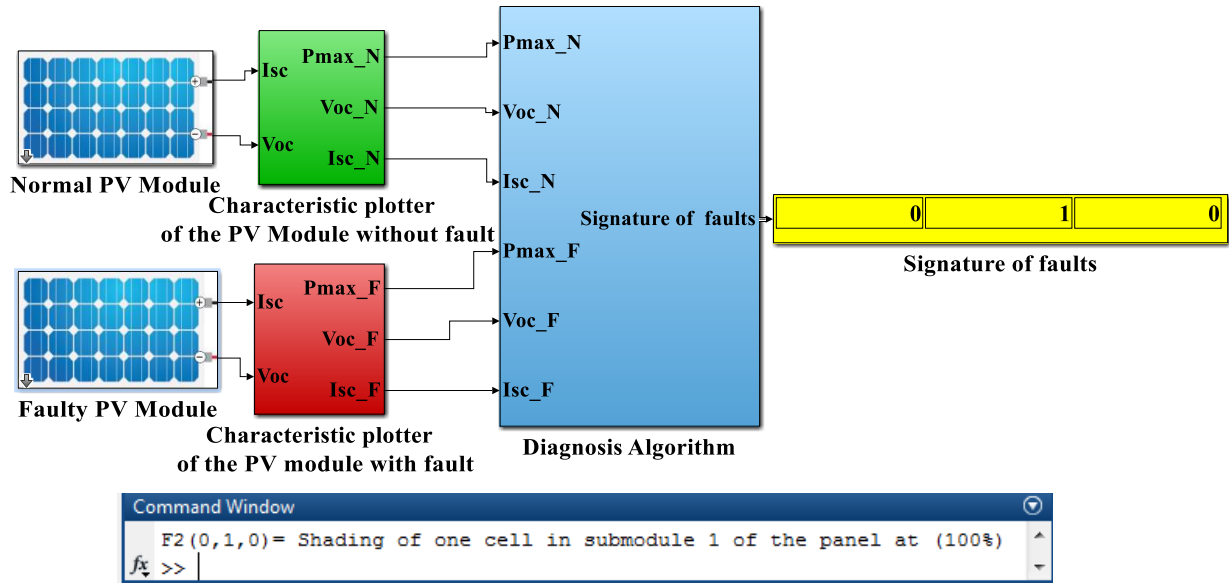


Figure.2.18: Diagnosis PV system results for F2 fault.

Table 2.8. The signatures of each of the symptom for each fault after integration of the fuzzy logic.

Faults	Amplitude of symptoms			Method
	S1 (W)	S2 (V)	S3 (A)	
F1	1	0	0	Fuzzy Logic
F2	0	1	0	
F3	1	0	1	Thresholding
F4	1	1	1	
F5	0	0	1	Fuzzy Logic
F6	0	0	0	Thresholding
F7	0	1	1	Fuzzy Logic
F8	1	1	0	

2.3. Part 2: Experimental Validation

2.3.1. EXPERIMENTAL COMPONENTS DESCRIPTION

In this section, a detection of faults is undertaken on an experimental PV panel situated at LGEB, University of Biskra, Algeria, where the schematic representation is given in Figure.2.19. It comprises of a SUNTECH PV panel of type poly crystalline silicon connected with a resistive load, through the intermediary current and voltage sensors are used to provide the performance of the PV panel implemented. The irradiances are measured using a Reference cell, while for temperature, it is measured using K-type thermocouple.

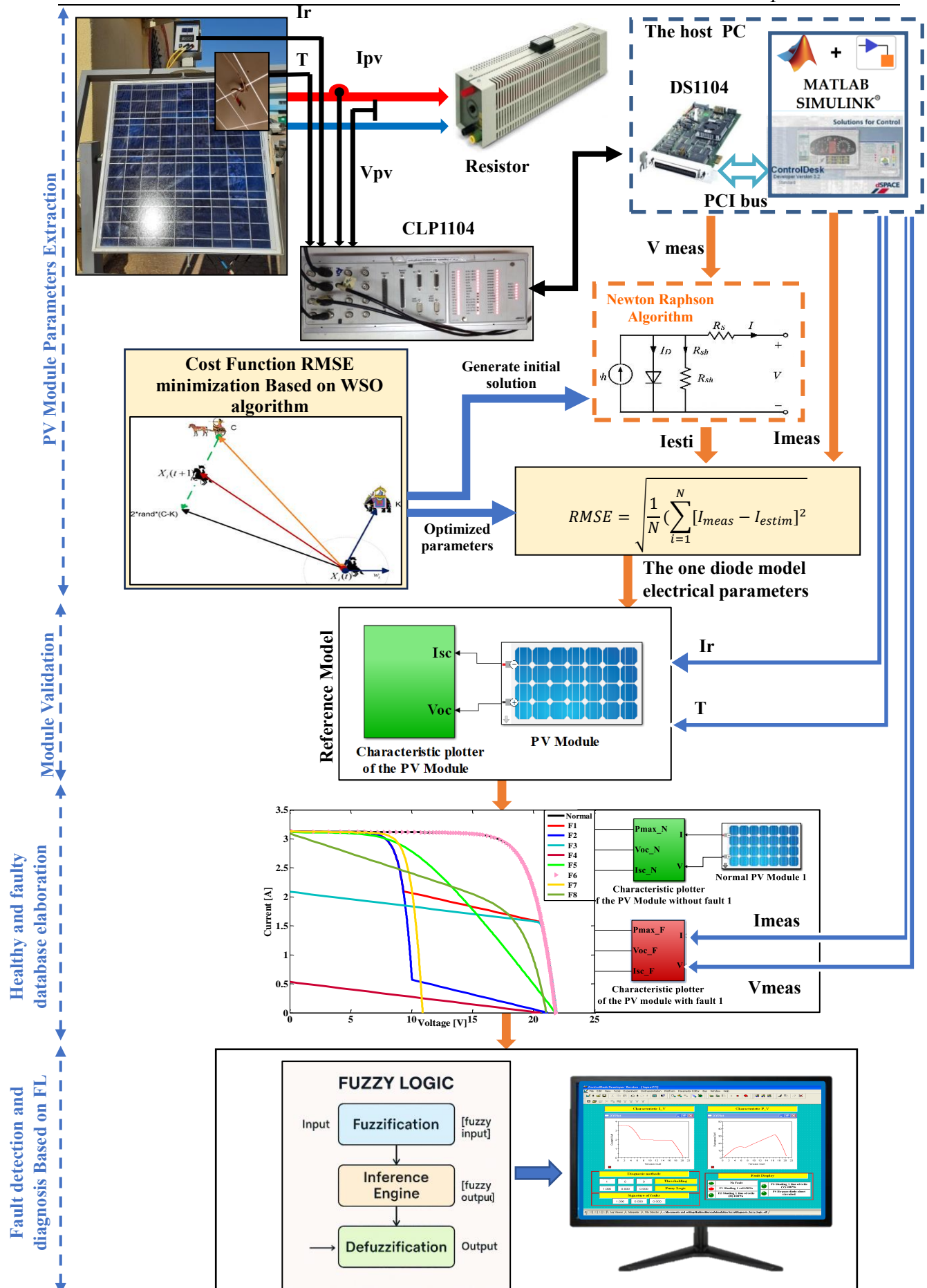


Figure. 2.19: Schematic of the experimental proposed technique.

The different data measured are realized by DS1104 controller board which is connected to the PC via PCI slot, and by the software Matlab/Simulink® and ControlDesk® we can monitor our experimental system using the implemented diagnosis technique.

A. Investigated Faults in the Experimental PV module

Four types of faults are established in our PV module, where F1 correspond to the shading of one cell in subpanel of the module at 50 %, the Fault 2 is shading horizontal line of cells at 100%, the Fault 3 is shading vertical line of cells at 100% and the Fault 4 is the diode by-pass short circuited. The investigated faults are shown in Figure 2.20.

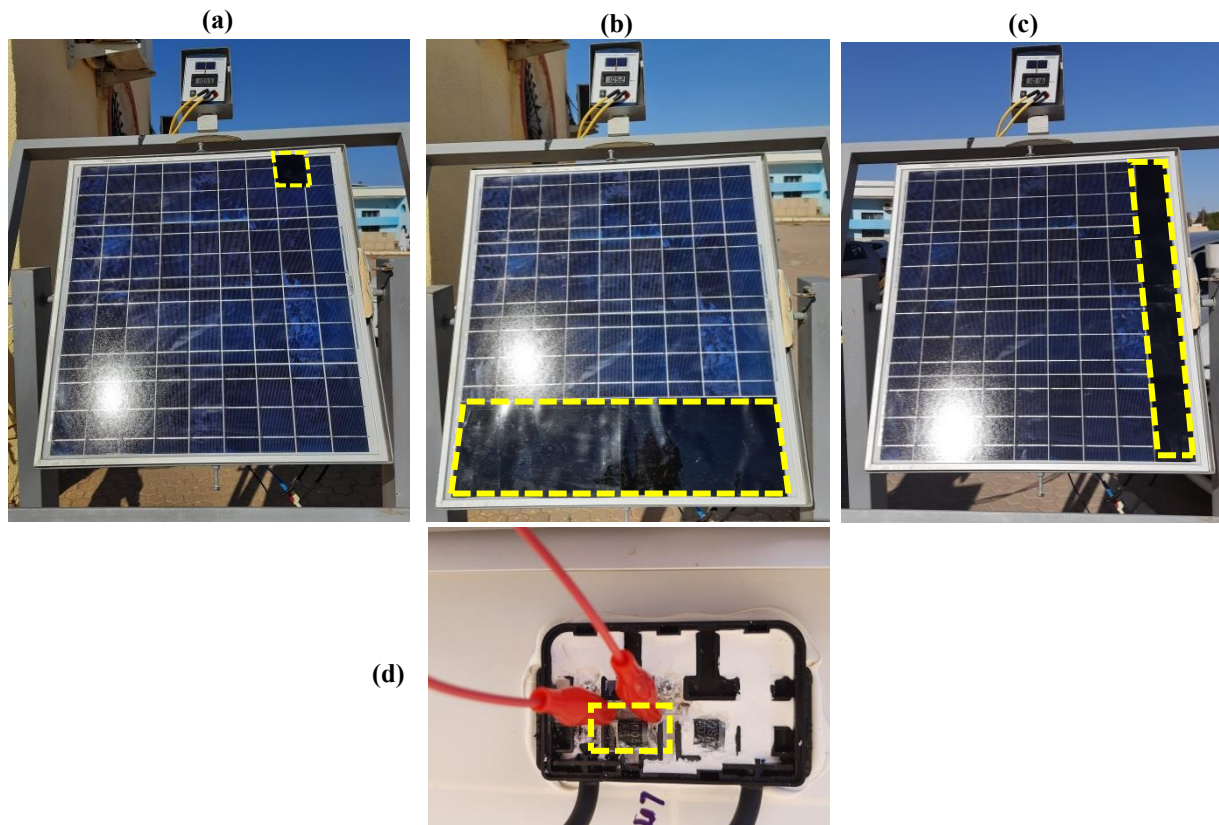


Figure 2.20: The investigated faults: (a) Shading 1 cell 50%, (b) Shading horizontal line of cells at 100%, (c) Shading vertical line of cells at 100%, (d) one diode by-pass short circuited.

B. Experimental SET-UP

To verify experimentally the diagnosis technique, as shown in Figure 2.21 a dSPACE DS1104 controller have been used as control platform since it enables the linking of the MATLAB/Simulink diagnosis simulated model to the experimental PV module. The electrical parameters generated by the faulty PV panel and the climatic parameters measured are read and then sent to the DS1104 board. After compiled the simulink model files with different extensions (SDF, PPC... etc.) are created and transferred automatically to DS1104 board.

Otherwise, the file with extension SDF appears in ControlDesk® which acts as a user-interface that we can use to control and monitor experiments.

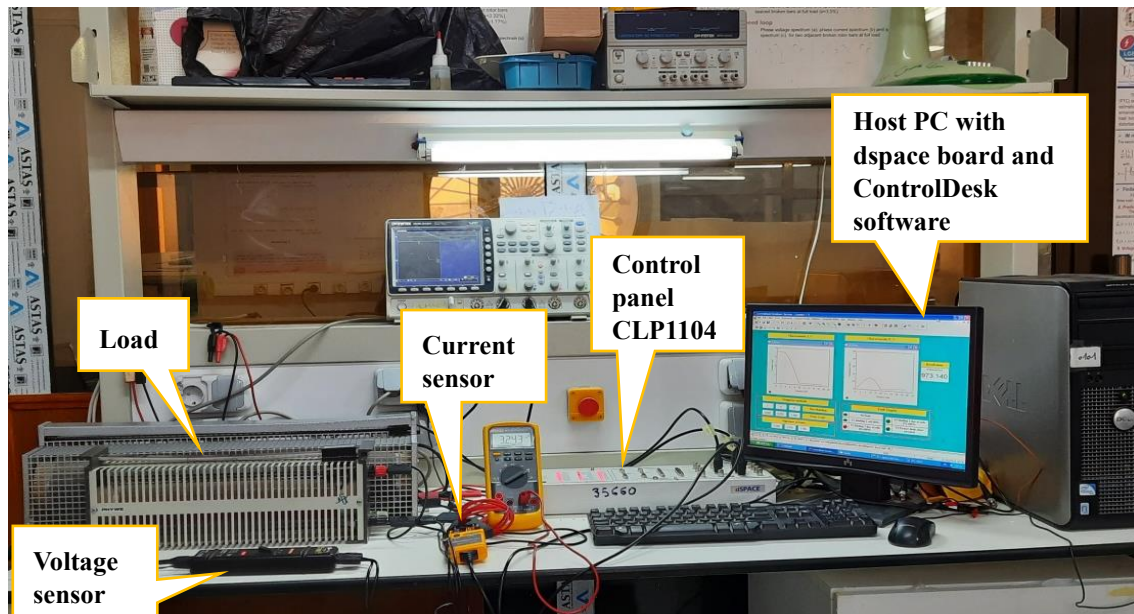


Figure 2.21: Experimental SET-UP.

2.3.2. Real-time Implementation: RESULTS AND DISCUSSION

This part presents the experimental diagnosis technique results for photovoltaic panel using only: The experimental database of climate (solar irradiance and temperature) and electrical parameters (voltage and current) of the faulty PV panel. The experiments have been carried out on temperature of 25 °C and irradiation of 1000 W/m². The proposed diagnosis technique is verified by the two different algorithms based on thresholding method and fuzzy logic method for the identification of four types of faults tested experimentally in a PV panel. To check the ability of the diagnosis technique, four types of faults are applied in an individual process on our PV panel. In Figure.2.22 the user-interface ControlDesk shows the Photovoltaic characteristics (I -V and P-V) for each faulty PV panel with the results of the two algorithms used, however the final signature of faults is also illustrated. To clearly indicate the type of fault, a display part is used to give its accurate location. As shown in Figure.2.22a and Figure.2.22b. The results of identification of the fault F1 and F2 by the thresholding method are the same combination of symptoms, which leads to automatic activation of the classification by the fuzzy logic method to classify the faults to different combination of symptoms. Hence, it can be clearly noticed that the two faults are detected and classified by the diagnosis technique, where the type of faults are indicated in the display part with a red LED. Figure.2.22c and Figure.2.22d show the results of identification of the fault F3 and F4. As can be seen, the faults have been

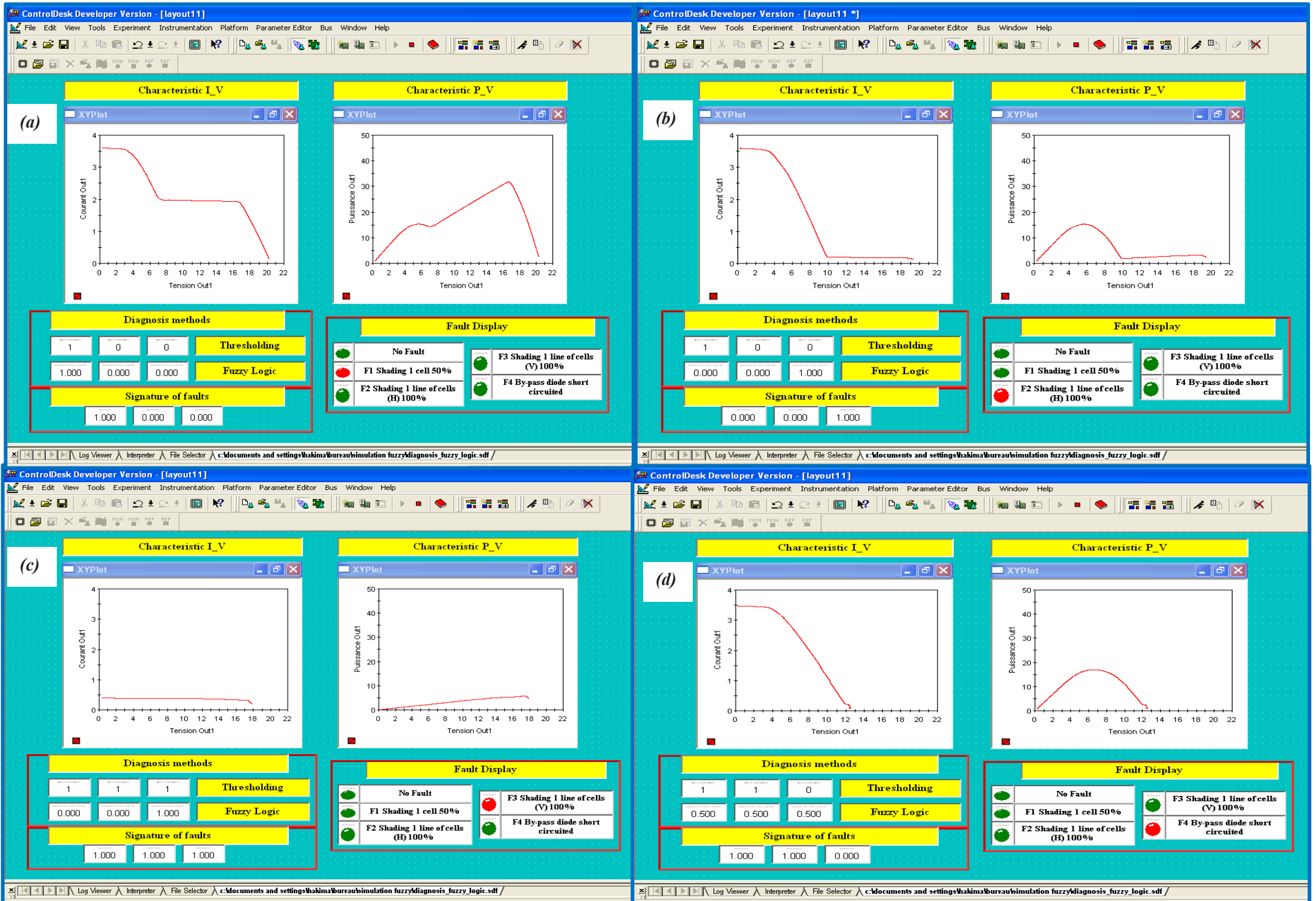


Figure. 2.22: The user-interface ControlDesk.

detected and classified by the thresholding method which gives a different combination of symptoms. Therefore, the diagnosis technique indicates in the display part the type of each fault.

2.4. Conclusion

This chapter presented both simulation and experimental approaches for fault detection and classification in PV panels using thresholding and fuzzy logic-based methods. In the simulation phase, eight types of faults were analyzed by comparing power, voltage, and current characteristics under normal and faulty conditions. While the thresholding method proved effective for some faults, it lacked the ability to distinguish all fault types, highlighting the need for a more advanced classification approach. The fuzzy logic method demonstrated superior diagnostic accuracy, successfully identifying all considered faults in a distinguishable manner.

The experimental phase validated the proposed diagnostic approach using real-world data collected from a PV panel at the LGEB Laboratory, University of Biskra. Implemented on the DS1104 platform and developed in Matlab/Simulink, the experimental results confirmed the efficiency of the fuzzy logic classification technique in accurately detecting and classifying various faults. Overall, the findings emphasize the effectiveness of fuzzy logic in PV fault diagnosis, offering a robust and reliable method for improving PV system performance.

Chapter 3

Diagnosis based on Artificial Neural Network: Simulation and real-time experimentation

3.1. Introduction

Fault detection and diagnosis in photovoltaic (PV) systems are essential for maintaining their performance, reliability, and longevity. This chapter presents a comprehensive approach to fault identification, classification, and localization using Artificial Neural Networks (ANN) through both simulation and experimental analysis.

In the first part, a diagnostic model is developed in Matlab/Simulink to simulate both normal and faulty conditions of a PV module. The model is designed to detect and classify five single- and multi-fault types of faults, including partial shading and bypass diode failures. Specifically, Fault 1 (F1) corresponds to 50% shading of a single cell in a subpanel, Fault 2 (F2) involves full shading of a horizontal line of cells, Fault 3 (F3) represents full shading of a vertical line of cells with open circuit fault, Fault 4 (F4) corresponds to a short-circuited bypass diode, and Fault 5 (F5) involves two short-circuited bypass diodes. The ANN-based fault detection method is trained to recognize patterns in voltage, current, and power variations, ensuring accurate fault classification.

The second part of this chapter focuses on the experimental validation of the proposed ANN-based fault detection technique. The same five single- and multi-fault types are introduced in a real PV module, and an experimental dataset of climatic and electrical parameters is collected. The developed ANN model is implemented in Matlab/Simulink and integrated with the dSPACE DS1104 controller to enable real-time fault diagnosis.

3.2. Description of Monitoring and Diagnosis PV System

The PV panel system under study was installed on LGEB Laboratory of the University of Biskra (Algeria). The actual system is shown in Figure 3.1. The PV system consist of mono-crystalline silicon module linked to a resistive load. The diverse data measurements are monitored such as module temperature and solar irradiance using a K-type thermocouple and Reference cell, outputs voltage and current which are measured by current and voltage sensors. These data collected is processed through a DS1104 controller board, seamlessly connected to a computer via a PCI slot. Employing the Matlab/Simulink® software alongside ControlDesk®. Collected data such as voltage, current, irradiance and temperature are displayed in a graphical and numerical form that creates using ControlDesk® user interface along with the state of the system. Figure 3.1 present the monitoring system.

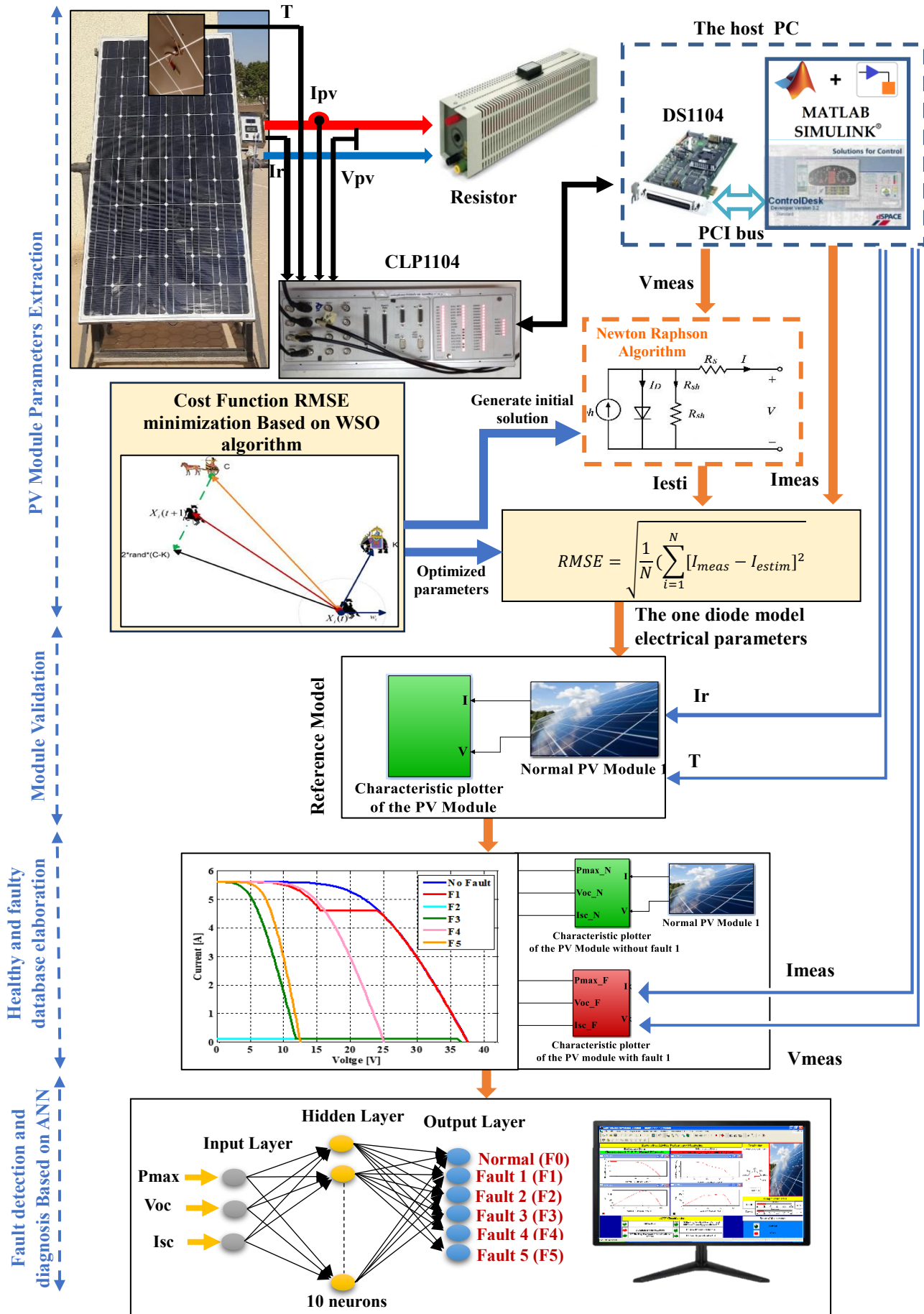


Figure. 3.1: Schematic Representation of the Electrical Configuration for the Experimental PV System.

3.2.1. Monitoring Unit

Firstly, the climatic-database of the experimental PV module which is solar irradiance and temperature are measured, which acts as inputs to the simulated PV module. Then, the difference between the experimental (Faulty) and the simulated (Normal or Reference) PV module electrical parameters were systematically compared to establish their relative effectiveness in fault detection. Subsequently, these parameters are classified using an Artificial Neural Network (ANN) algorithm to facilitate the detection and identification of faults in photovoltaic systems. The Figure. 3.2. presents the architecture of the realized monitoring with the PV system.

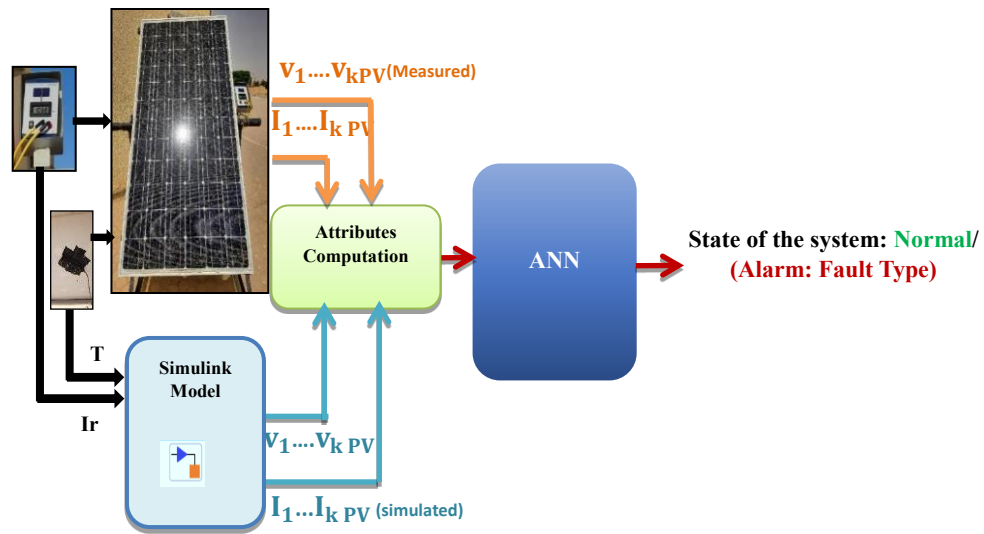


Figure. 3.2: Diagram Depicting the Proposed Monitoring and Diagnosis system.

3.2.2. Photovoltaic System Modeling

To assess the operational effectiveness of photovoltaic panels across different scenarios, the single diode model is commonly recognized as the predominant framework for elucidating the electrical characteristics of PV cells. The same strategy of PV module parameters extraction, which has been developed in chapter 2 utilizing the Newton-Raphson with the War Strategy Optimization (WSO) algorithm, is used to extract the set of five parameters ($I_{ph}, I_0, R_s, R_{sh}, n$) expounded in Table 3.1. This process exclusively relies upon the information intrinsic to the datasheet specific to the SUNTECH PV panel, characterized as mono-crystalline silicon and delineated in Table 3.1. It is observed that the extracted value of the shunt resistance is relatively low (1.5923Ω), indicating the presence of internal leakage paths within the PV cell. This may be caused by manufacturing defects, surface contamination, or aging effects. The low R_{sh} results in increased power losses and a reduced fill factor, which negatively affects the overall performance of the PV module. Notably, the configuration of this PV panel encompasses 72

photovoltaic cells, organized into groups of 24 cells, with each group featuring three bypass diodes in a bypass configuration, as visually represented in Figure 3.3.

Table 3.1. Electric Properties of the SUNTECH Photovoltaic Module

Electrical Propeties		Extracted Parameters	
Power at STC	123W	R_s	0.0259 Ω
V_{mp}	26.3 V	R_{sh}	1.5923 Ω
I_{mp}	4.80 A	I_{ph}	5.5580A
V_{oc}	38.29 V	I_0	2.3e-8A
I_{sc}	5.55 A	n	1.22
No. of cells in panel	72	RMSE	0.01807
No. of by-pass diodes	3		

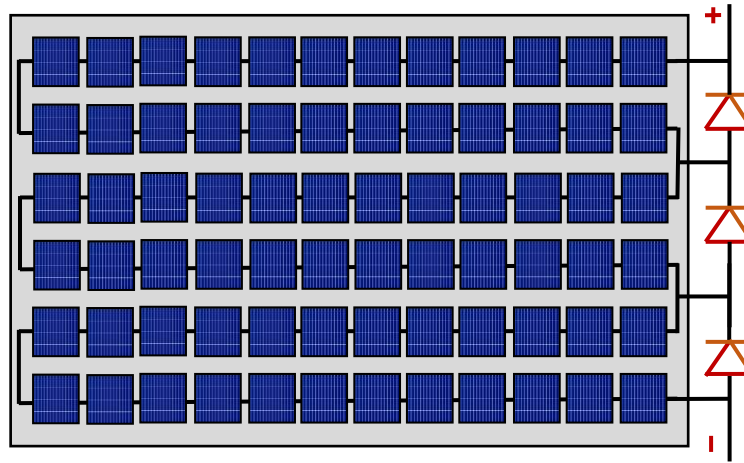


Figure. 3.3: PV module BP diode connections.

The Matlab/Simscape tool is then used to simulate a real PV panel under normal conditions using the identified parameters. before simulating the PV system to obtain accurate daily profiles of temperatures and irradiances. On the other side, Matlab/Simulink™ environment is used for data processing and the associated calculations. Finally, a comparison is made between the simulated and measured characteristics, in accordance with STC conditions, which provide for STC (25 °C and 1000 W/m²). Using Simulink/Matlab, the electrical I(V) and P(V) curves of a PV panel (simulation and experiments) are shown in Figures. 3.4 and 3.5. It has been noted that the simulated data is almost identical to the measured data, allowing for reliable PV module modeling. These graphs demonstrate that the electrical output characteristics of the simulated and experimental models are similar to those found in the PV module's datasheet. The curves display the highest power point determined by the data tips on the I-V and P-V curves, where P_{max} is equal to 123 (W), V_{mp} is equal to 26.3 (V), and I_{mp} is equal to 4.8 (A).

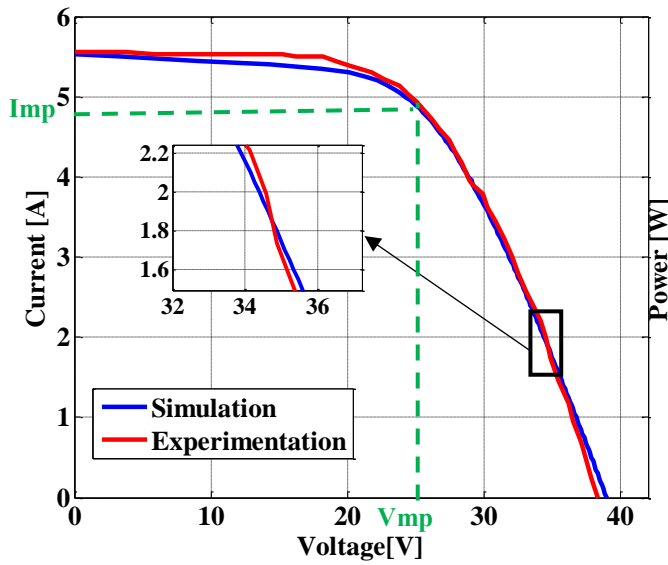


Figure. 3.4: I-V curve of a photovoltaic module under STC.

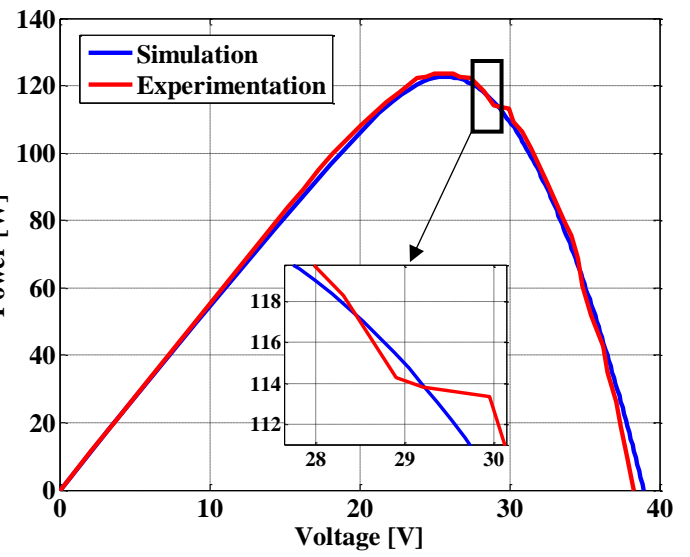


Figure. 3.5: P-V curve of a photovoltaic module under STC.

The reduced RMSE value (refer to Table 3.1) demonstrates the strong predictive capability of the WSO algorithm in identifying optimal parameter values. Additionally, the algorithm achieves this with a satisfactory convergence rate, as illustrated in Figure 3.6.

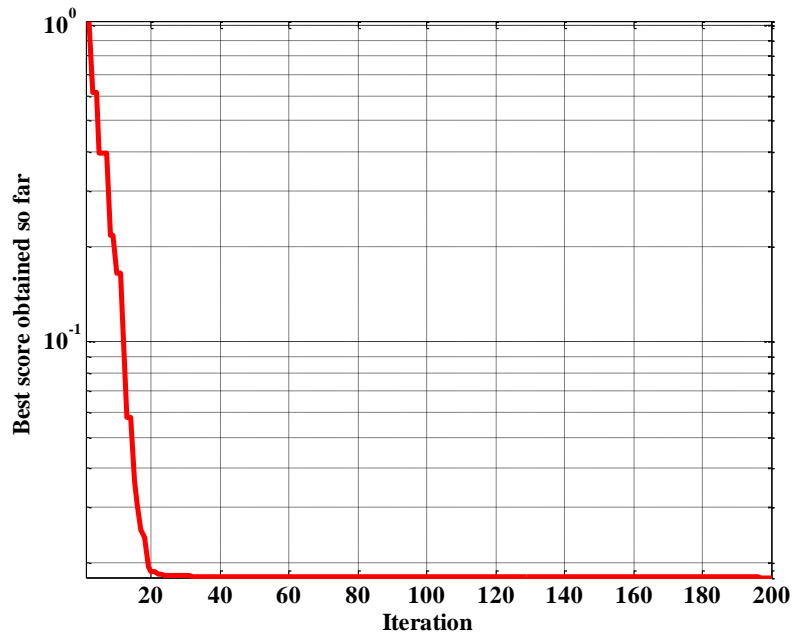


Figure. 3.6: Illustrates the convergence rate of the WSO algorithm during the parameter extraction process for PV module.

3.3. PV Faults

Five categories of faults have been identified in our photovoltaic module: Fault 1 refers to the shading of one cell in a subpanel at 50%, Fault 2 corresponds to the shading of a horizontal line of cells at 100%, Fault 3 refers to the shading of a vertical line of cells at 100% with open circuit of string of cells, Fault 4 refers to a short circuit in the bypass diode, and Fault 5 refers to a short circuit in two bypass diodes. The investigated faults are shown in Figure 3.7. The schematic representation of a photovoltaic panel exhibiting the five faults is highlighted in Figure 3.8.

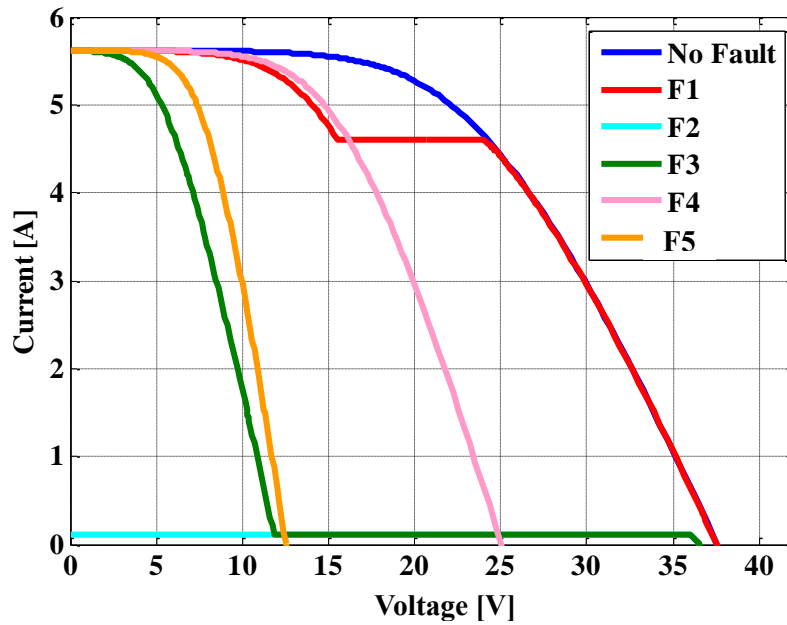


Figure. 3.7: The Investigated faults.

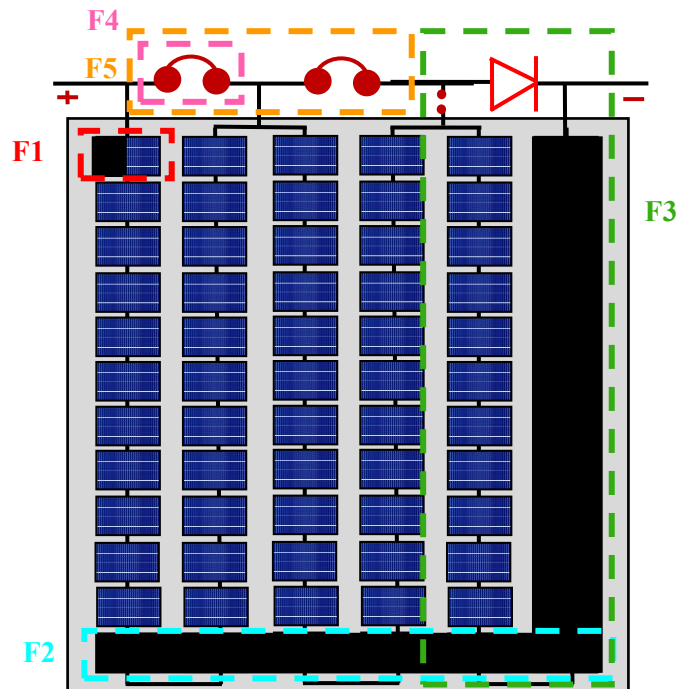


Figure. 3.8: Schematic representation of a photovoltaic panel exhibiting the five faults.

3.4. Implementation of the Artificial Neural Network Classifier

To make use of an Artificial Neural Network (ANN) it is important to develop a mechanism that imitates the structure and functioning of brain cells. In today's world ANN has proven its usefulness in fields such as pattern recognition, signal processing, modeling and computer vision. Within this thesis the Artificial Neural Network (ANN) is proposed. According to Figure 3.9 the ANN architecture consists of three layers:

- The input layer comprises three neurons representing the ratio between simulated and measured values of maximum power point current (P_{max}) open circuit voltage (V_{oc}) and short circuit current (I_{sc}).
- A hidden layer, with ten neurons that have chosen. *tansig* activation functions.
- The output layer contains six neurons representing five faults and the normal condition, which indicates a binary classification with a selected *purelin* activation function.

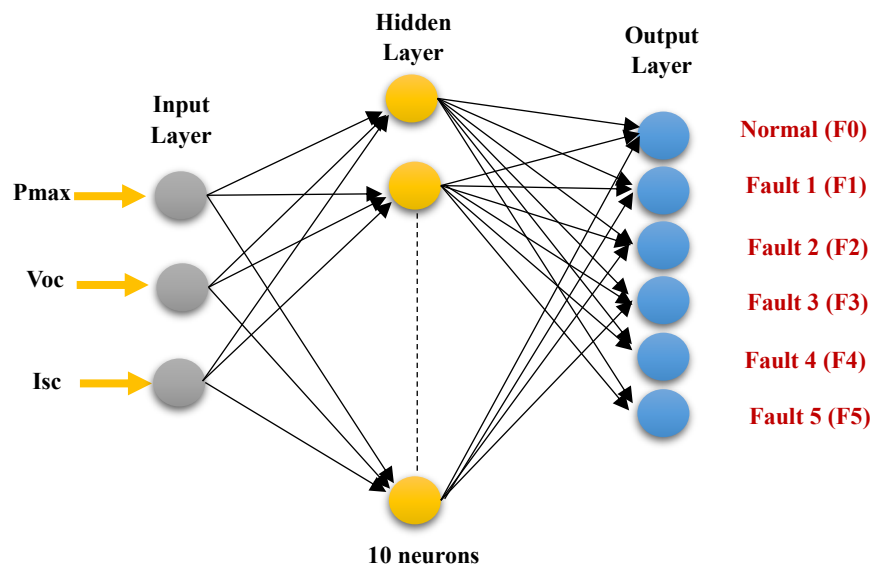


Figure 3.9: ANN configuration.

In this part, a Multilayer Perceptron (MLP) Feedforward Neural Network is employed as the network architecture. This MLP structure comprises a single hidden layer with 10 nodes, as depicted in Figure 3.10. The network undergoes training utilizing the Levenberg-Marquardt (LM) algorithm. The training dataset is generated from simulations that encompass both typical and fault-inducing operations for five distinct faults and the normal condition. Specifically, 70% of the patterns are allocated for training, while the remaining 30% are reserved for testing and model validation purposes.

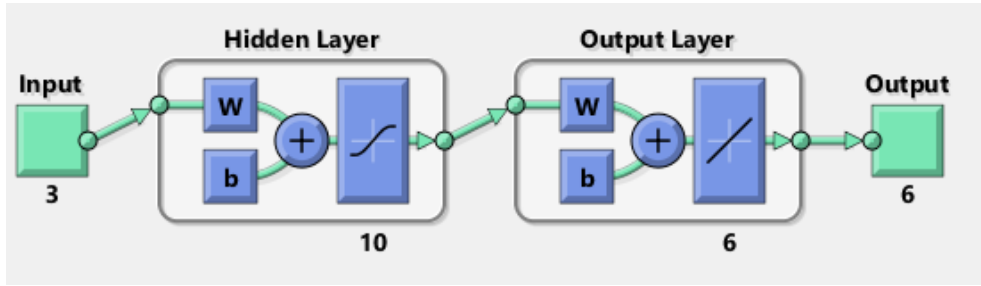


Figure 3.10: Schematic of the used ANN architecture.

3.5. Simulation results

To assess the proposed approach, a case study was conducted using MATLAB Simulink software. Data samples representing the distribution of three indicators were collected to generate input for the ANN model. The dataset consists of a total of $684 = (114 \times 6)$ samples, encompassing both standard conditions and five distinct fault scenarios. Each sample incorporates the three selected input indicators.

Figure 3.11 (a) Shows the minimum Mean Square Errors (MSE) variation concerning epoch for training, validating, and testing. Performance after training is 0.002 and the best validation performance is 0.00070178 after 33 iterations.

Generalization tests are aimed at assessing the neural network's performance and its ability to apply learned knowledge to new data. After the network's computation, it is essential to conduct tests to ensure that our network is providing accurate responses. The Figure 3.11 (b) illustrates the confusion matrix for the five faults including the normal case analyzed in the testing phase. The matrix cells that are colored green and red indicate the percentages of correctly and incorrectly classified faults, respectively. The confusion matrix provides the precision measurement for the training of the ANN fault detection and diagnosis model. It's noteworthy that a notably high precision rate of 99.7% has been achieved for the ANN diagnosis model. This result signifies the well-informed selection and effective training of the ANN model in detection and classification.

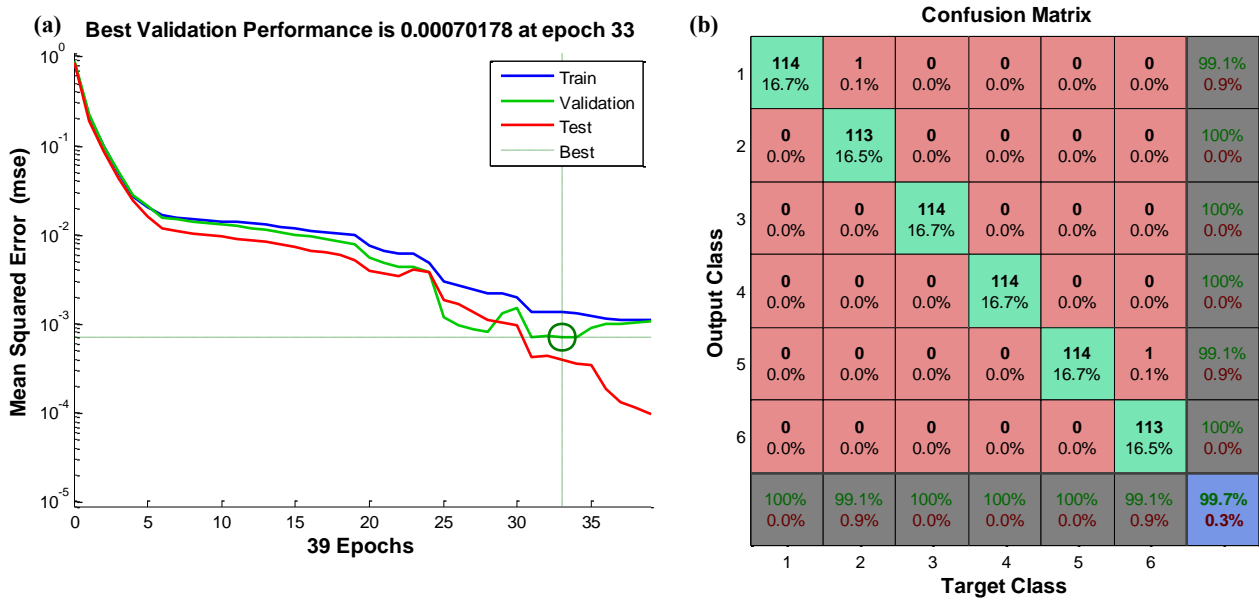


Figure 3.11: (a). Progression of Mean Squared Error (MSE) for the MLP Network. (b). Confusion Matrix for Classification in the MLP Network.

Figure 3.12 illustrates the outcomes of implementing fault 2, "Shading Horizontal line of cells at 100%" using simulation blocks. The simulation results validate the proposed approaches efficacy in detecting and classifying faults based on various symptom combinations. Notably, ANN categorized the fault by displaying "1" in the second output, corresponding to F2, and "0" in the remaining outputs. Upon fault detection and defect classification, a message is displayed in the command window to inform the user about the system's fault type.

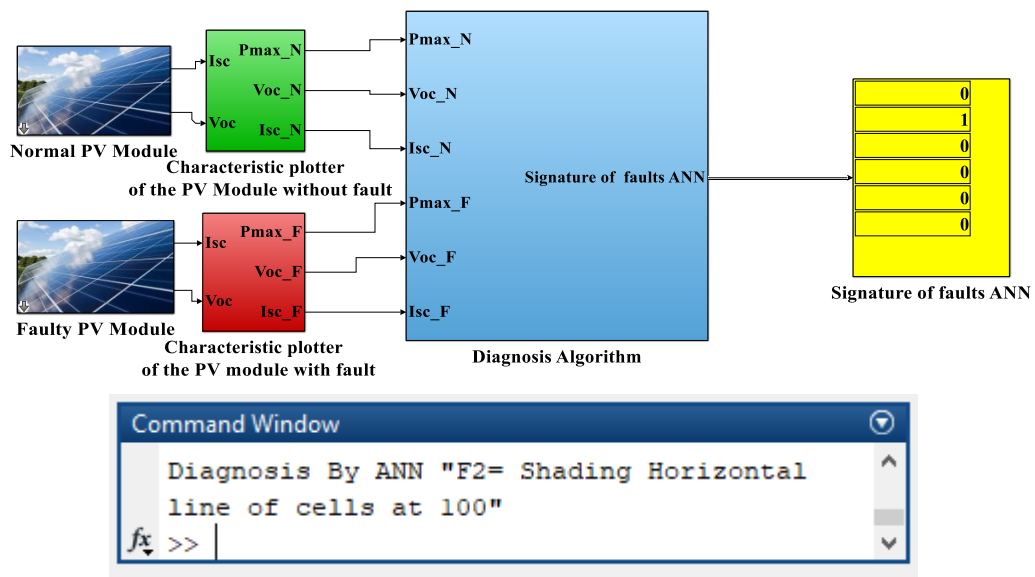


Figure 3.12: Detection and classification of Fault 2.

3.6. Experimental Validation

To prove the effectiveness of the proposed real-time monitoring and diagnosis system a laboratory experimental test bench is built.

First, this developed test bench is presented with its associated user interface, then the experimental results will be presented and analyzed. A commercial current and voltage monitor is used to acquire measurements. Figure 3.13 shows the investigated cases for the real PV panel: Normale operation and various faults mentioned in section 3.3, for implementing the shading fault (see Figure 3.13), the shaded module is conducted by covering the cells with a physical solid opaque.

The developed user interface is shown in Figures 3.14-3.19. The developed program is performed and allows the data acquisition of all the measured signals through the current and voltage PV monitor board. Furthermore, this interface allows real time visualization and presentation of these signals, as well as the presentation of different curves (power, current, voltage..., etc.) and the state of the system, detected and the classified faults. Several tests have been performed on the PV panel at measured temperature 25 °C and measured irradiation 1023W/m².

The Figure 3.14. illustrates the current-voltage (I-V) characteristic of the photovoltaic (PV) panel under typical operating conditions. Within this context, the observed I-V curve closely aligns with the anticipated performance, suggesting conformity between measured and estimated values. Specifically, parameters such as P_{max} (maximum power output), V_{oc} (open-circuit voltage), and I_{sc} (short-circuit current) exhibit consistency, denoting normal operation. This alignment is symbolized by the presence of a green LED indicator on the user interface, affirming normal functioning.

When the shading fault occurs (F1); in this case, the measured short-circuit current is the same with the estimated short-circuit current. Furthermore, the measured open-circuit voltage and measured maximum power output decrease of estimated values as shown in the Figure 3.15. The analysis demonstrates a direct correlation between the percentage of shading impacting the cell and the reduction in P_{max} and V_{oc}. This correspondence is further affirmed by the presence of an alarm with a red LED indicator on the user interface, symbolizing the panel's faulty functioning and indicates in the display part the type of fault. In fault 2, where three sub-strings are partially shaded, three bypass diodes are activated. Depending on the severity of the shading fault, scenario emerge: simultaneous conduction of diodes and the occurrence of a single

voltage peak (see Figure 3.16) leads to activate the alarm, identifies the type of fault with a red LED.

Figure 3.17 depicts the shading setup, wherein a vertical line of PV cells experiences partial shading at 100% with open circuit in string of cells. Shading of cells triggers the activation of one bypass diode, and the open circuit leads to the activation the second bypass diode, thereby deactivating the affected sub-strings. This phenomenon is corroborated by the sharp voltage variation resulting from the loss of this sub-strings, with the current value being directly proportional to the degree of shading (see Figure 3.17). The applied technique activates the alarm system and signals the specific fault type through a red LED indicator.

A short circuit diode defect (Figures 3.18 and 3.19) investigates two distinct scenarios: the short-circuiting of a single bypass diode and the short-circuiting of two bypass diodes. Both scenarios result in a reduced open-circuit voltage (V_{oc}) in comparison to the reference curve. Therefore, it is evident that the diagnosis technique is responsible for the detection and classification of the two defects. The display part of the interface indicates the type of fault with a red LED.

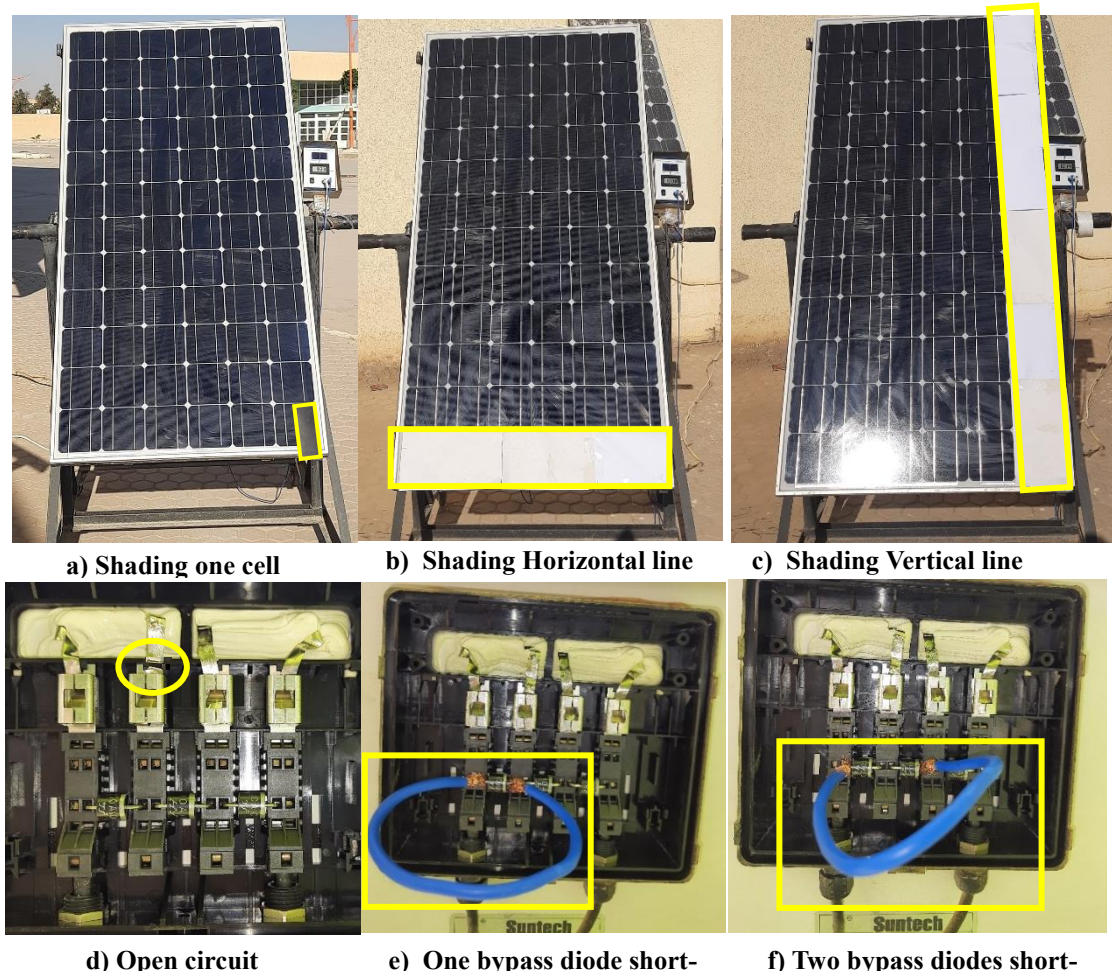


Figure 3.13: The investigated faults.

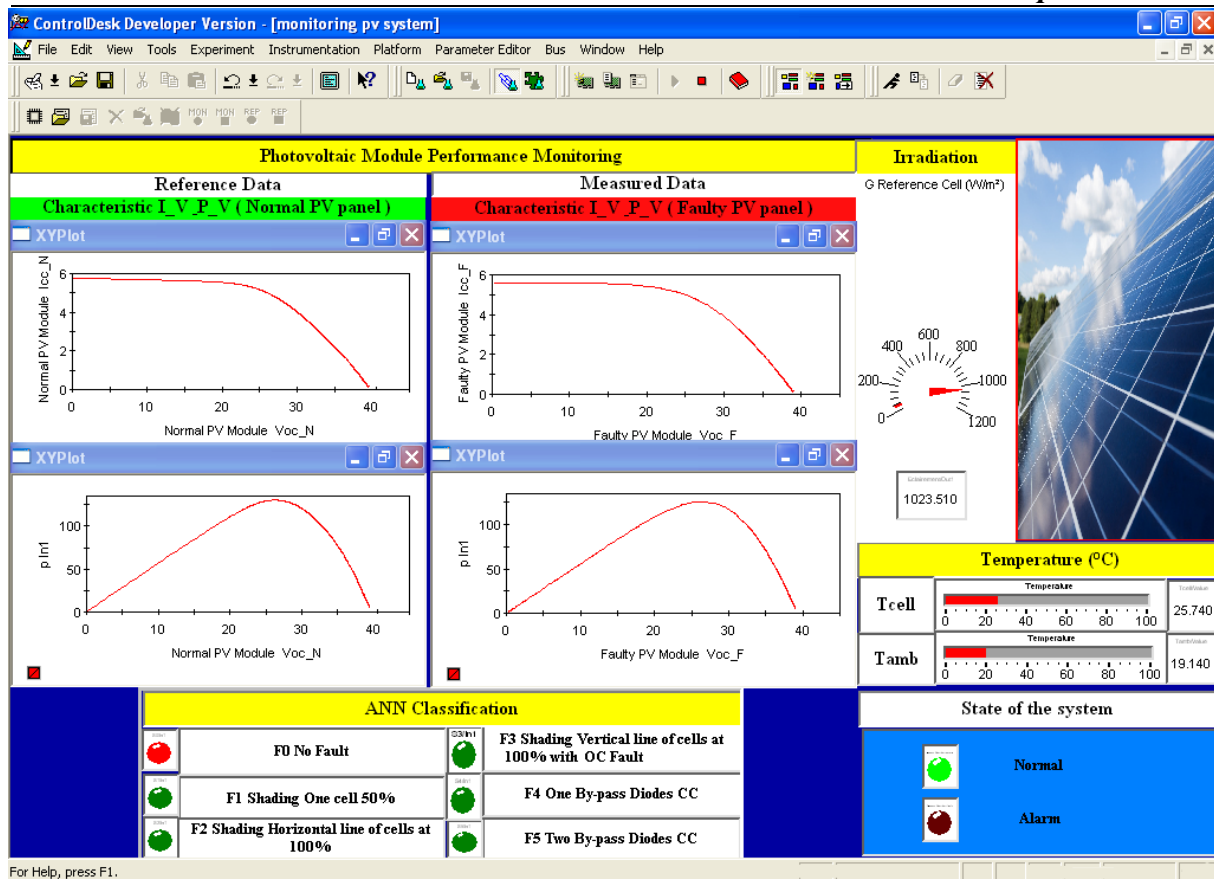


Figure 3.14: The ControlDesk User Interface Presents Real-Time Measurement Data in the Monitored PV Panel (Normal operation).

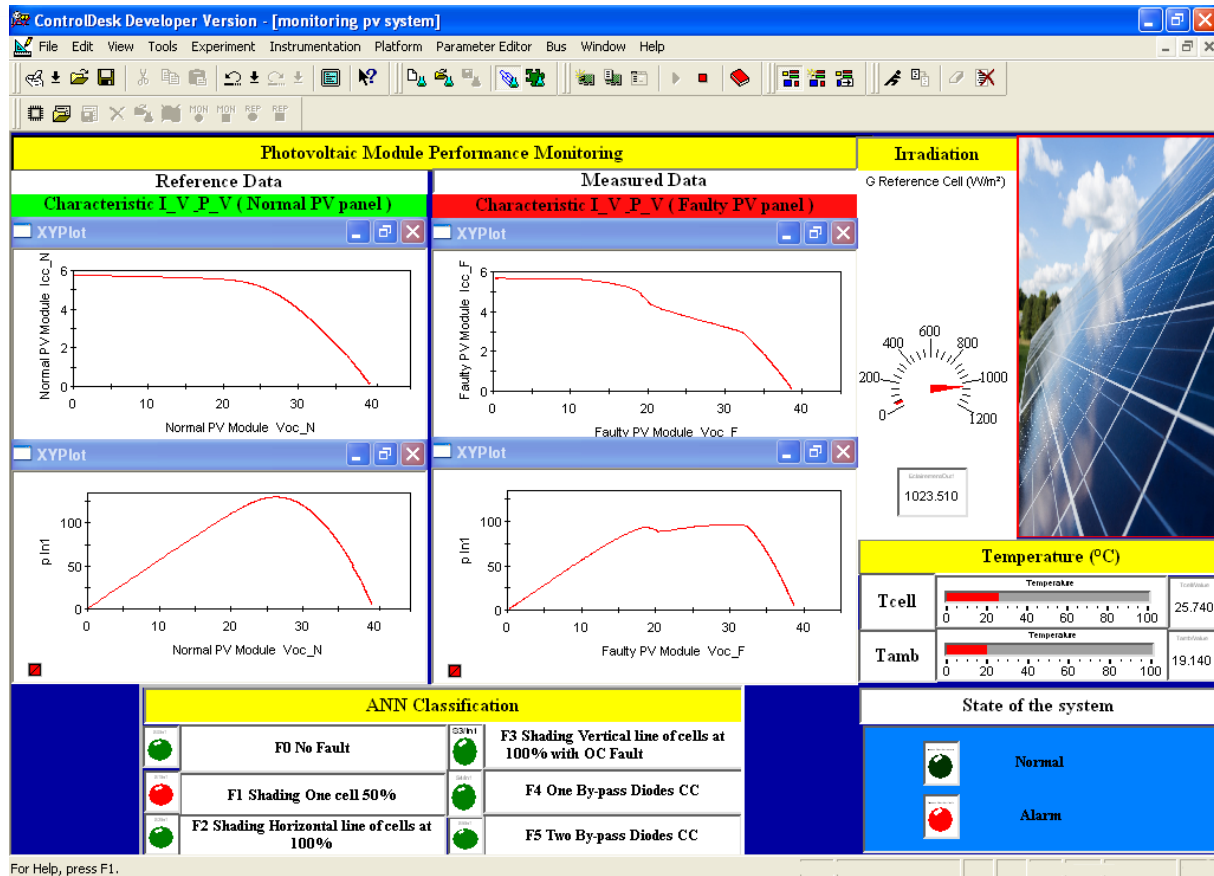


Figure 3.15: The ControlDesk User Interface Presents Real-Time Measurement Data in the Monitored PV Panel: Fault 1

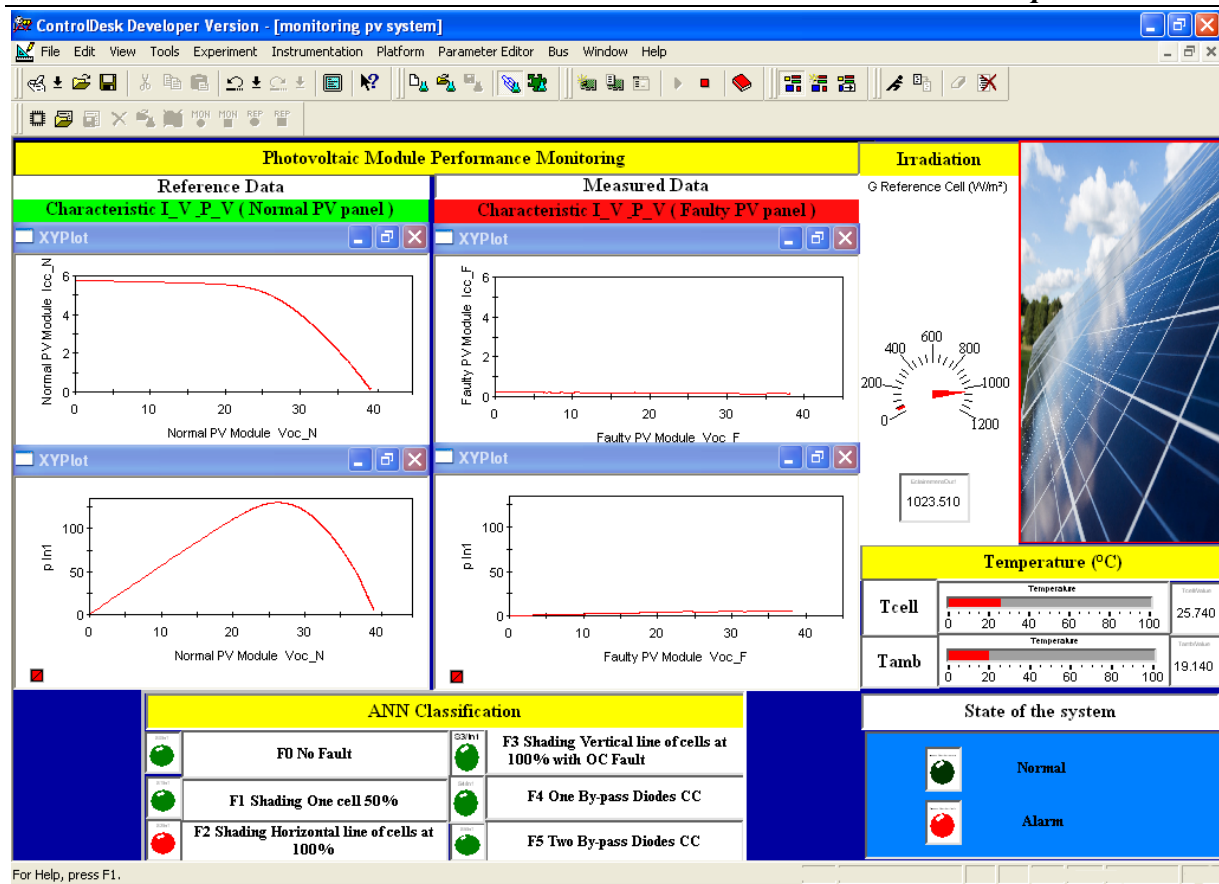


Figure 3.16: The ControlDesk User Interface Presents Real-Time Measurement Data in the Monitored PV Panel: Fault 2.

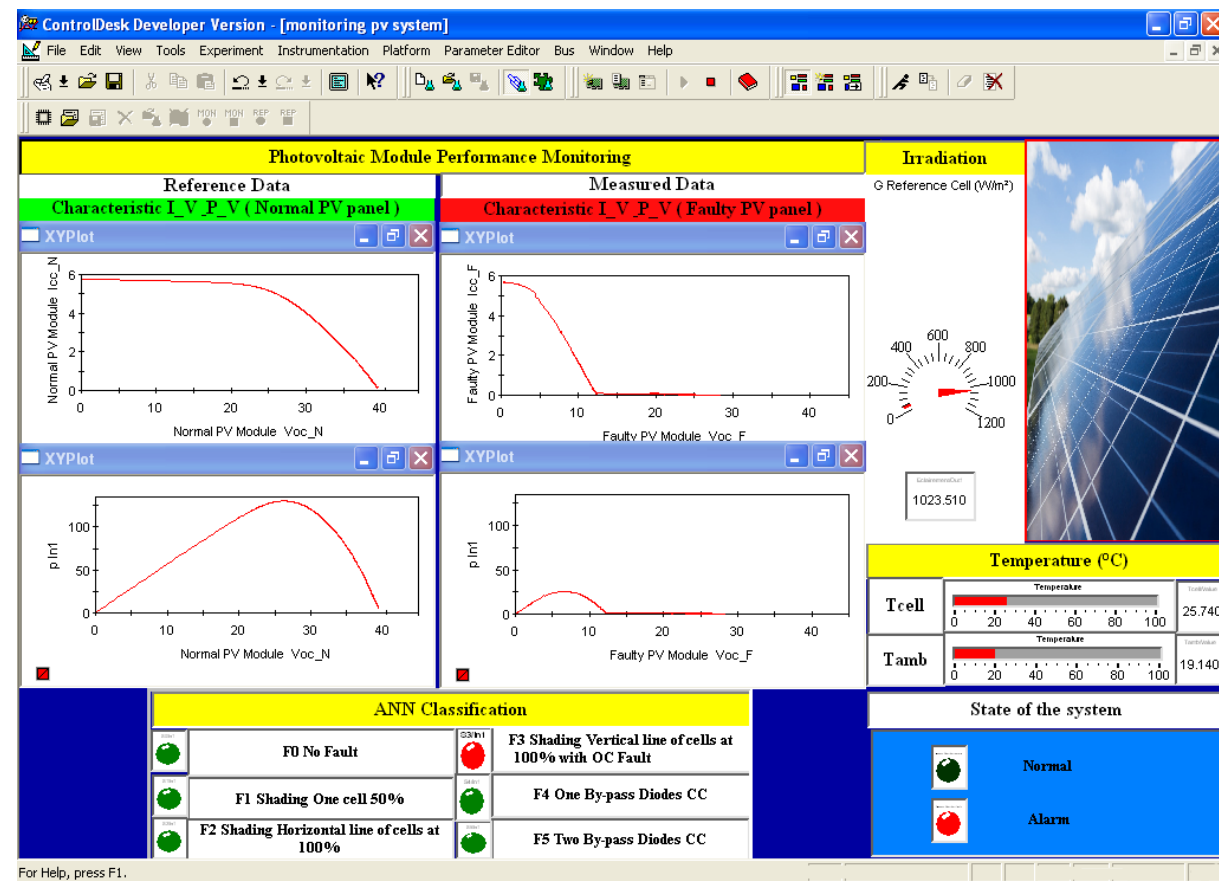


Figure 3.17: The ControlDesk User Interface Presents Real-Time Measurement Data in the Monitored PV Panel: Fault 3.

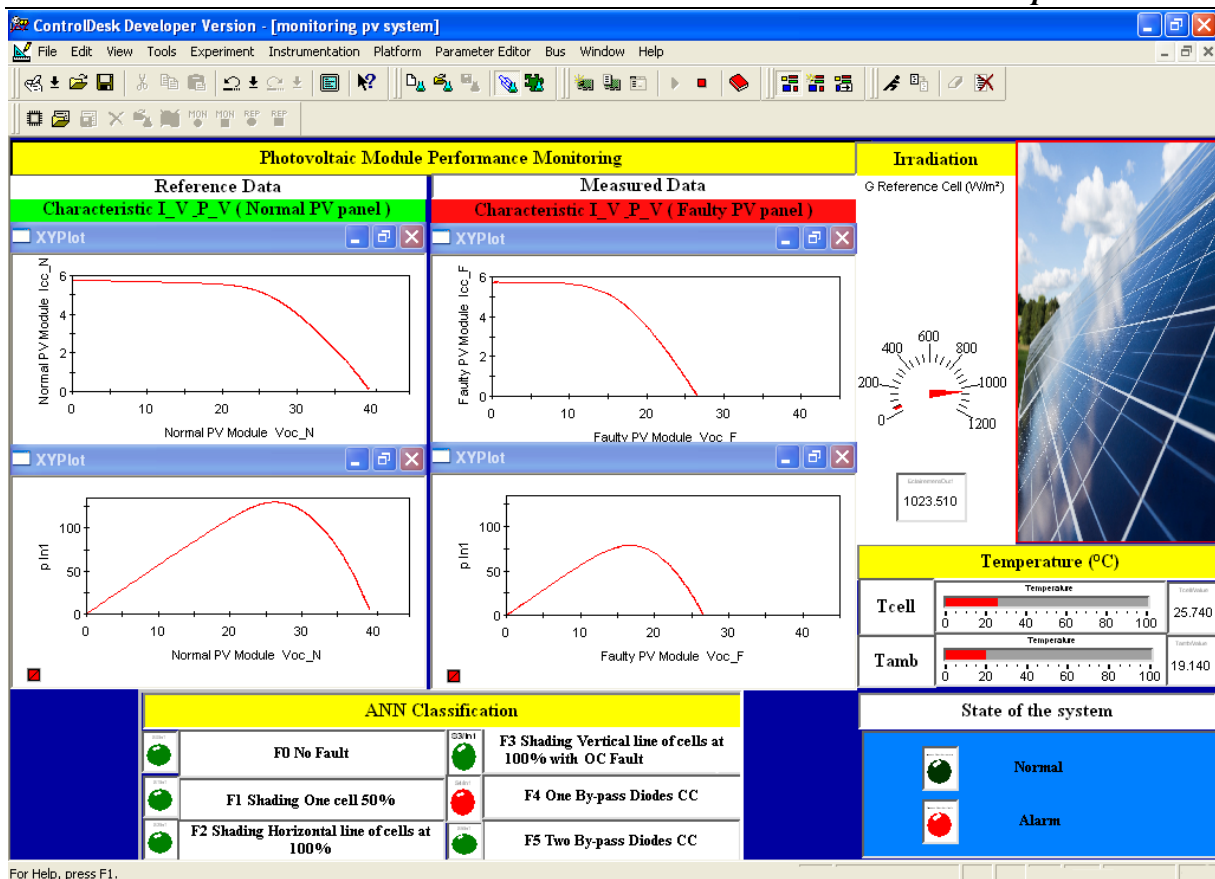


Figure 3.18: The ControlDesk User Interface Presents Real-Time Measurement Data in the Monitored PV Panel: Fault 4.

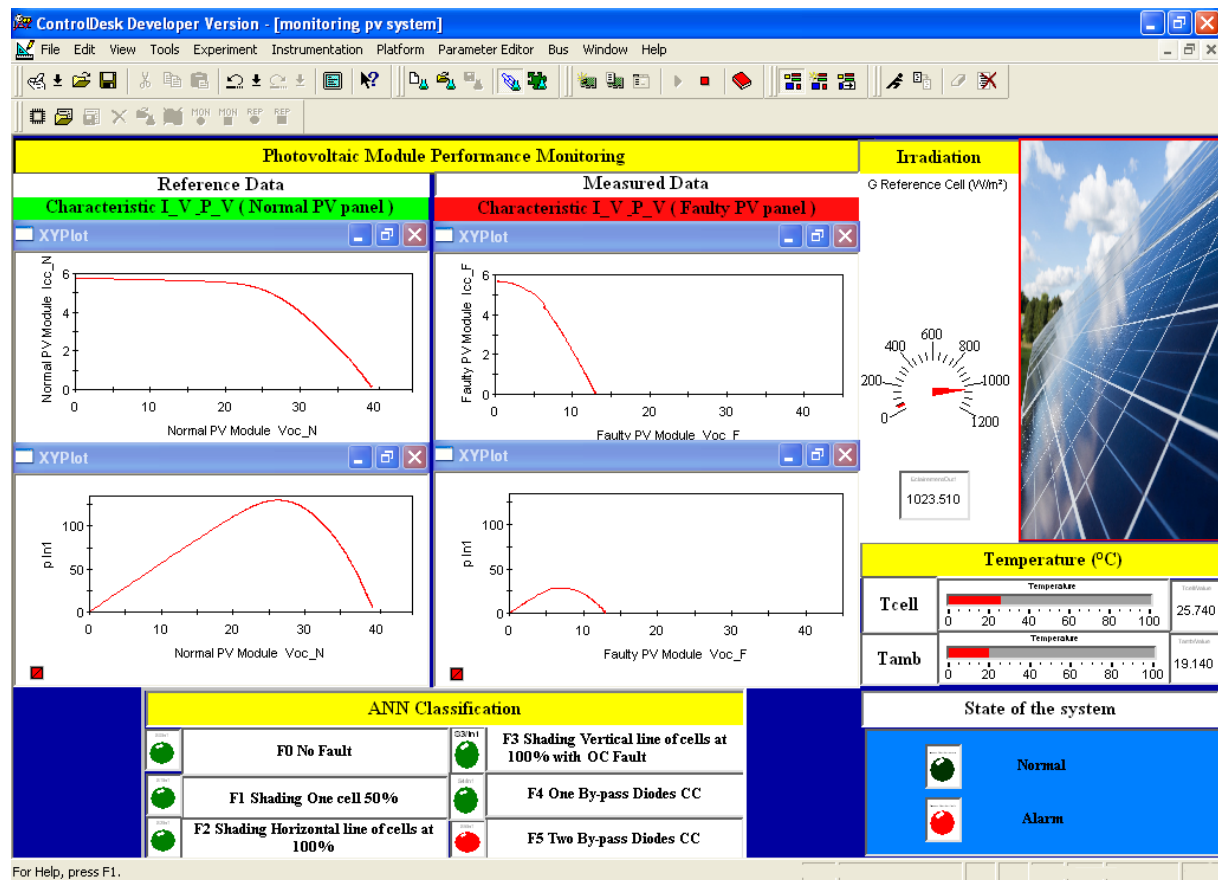


Figure 3.19: The ControlDesk User Interface Presents Real-Time Measurement Data in the Monitored PV Panel: Fault 5.

3.7. Conclusion

In this chapter, an Artificial Neural Network (ANN)-based fault detection and classification approach was successfully implemented and validated through both simulation and experimental analysis. Five distinct single- and multi-fault types of faults, including partial shading, open circuit and bypass diode failures, were applied to a PV module, and their effects were analyzed using voltage, current, and power variations. The simulation results demonstrated the effectiveness of the ANN model in accurately identifying and classifying all faults. Furthermore, the experimental validation, conducted using real PV module data and implemented through dSPACE DS1104 controller, confirmed the model's robustness and reliability. The ANN-based method achieved an impressive classification accuracy of 99.7%, proving its efficiency in detecting PV faults under varying conditions.

Chapter 4

Comparative Study of Real-Time Photovoltaic Fault Diagnosis: Fuzzy Logic and Neural Network Approaches

4.1. Introduction

Solar photovoltaic (PV) systems are becoming increasingly popular for renewable energy production. However, due to environmental and operational conditions, various faults can occur in PV modules, which can cause a significant reduction in system performance. This chapter proposes the use of two different methods, Fuzzy Logic (FL) and Artificial Neural Networks (ANN), for the real-time diagnosis of single and multi-type PV faults. The performance of these methods is compared both in simulation and experimentation. The simulation was conducted using MATLAB/Simulink, while the experiment was conducted using dSPACE DS1104 platform in order to implement the diagnosis model developed in Matlab/Simulink® software. The proposed methods have been validated using an experimental database of meteorological and electrical characteristics from a PV panel located at LGEB Laboratory of the University of Biskra (Algeria), for six different fault types, including shading, soiling, and by-pass diode faults.

4.2. Explanation of the Photovoltaic System and the Strategy for Detecting and Diagnosing Faults

4.2.1. PV system description

This section undertakes the examination of fault detection within an experimental photovoltaic (PV) panel installed at LGEB, University of Biskra, Algeria. The schematic representation of the electrical setup of the PV system under experimental conditions is presented in Figure 4.1. The validated PV system model, detailed in chapter 3, forms the basis for generating databases that capture the performance of the PV system under real outdoor conditions. Utilizing daily solar irradiance and module temperature profiles, this PV model is employed to create datasets comprising both optimal operation and intentionally simulated faults. The physical model of the PV system is implemented in the Matlab/Simulink® software platform. Subsequently, the values of the unknown parameters obtained under reference conditions are integrated into the physical PV array model.

The final stage of the proposed fault detection and localization strategy involves applying the ANN and FL, thereby facilitating the observation of the implemented diagnostic technique in the simulation.

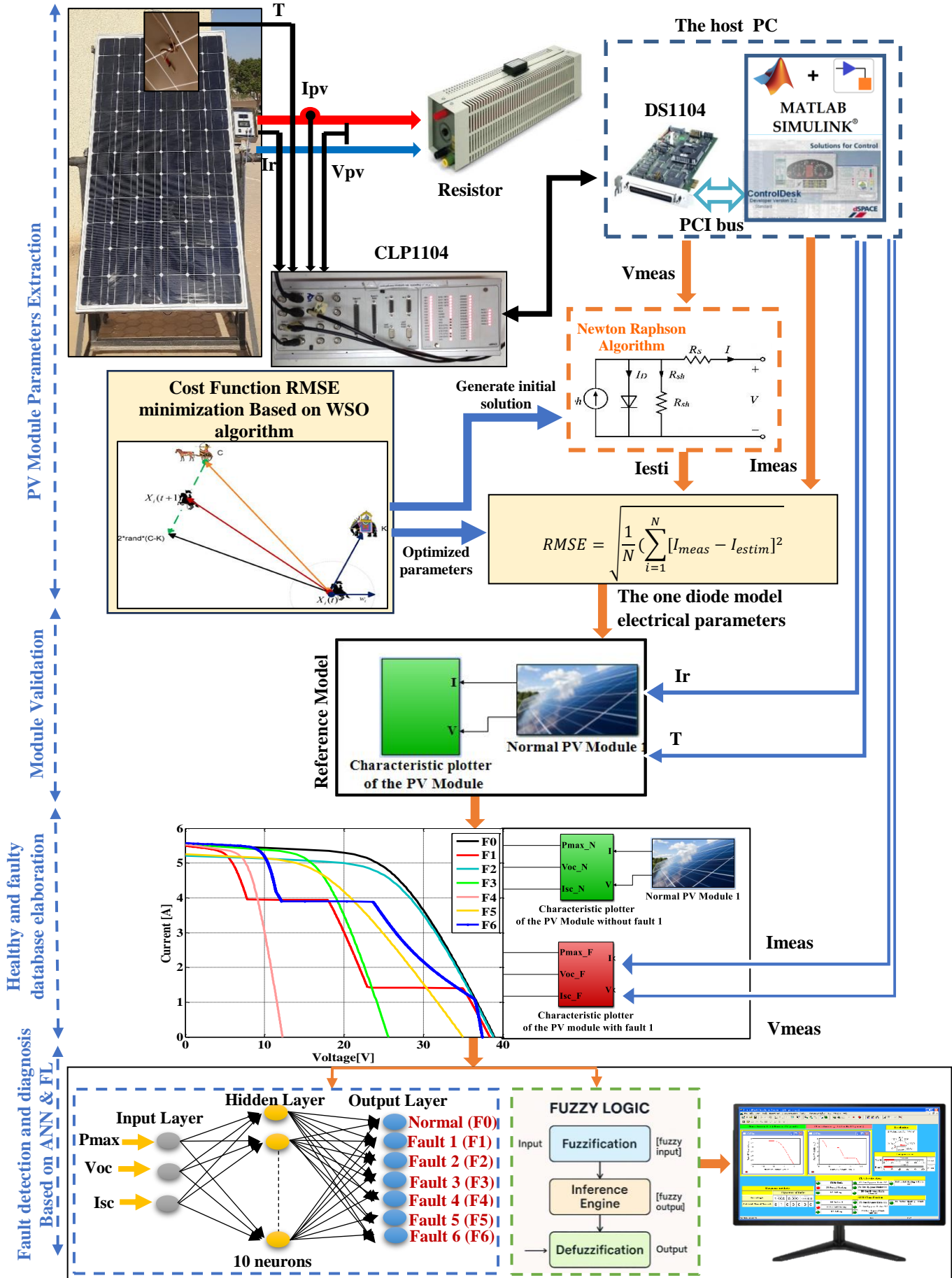


Figure. 4.1: Schematic representation of the electrical configuration for the experimental PV system.

4.2.2. The Implemented Diagnosis Technique

4.2.2.1 PV Module Faults

The main issues, with PV systems usually arise from the PV array inverter, storage system and electrical grid. The objective of this part is to pinpoint the faults that occur in the PV array. Six different faults are explored, as referenced in Table 4.1, and a schematic representation is depicted in Figure 4.2. Constructing a database on the faulty behavior of a PV panel requires creating a causal relation between faults and symptoms obtained from the I-V characteristic of the panel source. To accomplish this, a series of simulations must be carried out to obtain a complete list of the fault scenarios considered, as shown in Figure 4.3. Symptom S1 represents the reduction of the maximum power of the PV module, symptom S2 represents the reduction of Voc of the PV module and the symptom S3 describe the reduction of Isc of the PV module.

Table 4.1 Various categories of faults selected for the diagnosis.

Symbol	Types of faults
F1:	Shading of a cell of the subpanel 1 at 75% and another of the subpanel 2 of the PV module at 25 %.
F2:	Soiling.
F3:	One By-pass diode short circuited.
F4:	Two By-pass diodes short-circuited.
F5:	One by-pass diode shunted ($R_{sh} = 2\Omega$).
F6:	Shading of a cell of the subpanel 1 at 25% and another of the subpanel 2 of the module at 75 % with By-pass diode disconnected.

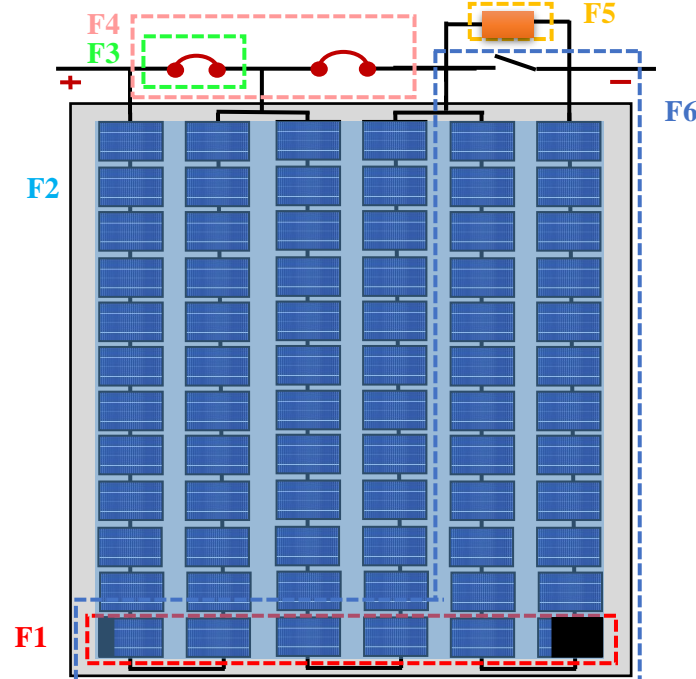


Figure. 4.2: Schematic representation of the six faults.

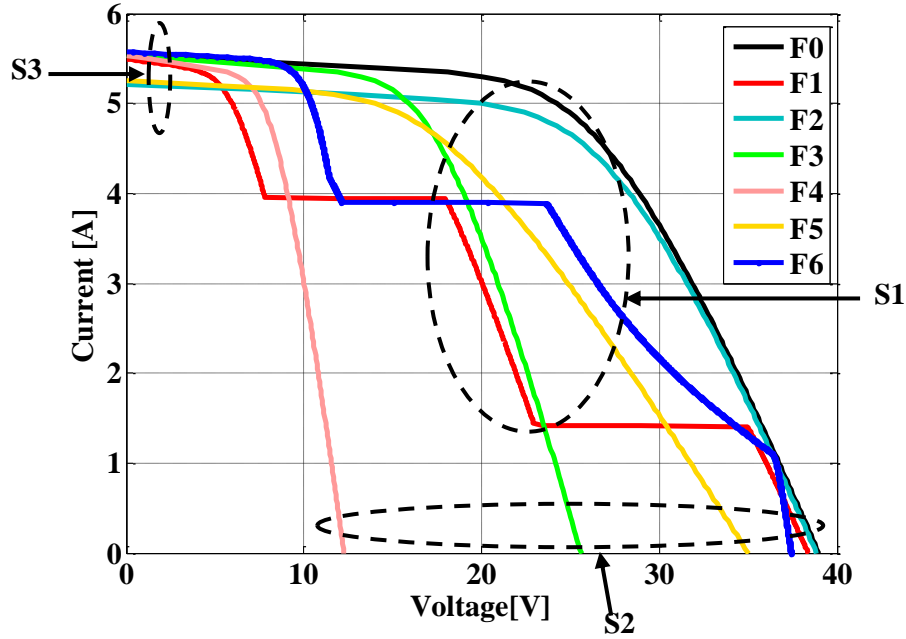


Figure 4.3: I-V Performance for various types

In this section, six faults of the PV module have been selected, as outlined in Table 4.1. To accurately model both the operational state and various fault scenarios within the PV array, a flexible fault simulation has been developed using a Simulink-based model, as depicted in Figure 4.3. The simulation enables the emulation of shading by adjusting the irradiance input to the relevant PV cells. Similarly, soiling can be simulated by modifying the irradiance input for all PV cells. For the simulation of short-circuit diode faults, wires are connected between the bypass diodes. Meanwhile, to simulate shunted diode faults, a parallel resistor (R_{sh}) with a value of 2Ω is added along with a bypass diode. Shading and bypass diode disconnection faults can also be simulated by manipulating the irradiance input to the relevant PV cells and disconnecting the bypass diode.

The datasets required for this study are directly obtained from the PV Simulink model under both faulty conditions, while varying parameters such as solar radiation (I_r) and temperature (T). During data generation, temperature is increased in increments of ten degrees Celsius from 0°C to 80°C , while solar irradiance is varied in increments of 50W/m^2 , ranging from 0W/m^2 to $1,100\text{W/m}^2$. Consequently, a total of 102 sets of samples is generated.

In each simulation, a single fault is considered, and the I-V characteristic resulting from this simulation is analyzed to determine the symptoms that can be used to identify the nature of the fault using two different methods, Fuzzy Logic (FL) and Artificial Neural Networks (ANN).

4.2.2.2. Photovoltaic System Fault Detection

In this part, the work consists of developing an algorithm to discriminate all the chosen defects. For this purpose, two methods, including their treatment concept have been applied. The first is a combined method based on threshold detection and the Fuzzy Logic approach of each symptom, which subsequently gives binary signatures (in the form of 1 and 0) as fault detection, the second method, is based on an Artificial Neural Network. The approach used for each of these methods can be summarized in the block diagram in Figure 4.4. It is used to obtain the signature for all the defects considered in our study, by simulating each defect separately from the other (Singular defects).

As depicted in Figure 4.5, the simulated diagnostic photovoltaic (PV) system comprises two SUNTECH PV modules, each module includes 72 solar cells and three by-pass diodes. In the initial phase, the simulation encompasses the characterization of both a reference PV panel, representing a healthy module, and a tested PV panel subjected to various fault conditions. Subsequently, three critical parameters (P_{max} , V_{oc} , I_{sc}) are extracted from each I-V curve. In the subsequent step, a diagnostic algorithm is employed to detect and classify PV faults, utilizing two distinct approaches: a combined method involving thresholding and a fuzzy logic classifier, as well as the utilization of an Artificial Neural Network.

The difference between predicted and measured values is used as a fault indicator. The fault diagnosis process will next be initiated and the alarm will trigger according to the identified fault category. Each malfunction produces a distinct set of symptoms that are identified and then displayed in the yellow blocs with a message on the Command Window to indicate the fault type (Fault F1), as depicted in Figure 4.6. Matlab/Simulink was used to apply the configuration shown in Figure 4.5.

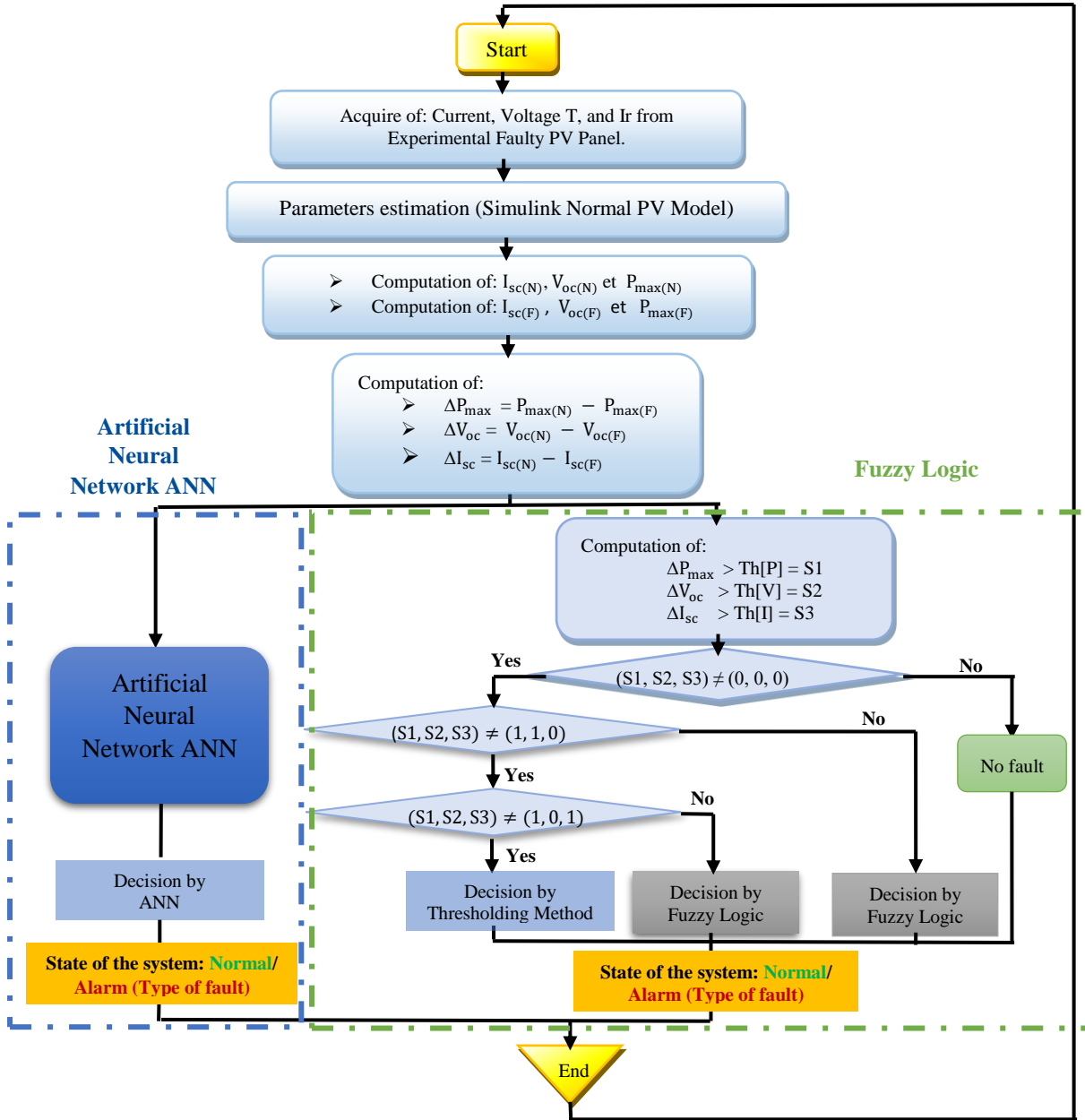


Figure 4.4: The proposed fault diagnosis technique.

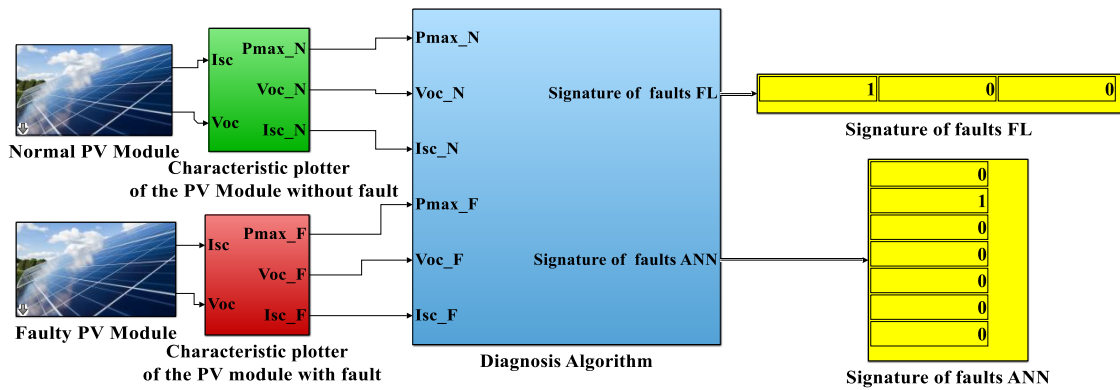


Figure 4.5: Photovoltaic System Fault Detection.

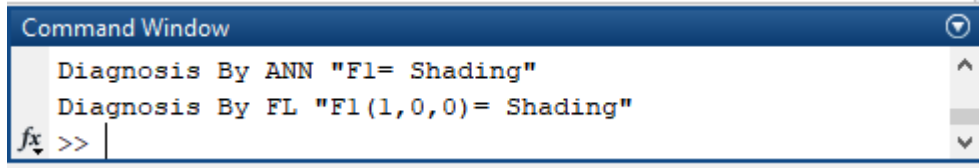


Figure 4.6: Result of the first fault, presented within the command window.

A. Thresholding method and Fuzzy Logic classifier

In this section, Figure 4.5 is analyzed to extract three parameters (P_{max} , V_{oc} , I_{sc}) from the I-V curves of both the standard and defective modules. The derived parameters are subsequently compared to calculate (ΔP_{max} , ΔV_{oc} , ΔI_{sc}). In the following step, these acquired parameters are compared with three relative errors accounting for potential deviations in measurement precision and modeling accuracy in power, voltage, and current. The standard IEC 61724 [97] prescribes a tolerance of 2% for power measurements, 1% for voltage measurements, and 1% for current measurements. Furthermore, the uncertainty inherent in the model is influenced by industrialization tolerances and sensor-related noise, as detailed in [33]. To incorporate this variability, a dispersion parameter is introduced into the simulation model parameters to calculate the allowable error. The relative errors for power, voltage, and current are determined as 5%, 3%, and 6%, respectively. Successful detection of defects is confirmed when these predefined thresholds are surpassed.

As shown in Table 4.2, three categories of defects can be identified using the threshold method:

Table 4.2 The distinctive signature of faults following the application of the threshold technique.

Groups	Fault type	Symptoms [S1, S2, S3]		
1	[F1]	S1=1	S2=0	S3=0
2	[F2, F6]	S1= 1	S2=0	S3 =1
3	[F3, F4, F5]	S1=1	S2=1	S3=0

According to these findings, the first algorithm is incapable of distinguishing between defects (F2, F6) and (F3, F4, F5), which share the same combination of symptoms. Therefore, a highly efficient classification method is required to identify these faults. In the next step, a diagnosis algorithm based on the Fuzzy Logic approach is used to detect and classify PV module faults into two groups:

- Defects with various combinations of symptoms. Using a signal threshold-based method, these defects are identified.

- Defects with the same set of symptoms. Using a Fuzzy Logic Classifier, this form of errors is isolated.

Fuzzy Logic Classifier

Fuzzy Logic classifier (FLC) stands as a contemporary artificial methodology utilized for fault diagnosis within photovoltaic systems. The characteristics of the FLC system are formulated through the establishment of connections between the IF condition and THEN statements across multiple uncertain input datasets. This process results in generating decisions denoted as membership function outputs.

In this section, A Fuzzy Logic (FL) method will be implemented, with (ΔP_{max} , ΔV_{oc}) as inputs. From Figure 4.7, In cases 1 where (S1, S2, S3) = (1, 1, 0) and case 2 (S1, S2, S3) = (1, 0, 1), the Fuzzy Logic classifier (FL) begins by fuzzifying the inputs through the use of membership functions.

Following this, the establishment of a rule base for inference is required. The fuzzy rules are selected to distinguish between defects that have the indication signatures. As shown in Tables 4.3 and 4.4 precise bases have been created to differentiate between the three faults (in case 1) and the two faults (in case 2). Table 4.3 consists of three rules while Table 4.4 contains two rules.

Finally, the acquired data has been analyzed and interpreted. At the output of the implemented FL system, the Takagi Sugeno Kang type one procedure is applied. Therefore, the outputs of membership functions are fixed values.

Table 4.3. Fuzzy rule set and the process of defuzzification employed in the fuzzy classifier (Case 1).

Rule N°	IF		THEN			Defuzzification
	PPM	Voc	S1	S2	S3	
1	PPM_M	Vco_S	S1=0	S2=1	S3=1	[0 1 1]
2	PPM_M	Vco_M	S1=1	S2=1	S3=0	[1 1 0]
3	PPM_M	Vco_L	S1=0	S2=1	S3=0	[0 1 0]

Table 4.4. Fuzzy rule set and the process of defuzzification employed in the fuzzy classifier (Case 2).

Rule N°	IF		THEN			Defuzzification
	PPM	Voc	S1	S2	S3	
1	PPM_S	Vco_S	S1=1	S2=0	S3=1	[1 0 1]
2	PPM_L	Vco_S	S1=0	S2=0	S3=1	[0 0 1]

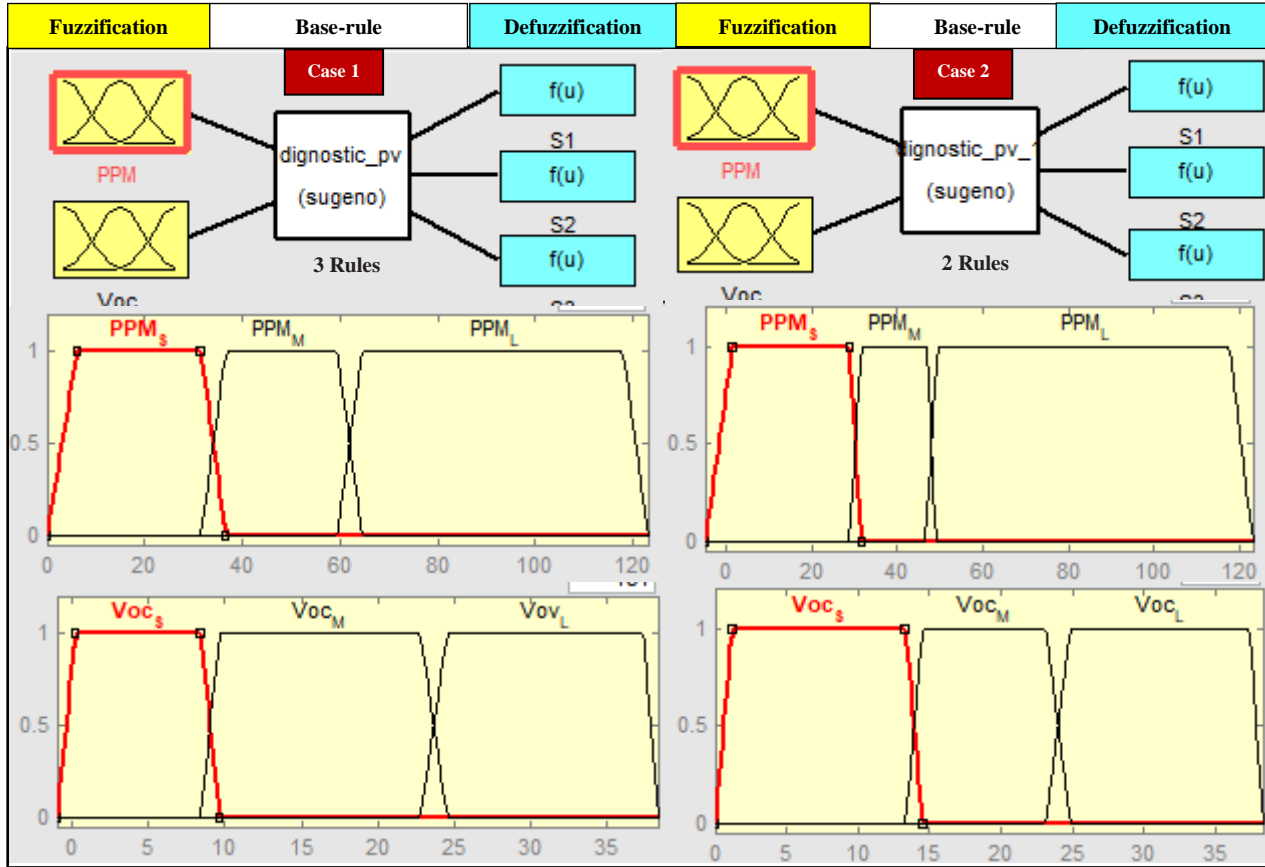


Figure 4.7: Structure of the fuzzy classifier and its input parameters.

B. Artificial Neural Network Classifier

In this section the Artificial Neural Network (ANN) is proposed. According to Figure 4.8 the ANN architecture consists of three layers:

- The input layer comprises three neurons representing the ratio between simulated and measured values of maximum power point current (P_{max}) open circuit voltage (Voc) and short circuit current (I_{sc}).
- A hidden layer, with ten neurons that have chosen. *tansig* activation functions.
- The output layer contains seven neurons representing six faults and the normal condition, which indicates a binary classification with a selected *purelin* activation function.

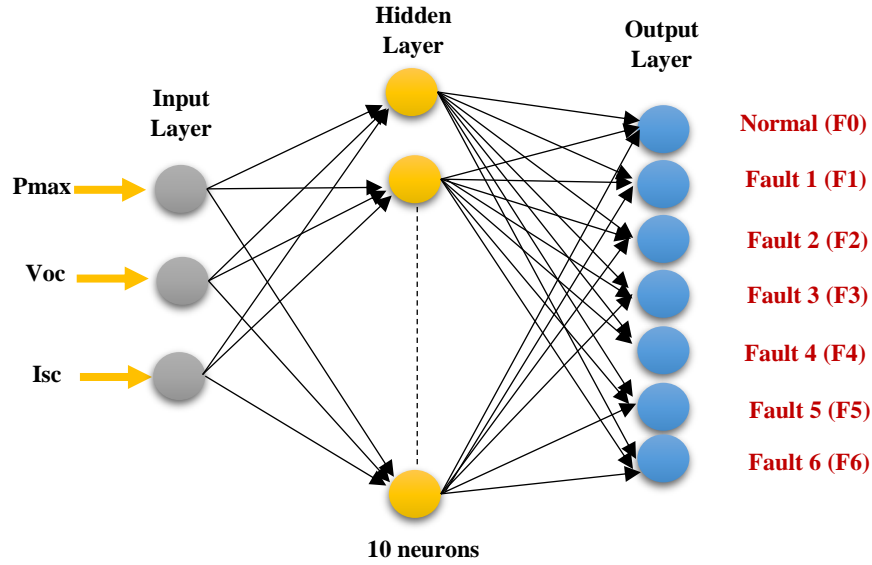


Figure 4.8: ANN configuration.

The network architecture is a Multilayer Perceptron (MLP) Feedforward Neural Network. As shown in Figure 4.9, this MLP structure consists of a single concealed layer with 10 nodes. The Levenberg-Marquardt (LM) algorithm is employed to train the network. The training dataset is produced from simulations that include both typical and fault-inducing operations for six distinct faults. In particular, 70% of the patterns are designated for training, while the remaining 30% are reserved for model validation and testing.

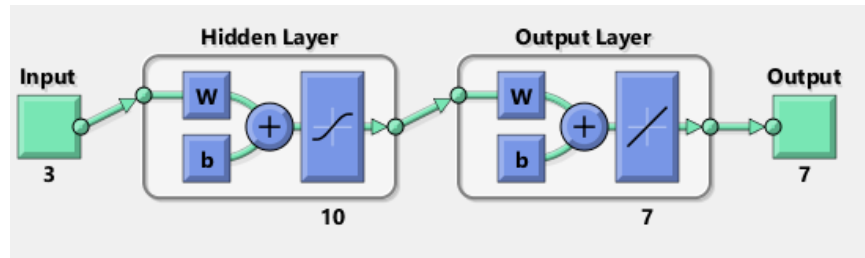


Figure 4.9: Schematic of the used ANN architecture.

4.3. Results Analysis

4.3.1. Simulation results for Simulink Model

To assess the efficacy of this intelligent approach, a simulation was conducted within the Matlab/Simulink environment, encompassing both normal and defective operational scenarios. The detection algorithm derives characteristics from two simulated photovoltaic systems: one emulates a real PV array with various faults, while the second represents the standard functioning.

4.3.1.1. Evaluation of the Proposed Method's Effectiveness

1) Evaluation of Algorithm 1

To assess the effectiveness of the algorithm, the suggested fault diagnosis method is simulated, for the SUNTECH photovoltaic (PV) module system.

The selected faults are individually applied to the faulty PV module, allowing the algorithm to detect and classify the faults based on various combinations of symptoms. These symptoms are then used for accurate fault localization.

Table 4.5 presents the results of various fault scenarios analyzed using the Sugeno FL and thresholding methods. Six different scenarios including normal case were tested, and all faults were successfully distinguished. The results clearly demonstrate that the combined method is highly effective in accurately and efficiently detecting, classifying, and locating different faults in PV panels, which achieved 100% accuracy. further details are reported in our previous studies [11-13].

Table 4.5. The Symptom Signatures for Individual Faults after Fuzzy Logic Integration.

Faults	Amplitude of symptoms			Method
	S1 (W)	S2 (V)	S3 (A)	
F0	0	0	0	Thresholding
F1	1	0	0	
F2	1	0	1	
F3	1	1	0	Fuzzy Logic
F4	0	1	0	
F5	0	1	1	
F6	0	0	1	

2) Evaluation of Algorithm 2

A case study was conducted using MATLAB Simulink software to evaluate the proposed approach. Data samples reflecting the distribution of three indicators were gathered to provide input for the ANN model. The dataset comprises 721 samples, calculated as (103×7) , which includes standard conditions and six unique fault scenarios. Each sample includes the three chosen input indicators. Figure 4.10 (a) illustrates the variation of minimum Mean Square Errors (MSE) with respect to epochs for training, validation, and testing. The performance following training is 0.002, while the optimal validation performance achieved is 0.0016615 after 96 iterations. Generalization tests evaluate the performance of neural networks and their capacity to apply acquired knowledge to novel data. Following the network's computation, it is

crucial to perform tests to verify that the network delivers accurate responses. Figure 4.10(b) presents the confusion matrix for the six faults, including the normal case, as analyzed during the testing phase. The matrix cells colored green and red represent the percentages of correctly and incorrectly classified faults, respectively. The confusion matrix offers a precision measurement for training the artificial neural network fault detection and diagnosis model. A precision rate of 99.7% has been achieved for the ANN diagnosis model. This result indicates the informed selection and efficient training of the ANN model for detection and classification.

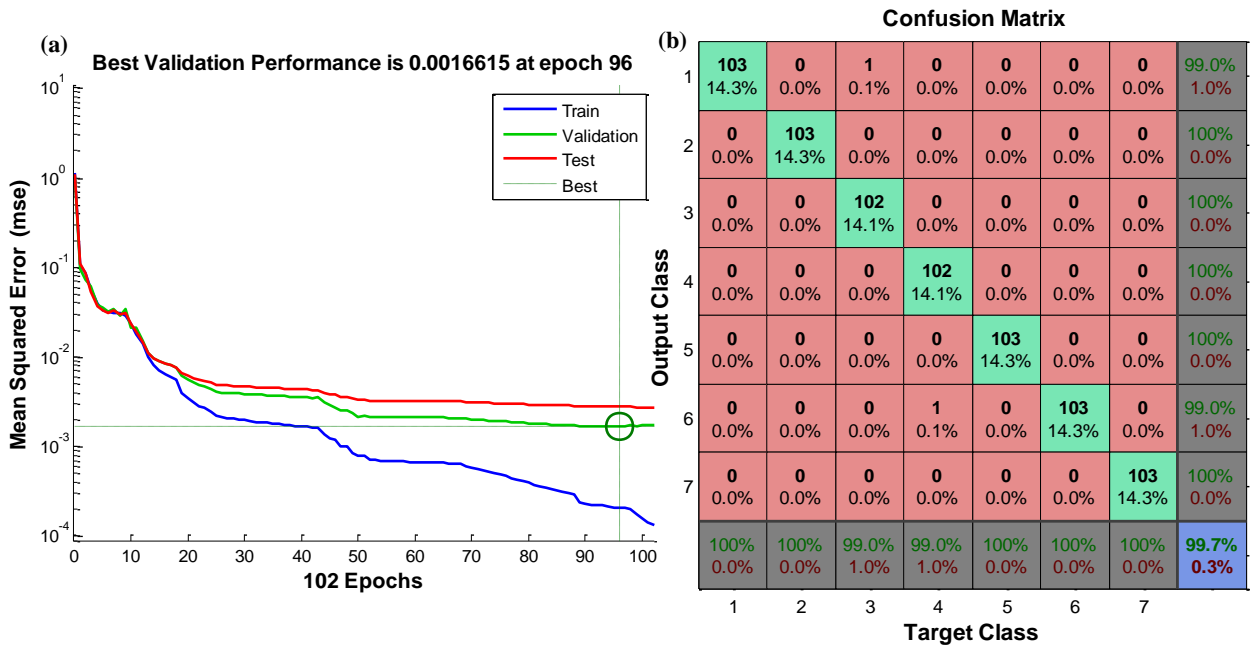


Figure 4.10: (a). Progression of Mean Squared Error (MSE) for the MLP Network. (b). Confusion Matrix for Classification in the MLP Network.

Figure 4.11 depicts the results of implementing fault 3, "One bypass diode CC," across simulation blocks. The simulation results confirm the effectiveness of the proposed approach in detecting and classifying defects based on diverse symptom combinations. FL designated F3 as the vector (1,1,0), while ANN identified the fault by indicating "1" in the fourth output, representing F3, and "0" in the other outputs. Upon detecting a fault and classifying the defect, a message is presented in the command window to notify the user of the system's fault type.

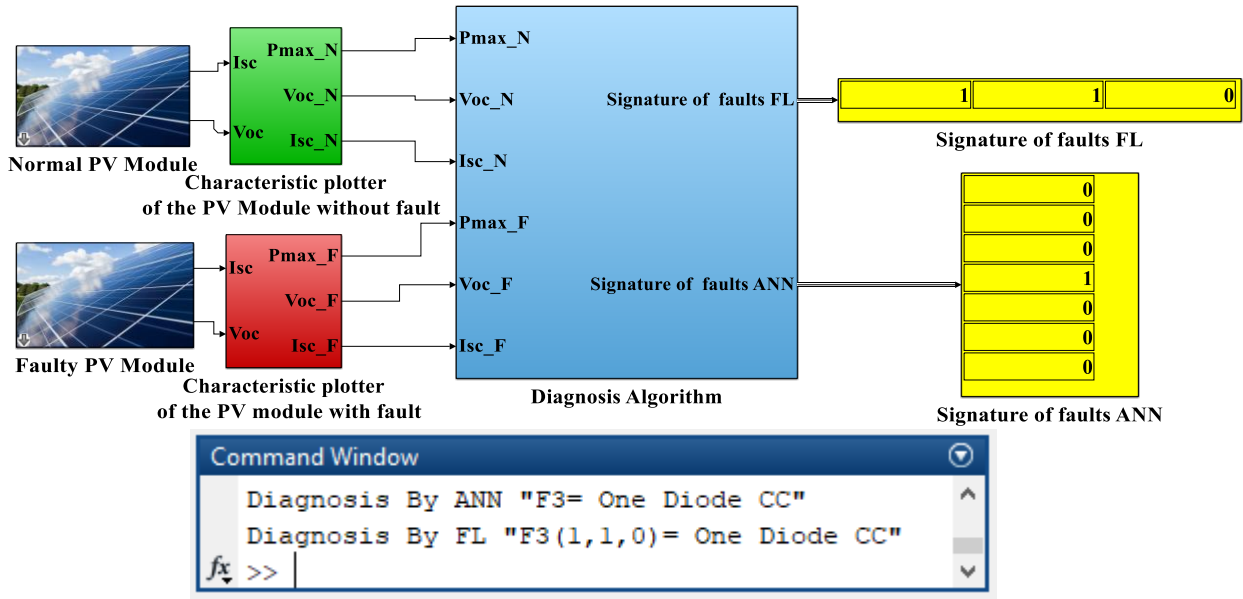


Figure 4.11: Detection of bypass diode CC fault.

4.4. Experimental validation

The experimental assessment of the performance of the diagnostic algorithms is conducted using the test bench as depicted in Figure 4.12 (a). This test setup was conceived and deployed within the LGEB Laboratory, University of Biskra, Algeria. The test bench consists of the following elements:

A SUNTECH PV photovoltaic solar panel of type mono-crystalline silicon was installed outside the building. The overall PV panel consists of 72 PV cells with three diodes (bypass type) each group of 24 cells connected to their bypass diode, where the electrical parameters of the module are previously presented in chapter 3. Following a reference cell and K-type thermocouple are used to record irradiance and temperature respectively. Which is used as inputs to our reference model. Due to practical limitations in reproducing each type of PV fault under varying real-world environmental conditions (irradiance and temperature), fault signatures were experimentally collected under standard test conditions. To simulate the variability of operating conditions, additional datasets were synthetically generated using MATLAB models calibrated with the real measurements, where the environmental conditions are that irradiance ranges from about 1000 to 1068 W/m² and the temperature ranges from about 23 to 25 °C.

As depicted in Figure 4.12 (b), the current sensor and voltage sensor are employed to obtain the current and voltage outputs of the solar panel. These data sets serve as input variables for

presenting the faulty PV panel, which are then compared to the simulated PV panel and diagnosed as shown in Figure 4.13.

The DS1104 Control Board is linked to a computer equipped with both the experimental ControlDesk software and the Matlab/Simulink software. The diagnostic algorithms being investigated are realized within Matlab/Simulink using blocks available in the Simulink libraries which are previously presented in Figure 4.5. To utilize the real-time interface toolbox, the implemented diagnosis algorithms are linked to the hardware.

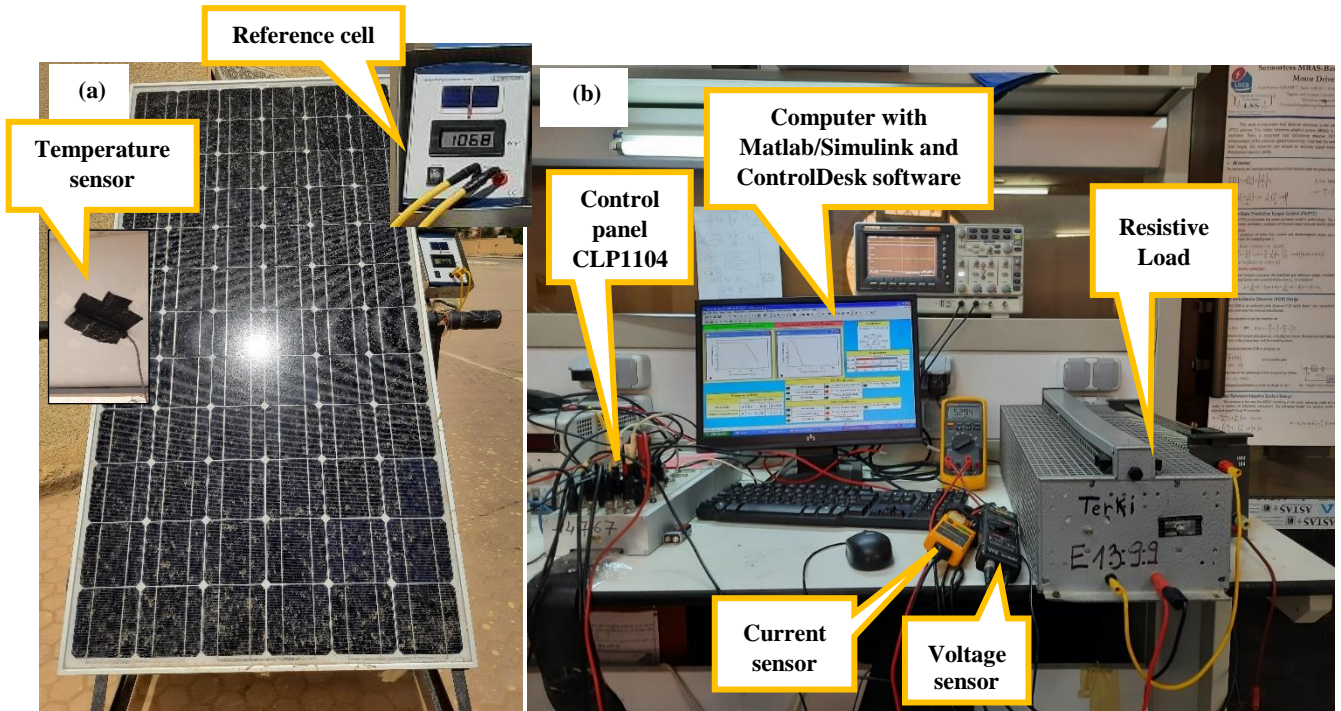


Figure 4.12: The experimental test bench setup.

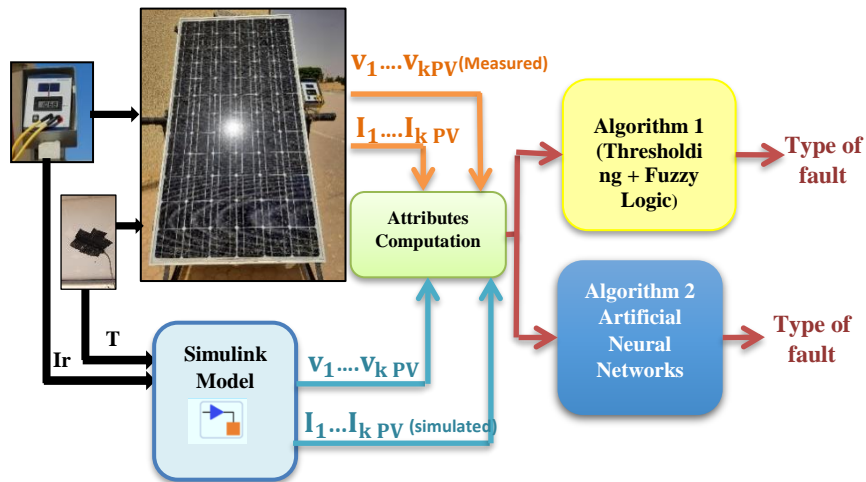


Figure 4.13: Diagram Depicting the Proposed Technique for Fault Diagnosis.

4.4.1. Investigated Faults

In this part, we can examine how diverse fault types influence a photovoltaic system across various parameters such as voltage and current variations and power losses. Consequently, this leads to the generation of distinct I-V characterization curves. Figure 4.14 shows the curves for several typical types of faults which show a visual concordance between real and simulated data. For implementing the shading fault (see Figure 4.15 (a)), the shaded module is conducted by covering the cells with a physical solid opaque, the I_{max} and V_{max} , are significantly affected, while I_{sc} and V_{oc} are similar to those of the normal condition. Soiling effect (Figure 4.15 (b)): The presence of dirt and debris on the surface of a PV panel can reduce the amount of sunlight reaching the solar cells thus decreasing the I_{sc} value. A shunted diode fault (Figure 4.15 (c)): the I_{max} and V_{max} , are significantly affected, which leads to a decrease in short circuit current and this leads also to a decrease in power. A short circuit diode fault (Figure 4.15 (d-f)): This section examines two distinct scenarios: the short-circuiting of a single bypass diode and the short-circuiting of two bypass diodes, both of which result in a decreased open-circuit voltage (V_{oc}) compared to the standard curve. Additionally, the presence of partial shading and disconnected bypass diode are also investigated (Figure 4.15 (a-e)), the result brings a reduction in the I_{max} and V_{max} , which leads to a decrease in power. As a result of the aforementioned factors, the detection of faults and the diagnostic processes for PV systems have emerged as critical endeavors and particularly interesting in this area.

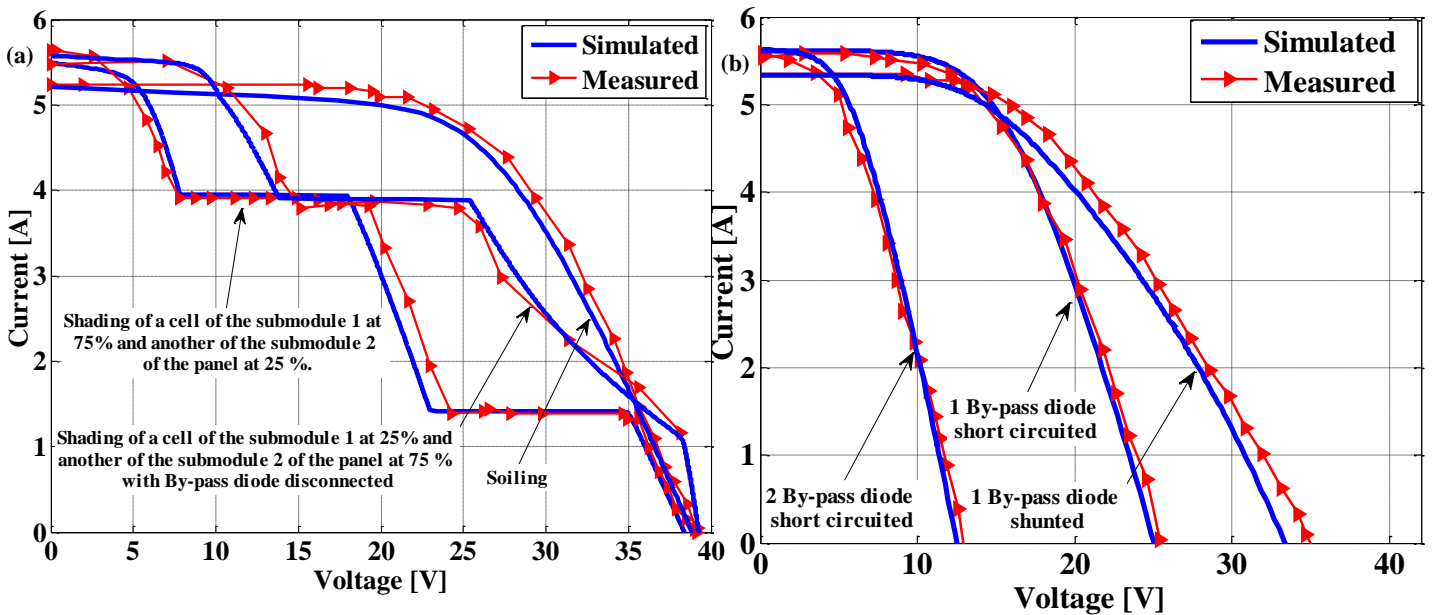


Figure 4.14:(a). PV module characteristics: case of soiling, shadow effect, shadow effect and bypass diode fault.
(b). PV module characteristics: case of bypass diode faults.

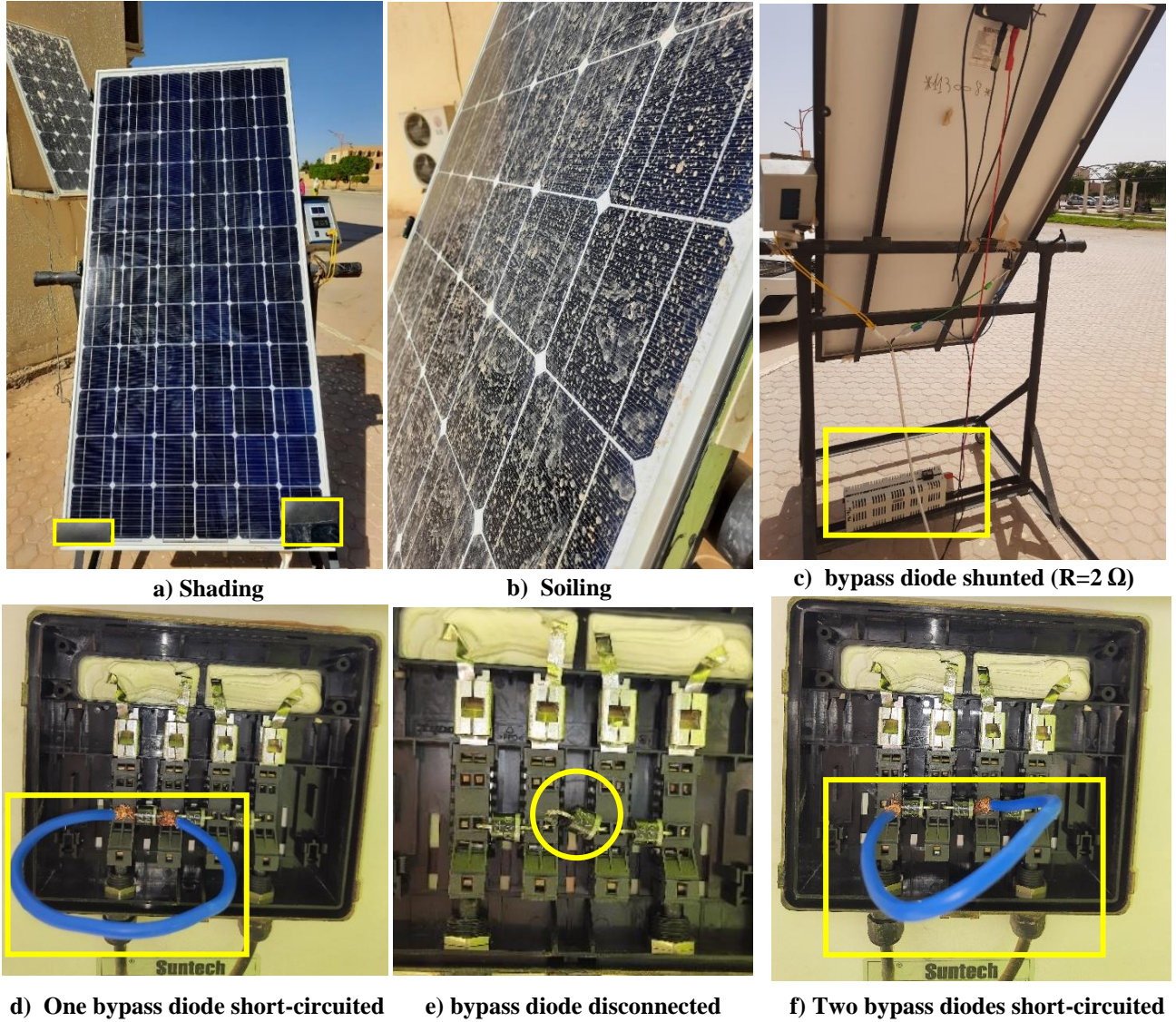


Figure 4.15: The investigated faults.

4.4.2. Experimental data Test off-line implementation

In this section, our contribution lies in the extension of this technique to render it suitable for off-line fault diagnosis and real-time implementation. For full supervision, a series of experiments were conducted over the course of seven consecutive days to assess a normal condition and six distinct fault types. For the off-line implementation, the data sample was collected from the experimental PV module consisting of $700 = (100 \times 7)$. Moreover, its data has been normalized in the same procedure mentioned previously in the simulation part (section 4.3.1.1). Finally, the data points have been divided into 70% and 30% for training and testing, respectively.

The learning algorithm's convergence is confirmed by examining the learning curve presented in Figure 4.16 (a). This curve clearly demonstrates that the error objective reaches a value of

0.0017085 after 31 iterations, which is indicative of an adequate performance level for achieving a high ranking rate.

The dataset (training + test) is examined to determine if ANN is capable of classifying defects. The results of the classification are shown in Figure 4.16 (b), where the green squares represent correctly classified data and the red squares represent the opposite. According to the classification confusion matrix, the MLP-based model's correct and false classification rates are 99.6% and 0.4%, respectively. This shows that the ANN model achieved a good performance in detecting classification faults.

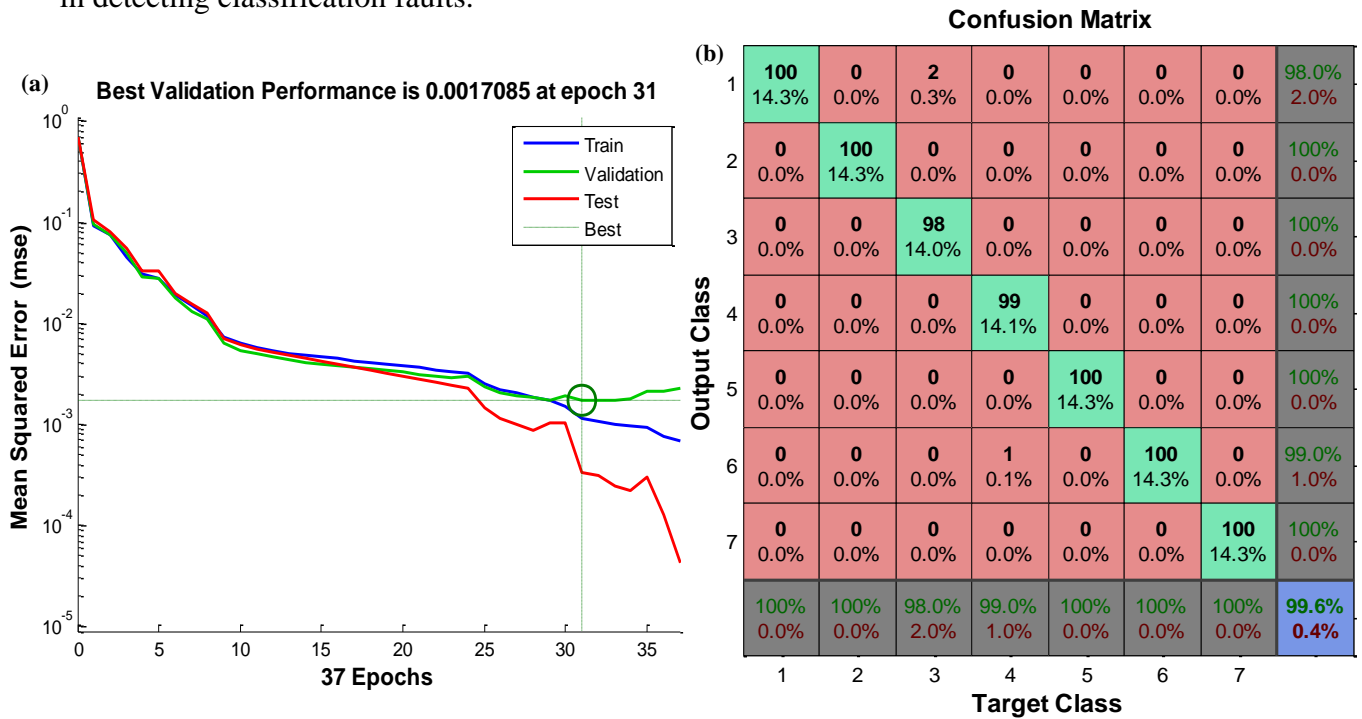


Figure 4.16: (a). Progression of Mean Squared Error (MSE) for the MLP Network. (b). Confusion Matrix for Classification in the MLP Network.

4.5. Real-time Experimental Application Results and Discussion

In order to guarantee that the simulated system accurately emulates the real system behavior, we compare experimentally multilayer neural network identification method and Fuzzy Logic method in the same data and the comparison result of fault diagnosis by day. Figures. 4.17-22 showcase the created ControlDesk user interface for real-time surveillance, which allows users to observe all instantaneous and integrated monitoring signals both electrical and environmental along with the state of the system, the Photovoltaic characteristics (I-V) for the normal operation and defective PV panel, accompanied by the outcomes obtained from the two employed algorithms (Detection part). Furthermore, the figures also demonstrate the ultimate classification of faults (Classification part). To provide a clear indication of the fault type, a

designated display component is utilized as an alarm triggered according to the identified fault category.

As shown in Figure 4.17. The results of the identification of the shading fault by the multilayer neural network identification method and Fuzzy Logic method successfully classified the fault into different combinations of symptoms. We can see in the monitoring platform that the graph of the measured PV panel (faulty) is not identical to the estimated one (normal), this indicates the existence of a fault in the panel. Hence, it can be seen clearly that the fault is detected and classified by the diagnosis technique, where the type of fault is indicated in the display part with a red LED. On the other hand, Figure 4.18. depicts the outcomes of the soiling fault identification. As can be seen, the fault has been detected by the FL and the ANN methods and classified only by the ANN method which gives a different combination of symptoms displayed with a red LED. However, the employment of the fuzzy logic method has resulted in a false alarm (indicated fault 6). The observed misclassification can be attributed to the existence of inherent measuring errors, which have consequently led to an inaccurate classification.

Figure 4.19 and 20 Present the result of the implementation of a single by-pass diode short-circuited and two by-pass diodes short-circuited. As observed, the measured (faulty) graphs of the PV panel differ from the predicted (normal) graph in the two cases. Thus, the results that were obtained of the by-pass diode short circuit faults identification using the ANN and FL methods successfully detect and classify the faults in the display part. Additionally, as depicted in Figure 4.21 and 22. The figures show the results of the shunted by-pass diode fault and the shading + open-circuit by-pass diode fault identification along with their corresponding characteristics (measured) compared to the predicted one (simulated). As can be seen, only the ANN technique which provides a unique combination of symptoms was able to detect and classify the defects in the display part. However, the use of fuzzy logic produced a fault detection, accompanied by a misclassification of the faults.

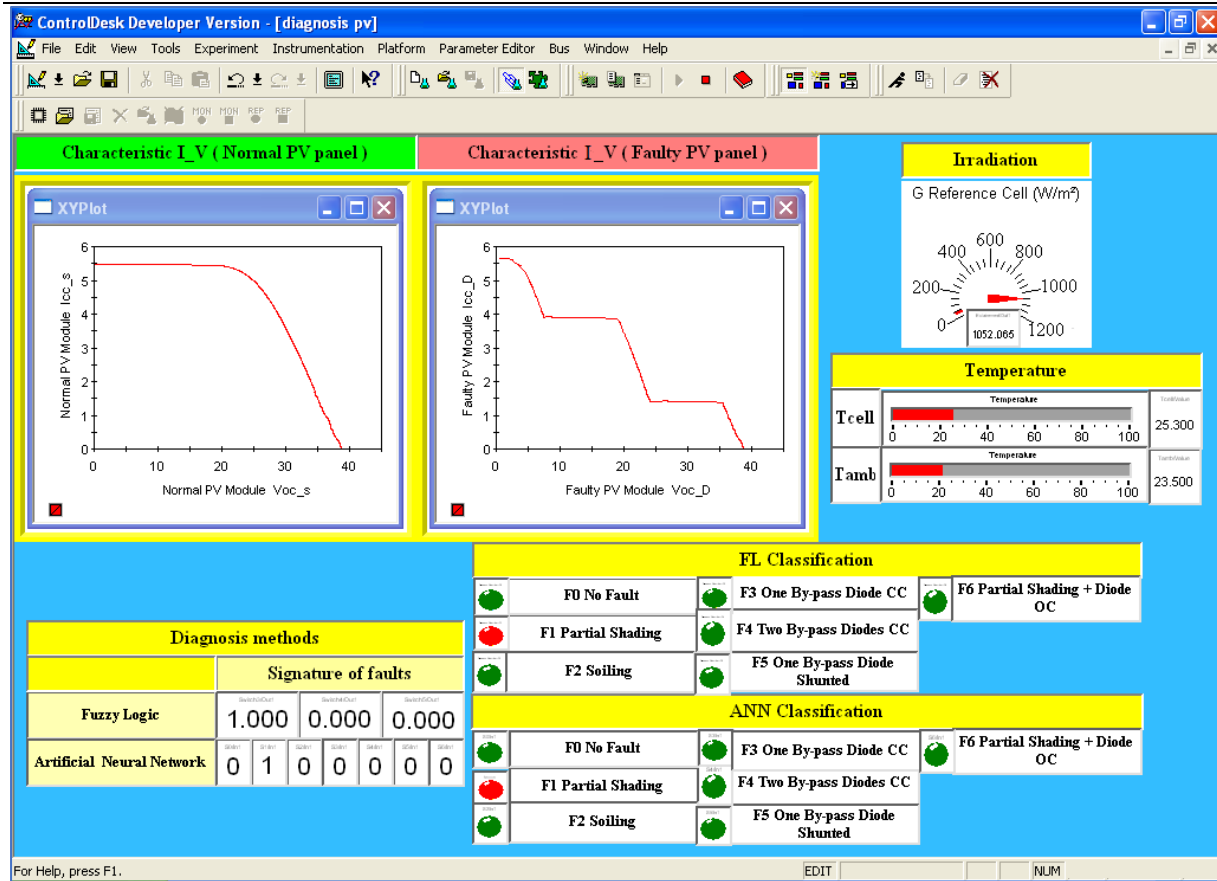


Figure 4.17: The ControlDesk User Interface Presents Real-Time Measurement Data and Detects Fault 1 in the Monitored PV Panel.

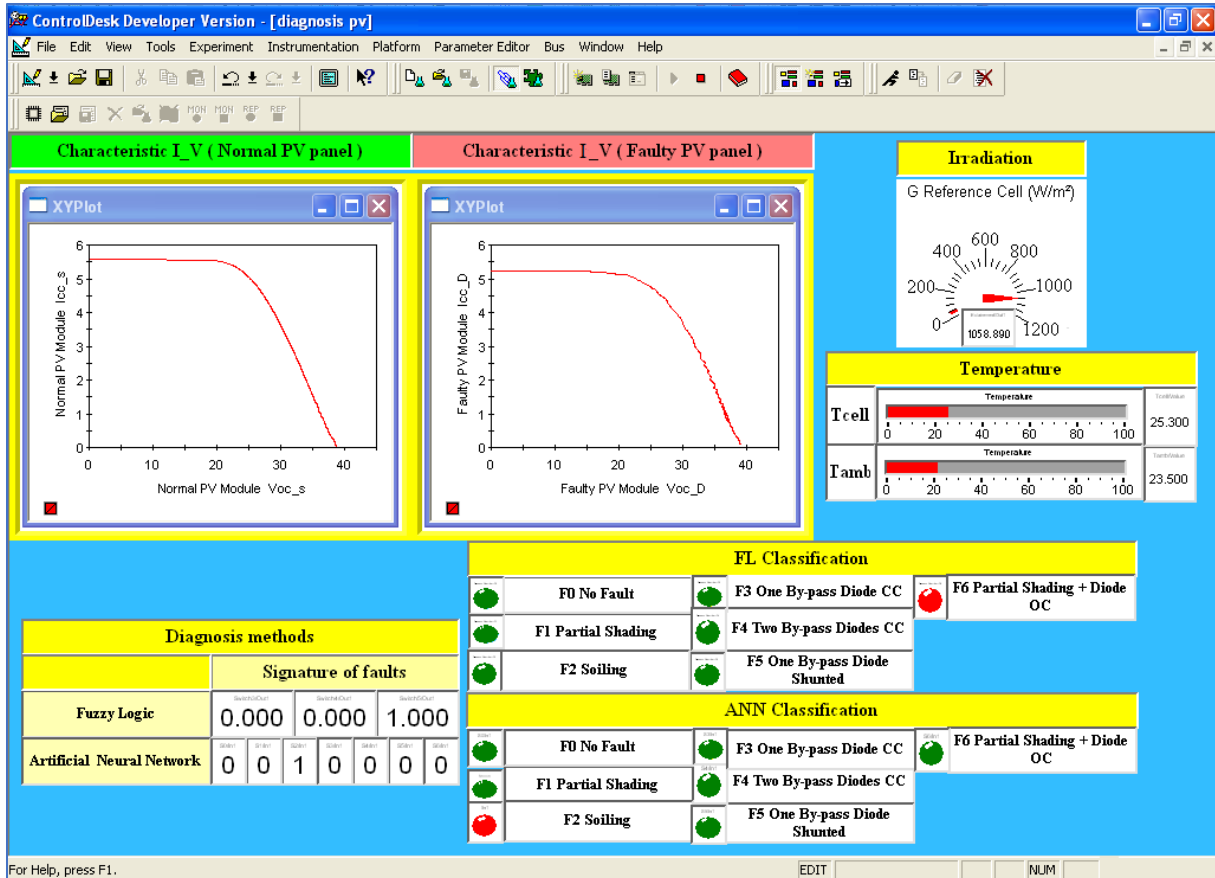


Figure 4.18: The ControlDesk User Interface Presents Real-Time Measurement Data and Detects Fault 2 in the Monitored PV Panel.

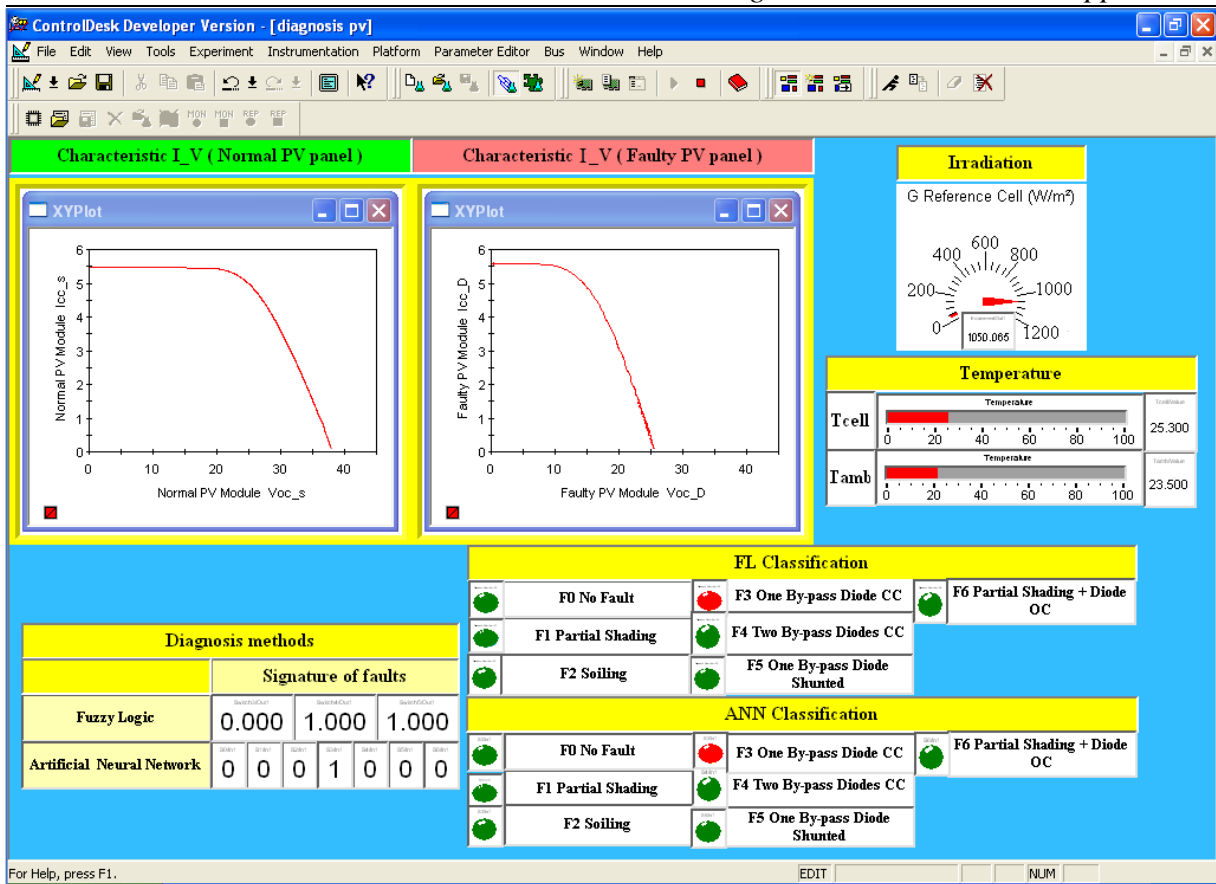


Figure 4.19: The ControlDesk User Interface Presents Real-Time Measurement Data and Detects Fault 3 in the Monitored PV Panel.

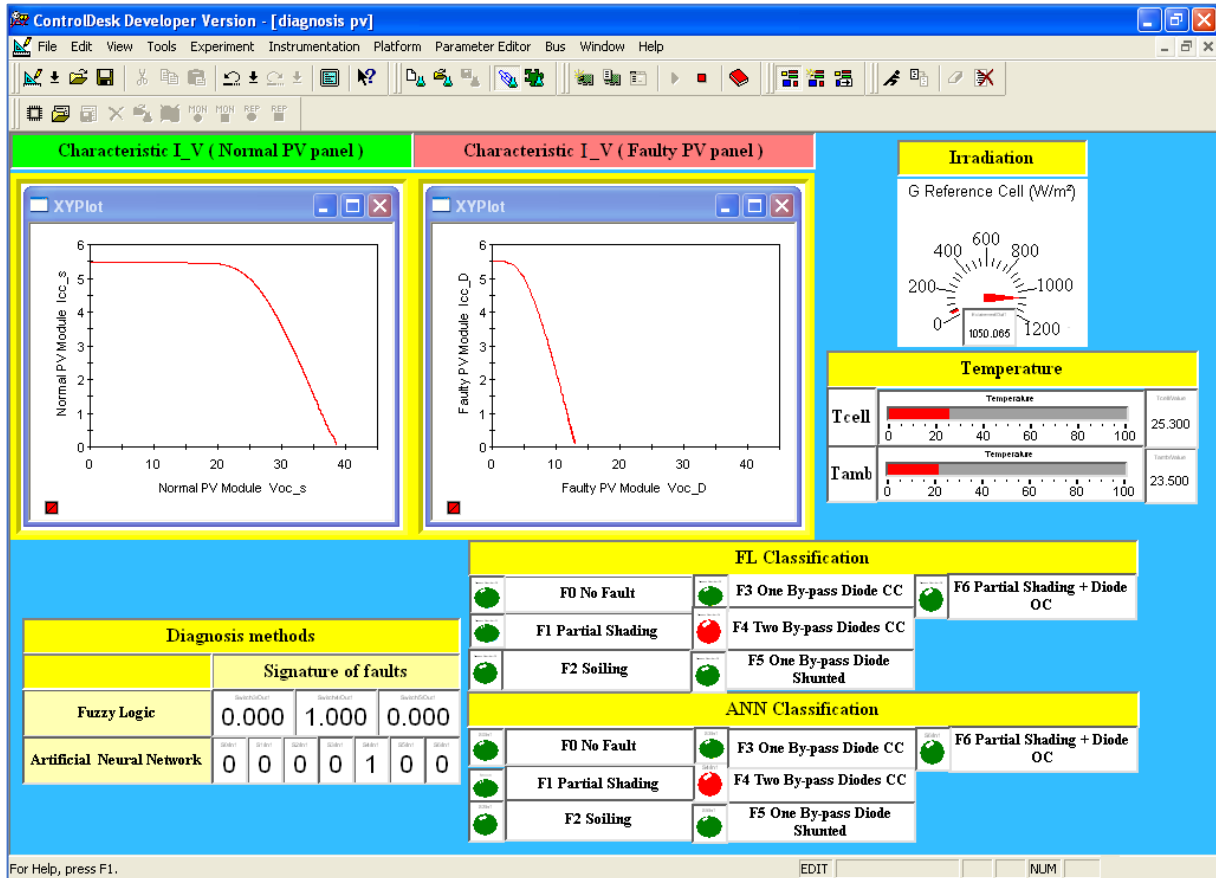


Figure 4.20: The ControlDesk User Interface Presents Real-Time Measurement Data and Detects Fault 4 in the Monitored PV Panel.

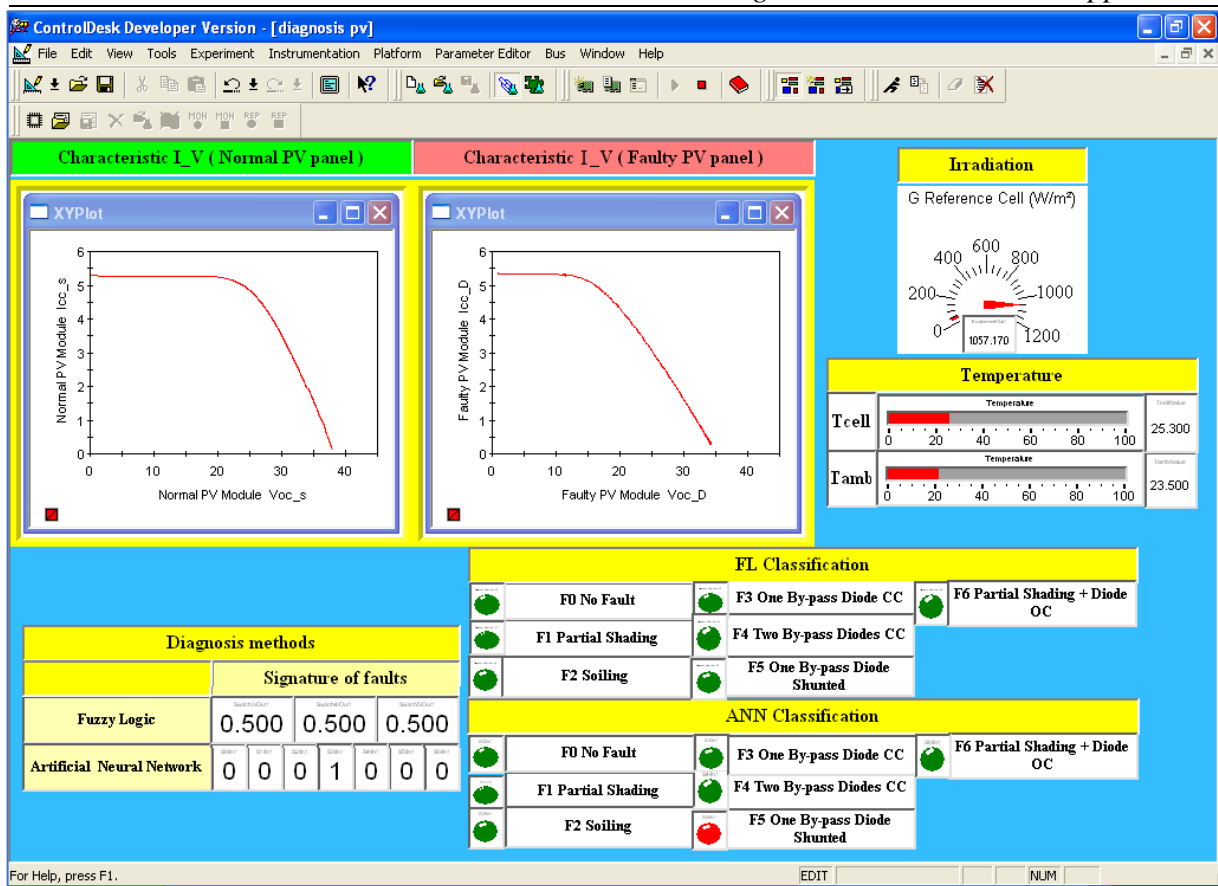


Figure 4.21: The ControlDesk User Interface Presents Real-Time Measurement Data and Detects Fault 5 in the Monitored PV Panel.

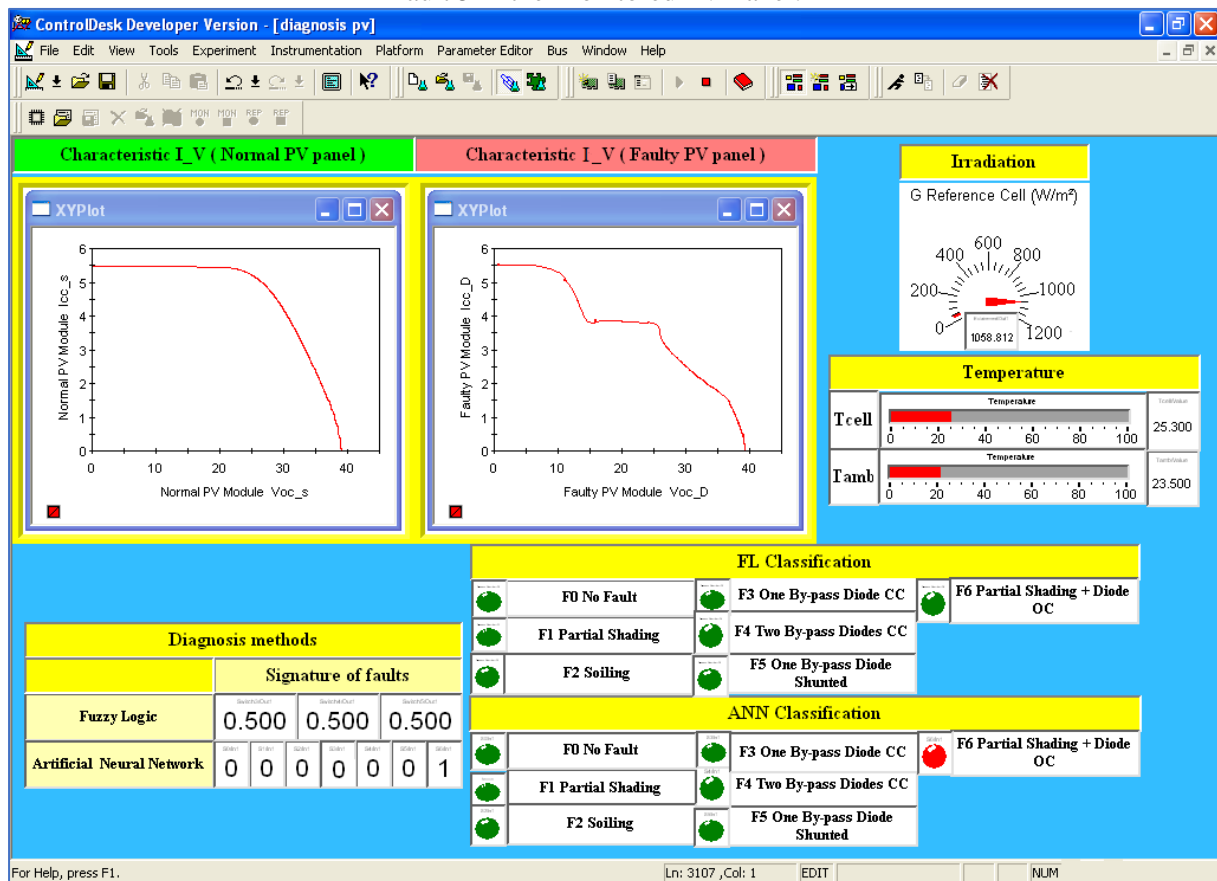


Figure 4.22: The ControlDesk User Interface Presents Real-Time Measurement Data and Detects Fault 6 in the Monitored PV Panel.

Most of the sampled data during the testing period are found to fall within the predetermined range of lower and upper thresholds. Nonetheless, in each case, a subset of samples demonstrates inaccurate detection, resulting in their classification as out-of-region instances. This situation arises due to the system's identification of a significant number of defective regions, a factor that could potentially be influenced by sensor efficiency and the computation of three ratios. The computation of Detection Accuracy (DA) for each examined scenario can be achieved through the subsequent calculation:

$$DA = \frac{\text{totale samples} - \text{out of region samples}}{\text{total samples}} \quad (4.1)$$

For each scenario examined in Figures 4.17-22, the employment of the Artificial Neural Network (ANN) method leads to a reduction in instances classified as out of region, as evidenced by the comparison with the Fuzzy Logic (FL) system state in Table 4.7. This unequivocally ensures a high degree of accurate classification for the majority of samples through the utilization of the Artificial Neural Network (ANN). Furthermore, the aggregate Detection Accuracy (DA) subsequent to the implementation of the ANN system, wherein only 3 instances out of a total of 700 are designated as out of the region, attains 99.6%. Similarly, employing the fuzzy logic approach (FL), 5 instances are categorized as out of region samples, contributing to a 99.2% DA level. On the aspect of speed, the execution time for generating the I-V curves is 20 seconds, due to manual variation of the load. Moreover, the diagnosis time using fuzzy logic method takes 3.02s, while ANN consumes only 1.04s for the execution of fault analysis, which in turn makes the system free from unwanted delays.

This enhancement significantly augments the monitoring efficacy of the Photovoltaic (PV) system. It is evident from the observations that the Artificial Neural Network (ANN) method adeptly and efficiently accomplishes the precise classification and detection of diverse fault data.

Table 4.7. The output DA and the execution time with FL and with ANN system.

Case	With FLC		With ANN		Duration of I-V Curves Generation (s)	Diagnosis time (s)	
	Out of region samples	DA (%)	Out of region samples	DA (%)		With FLC	With ANN
F1	0	100	0	100	20s	3.02s	1.04s
F2	1	99	0	100			
F3	0	100	2	98			
F4	0	100	1	99			
F5	2	98	0	100			
F6	2	98	0	100			

4.6. Comparative Study with Other ANN Solutions

Table 4.8 presents a comparative analysis of the characteristics of the proposed artificial neural network (ANN) architecture in contrast to other deep learning methodologies introduced in recent years. This comparative examination is succinctly addressed in the introductory section. The table exclusively encompasses methodologies pertinent to experimental diagnosis and fault detection in photovoltaic (PV) systems. The evaluation encompasses the ANN's accuracy, and the consideration of various types of detected faults (single- and multi-fault types), which could have significant implications for integration into embedded systems. This comparative analysis also underscores that all referenced studies encompass distinct test conditions and represent diverse scenarios. The results underscore the remarkable efficiency of the proposed fault diagnosis strategies, which consistently demonstrate their capability to accurately detect and classify single- and multi-fault types. It is notable that the parameter of training time is frequently omitted in the works reviewed. Nonetheless, this investigation underscores its relevance, particularly in the context of fault diagnosis. The outcomes affirm that the proposed fault diagnosis strategies exhibit rapid self-training, yielding a detection accuracy surpassing 99%.

Table 4.8. ANN techniques for PV diagnosis and faults identification.

References	Year of study	Types of faults detected	Fault Diagnosis Accuracy (%)
[22]	2024	Short-circuited modules, disconnected strings	87.56%
[23]	2024	Shading, short circuits, open circuits, and degradation of solar cells	99.64%
[24]	2024	Line-to-line defects, Open-circuit failures, Partial shading	99.4%
[25]	2024	line-ground (LG), line-line (LL), open-circuit (OC), string degradation, and array degradation faults	98.37%
This work	2024	Partial shading, Soiling, SC of one by-pass diode, SC of two by-pass diodes, by-pass diode shunted, Shading & by-pass diode disconnected	99.6%

4.7. Conclusion

In this chapter, the ANN and a combined method based on the FL classifier have been developed for fault detection and classification in photovoltaic panel, and both experimental

and simulation validations have been introduced using Matlab/Simulink® software. First, the WSO with Newton-Raphson optimization algorithm is used to determine the optimal PV simulation model parameters to improve the system's capability and performance. Second, three selected indicators are calculated and analyzed for normal (simulated PV panel) and measured (real PV panel) for various fault cases that represent: PV cells (shading and soiling) and bypass diode defects.

The simulation part has substantiated that both Artificial Neural Networks (ANN) and Fuzzy Logic (FL) are capable of detecting and classifying all faults effectively. However, when moving from simulation to experimental tests using dSPACE DS1104 platform, the results unequivocally showcased the superiority of the ANN classifier over the FL classifier. The experimental findings of real-time surveillance demonstrated that the ANN classifier outperformed the FL classifier in terms of fault classification accuracy performance and speed, the proposed FL and ANN model obtained classification accuracies of approximately 100% and 99.7% in simulation tests and 99.2% and 99.6% in experimental tests, respectively. These results highlight the potential of the ANN-based approach as a preferred choice for practical fault detection systems. Thus, incorporating ANN techniques in real-time applications can lead to enhanced fault detection capabilities and improved overall system performance.

Conclusion

Conclusion

The strategies developed in this research focus on the detection and diagnosis of faults in Photovoltaic system. The primary objective was to enhance the efficiency of PV systems and protect them from potential faults by implementing effective fault detection and diagnosis methods. In particular, the research emphasized the application of artificial intelligence (AI) techniques, such as artificial neural network classifier and Fuzzy Logic method as the core aim of the thesis.

Nonetheless, the use of AI tools for this purpose necessitates a high-quality database that, on one hand, accurately captures the relationship between system faults and PV parameters, and on the other hand, effectively characterizes system behavior under both normal and faulty conditions.

From a practical perspective, acquiring a comprehensive fault dataset through real-world experimentation is often challenging, as operating a PV system under faulty conditions can pose significant risks, including equipment damage and safety hazards. To address this limitation, this thesis employed a Matlab/Simulink co-simulation approach to develop a robust and realistic simulation model capable of accurately representing the system's behavior in both healthy and faulty states. Additionally, several types of faults were experimentally introduced in a controlled environment, and the resulting faulty data were collected. These experimental results were then compared with the outputs of the reference simulation model to validate its accuracy and reliability for fault diagnosis applications.

Moreover, the developed simulation model necessitates the use of the five electrical parameters of the One-Diode Model (ODM). To this end, an effective extraction methodology based on the War Strategy Optimization (WSO) algorithm and Newton-Raphson algorithm has been proposed. These algorithms were selected owing to their proven efficiency in solving complex optimization problems, rapid convergence characteristics, and suitability for real-time implementation. The performance of the proposed ODM parameter extraction method has been

experimentally validated using two of photovoltaic (PV) modules employing different technologies.

Subsequently, the extracted ODM parameters were employed to develop a robust strategy for Maximum Power Point (MPP) estimation. This estimation approach was validated through experimental testing with real measurement data obtained from photovoltaic system.

Second, both simulation and experimental methodologies were employed to investigate fault detection and classification in photovoltaic (PV) panels, utilizing thresholding and fuzzy logic-based techniques. During the simulation phase, eight distinct fault types were examined. Although the thresholding method proved effective in detecting certain faults, it was limited in its ability to accurately distinguish between all fault scenarios, thereby indicating the necessity for a more sophisticated classification strategy. In contrast, the fuzzy logic-based approach exhibited enhanced diagnostic performance, successfully and distinctly identifying all investigated faults. The experimental validation was carried out using real measurement data obtained from a PV panel tested at the LGEB Laboratory, University of Biskra. The implementation, carried out on the dSPACE DS1104 platform and developed in the Matlab/Simulink environment, further confirmed the effectiveness of the fuzzy logic method in reliably detecting and classifying multiple fault conditions.

Third, an Artificial Neural Network (ANN)-based approach for fault detection and classification was successfully developed and rigorously validated through both simulation and experimental investigations. The third chapter considered five distinct fault scenarios comprising both single and multiple faults, such as partial shading, open circuit faults, and bypass diode failures, applied to a photovoltaic (PV) module. The impact of these faults was assessed based on variations in voltage, current, and power. Simulation results confirmed the ANN model's high accuracy in identifying and classifying all fault types. In addition, experimental validation using real-time PV module data and implemented via dSPACE DS1104 controller further substantiated the model's robustness and reliability. The proposed method achieved a classification accuracy of 99.7%, demonstrating its strong potential for effective PV fault detection under diverse operating conditions.

Finally, the simulation of the comparative part of this thesis has substantiated that both Artificial Neural Networks (ANN) and Fuzzy Logic (FL) are capable of detecting and classifying single and multi-type faults effectively. However, when moving from simulation to experimental tests

using dSPACE DS1104 platform, the results unequivocally showcased the superiority of the ANN classifier over the FL classifier in terms of classifying the single fault (soiling) and the multi-fault (shading with By-pass diode disconnected). The experimental findings of real-time surveillance demonstrated that the ANN classifier outperformed the FL classifier concerning fault classification accuracy performance and speed for classifying the single and multi-faults types, the proposed FL and ANN model obtained classification accuracies of approximately 100% and 99.7% in simulation tests and 99.2% and 99.6% in experimental tests, respectively. These results highlight the potential of the ANN-based approach as a preferred choice for practical fault detection systems. Thus, incorporating ANN techniques in real-time applications can lead to enhanced fault detection capabilities and improved overall system performance.

As a perspective work, the future contribution is to implement the recommended technique on an extensive photovoltaic (PV) system could offer significant benefits owing to its notable advantages in effectively identifying common and multi-faults through heightened sensitivity and precision, also we will focus on evaluating the proposed embedded system for large-scale PV plants. Additionally, other type of multi-faults will be investigated, and also generalize the method for different PV module technologies. Furthermore, another avenue for enhancing the system involves the integration of Internet of Things (IoT) functionalities, which serves to enhance real-time online monitoring of performance analysis and the prompt issuance of malfunction alerts.

Bibliography

Bibliography

- [1] S. Ansari, A. Ayob, M.S.H. Lipu, M.H.M. Saad, A. Hussain, "A Review of Monitoring Technologies for Solar PV Systems Using Data Processing Modules and Transmission Protocols: Progress, Challenges and Prospects", *Sustainability*. 13 (2021) 8120.
- [2] F.S.M. Abdallah, M. N. Abdullah, I. Musirin, A. M. Elshamy, "Intelligent solar panel monitoring system and shading detection using artificial neural networks." *Energy Reports* 9 (2023): 324-334.
- [3] E. Perez-Anaya, D.A. Elvira-Ortiz, R.A. Osornio-Rios, J.A. Antonino-Daviu, "Methodology for the Identification of Dust Accumulation Levels in Photovoltaic Panels Based in Heuristic-Statistical Techniques", *Electronics*. 11 (2022) 3503.
- [4] M. Dhimish, A. M. Tyrrell. "Photovoltaic Bypass Diode Fault Detection Using Artificial Neural Networks". *IEEE Transactions on Instrumentation and Measurement* 72 (2023): 1-10.
- [5] A. Mehmood, H. A. Sher, A. F. Murtaza and K. Al-Haddad. "A diode-based fault detection, classification, and localization method for photovoltaic array". *IEEE Transactions on Instrumentation and Measurement*, 70 (2021).
- [6] A. Jäger-Waldau, "Snapshot of photovoltaics– March 2021," *EPJ Photovoltaics*, vol. 12, p. 2, 2021.
- [7] G. Di Lorenzo, R. Araneo, M. Mitolo, A. Niccolai, and F. Grimaccia, "Review of O&M Practices in PV Plants: Failures, Solutions, Remote Control, and Monitoring Tools," *IEEE Journal of Photovoltaics*, vol. 10, no. 4, pp. 914–926, Jul. 2020.
- [8] M. K. Alam, F. Khan, J. Johnson, and J. Flicker, "A Comprehensive Review of Catastrophic Faults in PV Arrays: Types, Detection, and Mitigation Techniques," *IEEE Journal of Photovoltaics*, vol. 5, no. 3, pp. 982–997, May 2015.
- [9] L. Hernández-Callejo, S. Gallardo-Saavedra, and V. Alonso-Gómez, "A review of photovoltaic systems: Design, operation and maintenance," *Solar Energy*, vol. 188, pp. 426–440, Aug. 2019.
- [10] S. K. Firth, K. J. Lomas, and S. J. Rees, "A simple model of PV system performance and its use in fault detection," *Solar Energy*, vol. 84, no. 4, pp. 624–635, Apr. 2010.
- [11] M. Bacha, A. Terki. "Diagnosis algorithm and detection faults based on fuzzy logic for PV panel. *Materials Today: Proceedings*", Vol. 51, Part 7, Pp. 2131-2138 (2022).
- [12] M. Bacha, A. Terki and M. Bacha. "Real-Time implementation of Diagnosis and Fault Detection for PV panel Based on Fuzzy Logic Classification", 2022 2nd International Conference on Advanced Electrical Engineering (ICAEE), Constantine, Algeria, (2022), pp. 1-6.
- [13] M. Bacha, A. Terki and M. Bacha. "Comparative study of real-time photovoltaic fault diagnosis using artificial intelligence: Fuzzy logic and neural network approaches," *Energy Sources, Part A: Recovery, Utilization, and Environmental Effects*, vol. 46, no. 1, pp. 13536–13560, 2024.

- [14] Shweta, R., Sivagnanam, S., & Kumar, K. A. (2022). Fault detection and monitoring of solar photovoltaic panels using internet of things technology with fuzzy logic controller. *Electrical Engineering & Electromechanics*, (6), 67-74.
- [15] M. Dhimish, V. Holmes, B. Mehrdadi, M. Dales, "Comparing Mamdani Sugeno fuzzy logic and RBF ANN network for PV fault detection". *Renewable energy* 117 (2018): 257-274.
- [16] A. Seghiour, H.A. Abbas, A. Chouder. A. Rabhi. "Deep learning method based on autoencoder neural network applied to faults detection and diagnosis of photovoltaic system". *Simulation Modelling Practice and Theory* 123 (2023): 102704.
- [17] A. Aallouche, H. Ouadi. "Online fault detection and identification for an isolated PV system using ANN", *IFAC-PapersOnLine* 55.12 (2022): 468-475.
- [18] Y. Liu, K. Ding, J. Zhang, Y. Li, Z. Yang, W. Zheng, X. Chen, "Fault diagnosis approach for photovoltaic array based on the stacked auto-encoder and clustering with I-V curves", *Energy Convers. Manag.* 245 (2021) 114603.
- [19] X. Cai, R Wai, "Intelligent DC Arc-fault detection of solar PV power generation system via optimized VMD-based signal processing and PSO–SVM classifier", *IEEE J. Photovolt.* 12 (4) (2022) 1058–1077.
- [20] J. Qu, Z. Qian, Y. Pei, L. Wei, H. Zareipour, Q. Sun, "An unsupervised hourly weather status pattern recognition and blending fitting model for PV system fault detection", *Appl. Energy* 319 (2022) 119271.
- [21] Z. He, P. Chu, C. Li, K. Zhang, H. Wei, Y. Hu, "Compound fault diagnosis for photovoltaic arrays based on multi-label learning considering multiple faults coupling". *Energy Conversion and Management* 279 (2023): 116742.
- [22] F. Suliman, F. Anayi, M. Packianather. "Electrical Faults Analysis and Detection in Photovoltaic Arrays Based on Machine Learning Classifiers". *Sustainability*. 2024; 16(3):1102.
- [23] B. Gong, A. An, Y. Shi, X. Zhang, "Fast fault detection method for photovoltaic arrays with adaptive deep multiscale feature enhancement", *Appl. Energy* 353 (2024) 122071.
- [24] A. F. Amiri, H. Oudira, A. Chouder, S. Kichou, "Faults detection and diagnosis of PV systems based on machine learning approach using random forest classifier". *Energy Conversion and Management*, (2024), 301, Article 118076.
- [25] E. Aref, N. Amir, M. Jafar, A. Mohammadreza, "A multilayer integrative approach for diagnosis, classification and severity detection of electrical faults in photovoltaic arrays, *Expert Systems with Applications*", Volume 252, Part A, (2024), 124111, ISSN 0957-4174.
- [26] T.S. Ayyarao and P.P. Kumar. "Parameter estimation of solar PV models with a new proposed war strategy optimization algorithm." *International Journal of Energy Research* 46.6 (2022): 7215-7238.
- [27] Ayyarao, TummalaS LV, N. S. S. RamaKrishna, Rajvikram Madurai Elavarasam, Nishanth Polumahanthi, M. Rambabu, Gaurav Saini, Baseem Khan, and Bilal Alatas. "War Strategy Optimization Algorithm: A New Effective Metaheuristic Algorithm for Global Optimization." *IEEE Access* (2022).
- [28] Geretschlager, K. J., Wallner, G. M., & Fischer, J. (2016). Structure and basic properties of photovoltaic module backsheet films. *Solar Energy Materials and Solar Cells*, 144, 451-456.

- [29] Bastidas-Rodríguez, J. D., Ramos-Paja, C. A., & Serna-Garcés, S. I. (2022). Improved modelling of bypass diodes for photovoltaic applications. *Alexandria Engineering Journal*, 61(8), 6261-6273.
- [30] Vieira, R. G., de Araújo, F. M., Dhimish, M., & Guerra, M. I. (2020). A comprehensive review on bypass diode application on photovoltaic modules. *Energies*, 13(10), 2472.
- [31] Solar, A. AE Smart Hot-Spot Free; WEE DE 20958316; AE Solar Alternative Energie: Konigsbrunn, Germany, 2019.
- [32] Alqaisi, Z., & Mahmoud, Y. (2019). Comprehensive study of partially shaded PV modules with overlapping diodes. *IEEE access*, 7, 172665-172675.
- [33] Bun, L. (2011). Détection et Localisation de Défauts pour un Système PV (Doctoral dissertation, Université de Grenoble).
- [34] Kato, K., & Koizumi, H. (2015, May). A study on effect of blocking and bypass diodes on partial shaded PV string with compensating circuit using voltage equalizer. In 2015 IEEE international symposium on circuits and systems (ISCAS) (pp. 241-244). IEEE.
- [35] K. Abdulmawjood, S. S. Refaat, and W. G. Morsi, "Detection and prediction of faults in photovoltaic arrays: A review," in *Proceedings - 2018 IEEE 12th International Conference on Compatibility, Power Electronics and Power Engineering, CPE-POWERENG 2018*, 10-12 April 2018, pp. 1–8.
- [36] A. Triki-Lahiani, A. Bennani-Ben Abdelghani, and I. Slama-Belkhodja, "Fault detection and monitoring systems for photovoltaic installations: A review," *Renewable and Sustainable Energy Reviews*, vol. 82, no. March 2017, pp. 2680–2692, 2018.
- [37] D. S. Pillai and N. Rajasekar, "A comprehensive review on protection challenges and fault diagnosis in PV systems," *Renewable and Sustainable Energy Reviews*, vol. 91, no. July 2017, pp. 18–40, 2018.
- [38] Sun, M., Lv, S., Zhao, X., Li, R., Zhang, W., & Zhang, X. (2018). Defect detection of photovoltaic modules based on convolutional neural network. In *Machine Learning and Intelligent Communications: Second International Conference, MLICOM 2017, Weihai, China, August 5-6, 2017, Proceedings, Part I 2* (pp. 122-132). Springer International Publishing.
- [39] B. Adothu, P. Bhatt, S. Chattopadhyay, S. Zele, J. Oderkerk, H. P. Sagar, F. R. Costa, and S. Mallick, "Newly developed thermoplastic polyolefin encapsulant—A potential candidate for crystalline silicon photovoltaic modules encapsulation," *Solar Energy*, vol. 194, pp. 581–588, Dec. 2019.
- [40] M. Koentges, S. Kurtz, C. E. Packard, U. Jahn, K. A. Berger, K. Kato, T. Friesen, H. Liu, M. Van Iseghem, and J. Wohlgemuth, "T13-01:2014 Review of failures of photovoltaic modules," *Technical Report*, IEA International Energy Agency, 2014.
- [41] García-Gutiérrez, L. A. (2019). Développement d'un contrôle actif tolérant aux défaillances appliquées aux systèmes PV (Doctoral dissertation, Toulouse 3).
- [42] Moyo, R. T., Dewa, M., Romero, H. F. M., Gómez, V. A., Aragonés, J. I. M., & Hernández-Callejo, L. (2024). An Adaptive Neuro-fuzzy Inference Scheme for Defect Detection and Classification of Solar Pv Cells. *Renewable Energy & Sustainable Development*, 10(2).

-
- [43] Kherici, Z., Kahoul, N., Cheghib, H., Younes, M., & Affari, B. C. (2021). Main degradation mechanisms of silicon solar cells in Algerian desert climates. *Solar Energy*, 224, 279-284.
 - [44] Sun, Y., Chen, S., Xie, L., Hong, R., & Shen, H. (2014). Investigating the impact of shading effect on the characteristics of a large-scale grid-connected PV power plant in Northwest China. *International Journal of Photoenergy*, 2014(1), 763106.
 - [45] ‘PV magazine’, <https://www.pv-magazine.fr/2024/07/03/augmentation-des-cas-de-bris-de-verre-spontanes-sur-les-panneaux-solaires/> , July 2024.
 - [46] Canal Solar. <https://canalsolar.com.br/principais-problemas-encontrados-em-modulos-fotovoltaicos/>.
 - [47] Burhandono, A., & Sinaga, N. (2022). Menjaga Keandalan Sistem PLTS dengan Metode Failure Mode Effect Analysis (FMEA). *Jurnal Teknik Industri*, 12(1), 30-39.
 - [48] Winaico. <https://www.winaico.com.au/blog/common-solar-panel-defects>.
 - [49] Köntges, M., Kurtz, S., Packard, C. E., Jahn, U., Berger, K. A., Kato, K., ... & Friesen, G. (2014). Review of failures of photovoltaic modules.
 - [50] Testo. (n.d.). <https://www.testo.com/fr-FR/applications/solar-energy>.
 - [51] Hidayathulla, M. (2019, October 17). Testing and certification of solar PV modules and components: Recent changes and its requirements [Presentation]. TÜV Rheinland India.
 - [52] P. Manganiello, M. Balato, and M. Vitelli, “A Survey on Mismatching and Aging of PV Modules: The Closed Loop,” *IEEE Transactions on Industrial Electronics*, vol. 62, no. 11, pp. 7276–7286, Nov. 2015.
 - [53] Kim, J., Rabelo, M., Padi, S. P., Yousuf, H., Cho, E.-C., & Yi, J. A Review of the Degradation of Photovoltaic Modules for Life Expectancy. *Energies*, 14(14), 4278, (2021).
 - [54] S.R. Madeti, S.N. Singh, Monitoring system for photovoltaic plants: a review, *Renew. Sustain. Energy Rev.* 67 (2017) 1180–1207.
 - [55] P. Hacke, S. Lokanath, P. Williams, A. Vasan, P. Sochor, G.S.T. Mani, H. Shinohara, S. Kurtz, A status review of photovoltaic power conversion equipment reliability, safety, and quality assurance protocols, *Renew. Sustain. Energy Rev.* 82 (2018) 1097–1112.
 - [56] S. Shivashankar, S. Mekhilef, H. Mokhlis, M. Karimi, Mitigating methods of power fluctuations of photovoltaic (PV) sources – a review, *Renew. Sustain. Energy Rev.* 59 (2016) 1170–1184.
 - [57] A. Colli, Failure mode and effect analysis for photovoltaic systems, *Renew. Sustain. Energy Rev.* 50 (2015) 804–809.
 - [58] D. S. Pillai, F. Blaabjerg, and N. Rajasekar, “A Comparative Evaluation of Advanced Fault Detection Approaches for PV Systems,” *IEEE J. Photovoltaics*, vol. 9, no. 2, pp. 513–527, 2019.
 - [59] A. Livera, M. Theristis, G. Makrides, and G. E. Georghiou, “Recent advances in failure diagnosis techniques based on performance data analysis for grid-connected photovoltaic systems,” *Renew. Energy*, vol. 133, pp. 126–143, 2019.
 - [60] I. U. Khalil et al., “Comparative Analysis of Photovoltaic Faults and Performance Evaluation of its Detection Techniques,” *IEEE Access*, vol. 8, pp. 26676–26700, 2020.

- [61] A. Mellit, "Recent Applications of Artificial Intelligence in Fault Diagnosis of Photovoltaic Systems," in *A Practical Guide for Advanced Methods in Solar Photovoltaic Systems*, vol. 128, Springer International Publishing, 2020, pp. 257–271.
- [62] IEA-PVPS, *Review on Infrared and Electroluminescence Imaging for PV Field Applications*. 2018.
- [63] R. Ebner, B. Kubicek, and G. Ujvari, "Non-destructive techniques for quality control of PV modules: Infrared thermography, electro- and photoluminescence imaging," *IECON Proc. (Industrial Electron. Conf.)*, pp. 8104–8109, 2013.
- [64] X. Li, W. Li, Q. Yang, W. Yan, and A. Y. Zomaya, "An Unmanned Inspection System for Multiple Defects Detection in Photovoltaic Plants," *IEEE J. Photovoltaics*, vol. 10, no. 2, pp. 568–576, 2020.
- [65] M. Alsafasfeh, I. Abdel-Qader, B. Bazuin, Q. Alsafasfeh, and W. Su, "Unsupervised fault detection and analysis for large photovoltaic systems using drones and machine vision," *Energies*, vol. 11, no. 9, pp. 1–18, 2018.
- [66] G. Alves Dos Reis Benatto et al., "Drone-Based Daylight Electroluminescence Imaging of PV Modules," *IEEE J. Photovoltaics*, vol. 10, no. 3, pp. 872–877, 2020.
- [67] V. Carletti, A. Greco, A. Saggese, and M. Vento, "An intelligent flying system for automatic detection of faults in photovoltaic plants," *J. Ambient Intell. Humaniz. Comput.*, vol. 11, no. 5, pp. 2027–2040, 2020.
- [68] B. TAGHEZOUIT, (2022). *Contribution to monitoring and performance analysis of photovoltaic systems* (Doctoral dissertation, école nationale polytechnique).
- [69] D. L. King, W. E. Boyson, and J. A. Kratochvil, "Photovoltaic array performance model," *Sandia Rep. No. 2004-3535*, vol. 8, no. December, pp. 1–19, 2004.
- [70] R. Rawat, S. C. Kaushik, and R. Lamba, "A review on modeling, design methodology and size optimization of photovoltaic based water pumping, standalone and grid connected system," *Renew. Sustain. Energy Rev.*, vol. 57, pp. 1506–1519, 2016.
- [71] Huawei, "Smart I-V Curve Diagnosis," no. 03, 2020, [Online]. Available: <https://solar.huawei.com/enGB/download?p=%2F%2Fmedia%2FSolar%2Fattachment%2Fpdf%2Fcu%2Fdatasheet%2FIV-Curve.pdf>.
- [72] S. Roy, M. K. Alam, F. Khan, J. Johnson, and J. Flicker, "An Irradiance Independent, Robust Ground Fault Detection Scheme for PV Arrays Based on Spread Spectrum Time Domain Reflectometry (SSTDR)," *IEEE Trans. Power Electron.*, vol. 8993, no. c, pp. 1–1, 2017.
- [73] Q. Xiong et al., "Detecting and localizing series arc fault in photovoltaic systems based on time and frequency characteristics of capacitor current," *Sol. Energy*, vol. 170, no. May, pp. 788–799, 2018.
- [74] Z. Wang, S. McConnell, R. S. Balog, and J. Johnson, "Arc fault signal detection - Fourier transformation vs. wavelet decomposition techniques using synthesized data," *2014 IEEE 40th Photovolt. Spec. Conf. PVSC 2014*, pp. 3239–3244, 2014.
- [75] J. Flicker and J. Johnson, "Photovoltaic ground fault detection recommendations for array safety and operation," *Sol. Energy*, vol. 140, pp. 34–50, 2016.
- [76] D. Gianola, "Theory and analysis of threshold characters," *Journal of animal Science*, vol. 54, no. 5, pp. 1079–1096, 1982.

- [77] M. Hosseinzadeh and F. Rajaei Salmasi, "Determination of maximum solar power under shading and converter faults - A prerequisite for failure-tolerant power management systems," *Simulation Modelling Practice and Theory*, vol. 62, pp. 14–30, Mar. 2016.
- [78] A. Umana and A. P. S. Meliopoulos, "Detection of cell-level fault conditions within a photovoltaic array system," in *Proceedings of the IEEE Power Engineering Society Transmission and Distribution Conference*, Dallas, TX, USA, 3-5 May 2016.
- [79] T. Shimakage, K. Nishioka, H. Yamane, M. Nagura, and M. Kudo, "Development of fault detection system in PV system," in *INTELEC, International Telecommunications Energy Conference (Proceedings)*, Amsterdam, Netherlands, 9-13 Oct. 2011.
- [80] M. Alajmi and I. Abdel-Qader, "Fault detection and localization in solar photovoltaic arrays using the current-voltage sensing framework," in *IEEE International Conference on Electro Information Technology*, Grand Forks, ND, USA, 19-21 May 2016, vol. 2016-Augus, pp. 307–312.
- [81] W. J. Dixon and F. J. Massey Jr, *Introduction to statistical analysis*, Book. McGraw-Hill, 1951.
- [82] N. R. Draper and H. Smith, *Applied regression analysis*, Book, vol. 326. John Wiley & Sons, 1998.
- [83] T. Li, S. Zhu, and M. Ogihara, "Using discriminant analysis for multi-class classification: An experimental investigation," *Knowledge and Information Systems*, vol. 10, no. 4, pp. 453–472, Nov. 2006.
- [84] C. Voyant, G. Notton, S. Kalogirou, M. L. Nivet, C. Paoli, F. Motte, and A. Foulloy, "Machine learning methods for solar radiation forecasting: A review," *Renewable Energy*, vol. 105, pp. 569–582, May 2017.
- [85] R. Fazai, K. Abodayeh, M. Mansouri, M. Trabelsi, H. Nounou, M. Nounou, and G. E. Georgiou, "Machine learning-based statistical testing hypothesis for fault detection in photovoltaic systems," *Solar Energy*, vol. 190, pp. 405–413, Sep. 2019.
- [86] A. H. Elsheikh, S. W. Sharshir, M. Abd Elaziz, A. E. Kabeel, W. Guilan, and Z. Haiou, "Modeling of solar energy systems using artificial neural network: A comprehensive review," *Solar Energy*, vol. 180, pp. 622–639, Mar. 2019.
- [87] D. E. Rumelhart, G. E. Hinton, and R. J. Williams, "Learning representations by back-propagating errors," *Nature*, vol. 323, no. 6088, pp. 533–536, Oct. 1986.
- [88] V. Cherkassky and Y. Ma, "Practical selection of SVM parameters and noise estimation for SVM regression," *Neural Networks*, vol. 17, no. 1, pp. 113–126, Jan. 2004.
- [89] J. Wang, D. Gao, S. Zhu, S. Wang, and H. Liu, "Fault diagnosis method of photovoltaic array based on support vector machine," *Energy Sources, Part A: Recovery, Utilization and Environmental Effects*, 2019.
- [90] M. Manohar and E. Koley, "SVM based protection scheme for microgrid," in *2017 International Conference on Intelligent Computing, Instrumentation and Control Technologies, ICICICT 2017, 2018*, vol. 2018-Janua, pp. 429–432.
- [91] L. A. Zadeh, "Fuzzy Logic," *Computer*, vol. 21, no. 4, pp. 83–93, 1988.
- [92] S. R. Safavian and D. Landgrebe, "A Survey of Decision Tree Classifier Methodology," *IEEE Transactions on Systems, Man and Cybernetics*, vol. 21, no. 3, pp. 660–674, 1991.

- [93] B. Kamiński, M. Jakubczyk, and P. Szufel, “A framework for sensitivity analysis of decision trees,” *Central European Journal of Operations Research*, vol. 26, no. 1, pp. 135–159, Mar. 2018.
- [94] IEA-PVPS, “Review of Failures of Photovoltaic Modules,” 2014. [Online]. Available : iea-pvps.org.
- [95] E. Garoudja, A. Chouder, K. Kara, S. Silvestre, An enhanced machine learning based approach for failures detection and diagnosis of PV systems, *Energy Convers. Manag.* (2017).
- [96] Garoudja, E. (2018). Faults detection and diagnosis of photovoltaic systems using artificial intelligence tools (Doctoral dissertation, Blida 1 University).
- [97] International Electrotechnical Commission, Photovoltaic System Performance Monitoring—Guidelines for Measurement, Data Exchange and Analysis, IEC 61724 (1998).

Scientific Productions

Publications in journals

- **Bacha, M.**, Terki, A., & Bacha, M. (2024). Comparative study of real-time photovoltaic fault diagnosis using artificial intelligence: Fuzzy logic and neural network approaches. *Energy Sources, Part A: Recovery, Utilization, and Environmental Effects*, 46(1), 13536–13560.
- Slimani, A., Bourek, A., Ammar, A., Kakouche, K., Hattab, W., & **Bacha, M.** (2025). Artificial Neural Network-Based Deadbeat Predictive Current Control with Dead-Time Compensation for PMSMs. *ITEGAM-JETIA*, 11(51), 197-205.

International Conferences

- **Bacha, M.**, & Terki, A. (2022). Diagnosis algorithm and detection faults based on fuzzy logic for PV panel. *Materials Today: Proceedings*, 51, 2131-2138.
- **Bacha, M.**, Terki, A., & Bacha, M. (2022, October). Real-time implementation of diagnosis and fault detection for PV panel based on fuzzy logic classification. In *2022 2nd International Conference on Advanced Electrical Engineering (ICAEE)* (pp. 1-6). IEEE.
- **Bacha, M.**, Terki, A., & Houili, R. (2024, May). An Intelligent Diagnosis and Fault Detection Model Based on Fuzzy Logic for Photovoltaic Panels. In *Proceedings* (Vol. 105, No. 1, p. 105). MDPI.
- Houili, R., Hammoudi, M. Y., **Bacha, M.**, Betka, A., & Titaouine, A. (2024, May). Hybrid Particle Swarm Optimization and Manta Ray Foraging Optimization for Parameter Estimation of Induction Motors. In *Proceedings* (Vol. 105, No. 1, p. 86). MDPI.
- Slimani, A. A., Bourek, A., Ammar, A., Kakouche, K., Hattab, W., & **Bacha, M.** (2024, May). Model Predictive Current Controlled PMSM Drive with Fuzzy Logic for Electric Vehicle Applications. In *2024 2nd International Conference on Electrical Engineering and Automatic Control (ICEEAC)* (pp. 1-6). IEEE.

- Belaroussi, O., Terki, A., & **Bacha, M.** (2022, October). Performances Improvement of PV Water Pumping System. In 2022 2nd International Conference on Advanced Electrical Engineering (ICAEE) (pp. 1-5). IEEE.

National Conferences

- **Bacha, M.**, Terki, A., Houili, R., Bacha, M., Youcef, I. Analyzing the Influence of partial shading on photovoltaic system performance. The 1ST National Conference on Mechanics and Materials ,06- 07 December 2023, Boumerdes University- Algeria (NCMM'2023).
- **Bacha, M.**, Terki, A., Houili , R.,Zabia D. E., Youcef, I, & Bacha, M. Study of the Effect of Partial shading on photovoltaic panels. The 1ST National Conference on Emergent Technologies in Electrical Engineering ,16- 17 December 2023, Ferhat Abbas University Setif 1- Algeria (NCETEE'2023)
- **Bacha, M.**, Terki, A., Houili, R., Bacha, M., & Youcef, I. Analysis of the Impact of Bypass Diode Failure on Solar PV Module Performance. The 1ST National Conference on Matter Science ,20 December 2023, Djelfa University- Algeria (NCSM2023).
- Houili, R., Hammoudi, M.Y., **Bacha, M.**, & Titaouine, A. New state feedback con troller of ts fuzzy systems with unmeasured premise variables: Application to single link flexible joint robot.The 1ST National Conference on Mechanics and Materials ,06- 07 December 2023, Boumerdes University- Algeria (NCMM'2023).
- Houili, R., Hammoudi, M.Y., **Bacha, M.**, & Titaouine, A. Enhanced Identification and Simulation of Photovoltaic Systems.The 1ST National Conference on Matter Science ,20 December 2023, Djelfa University- Algeria (NCSM2023).